Performance Prediction and Improvement of a Bistatic Passive Coherent Location Radar

Gunther Erich Lange

A dissertation submitted to the Department of Electrical Engineering,
University of Cape Town, in fulfilment of the requirements
for the degree of Master of Science in Engineering.

Cape Town, May 2009

Declaration

I declare that this dissertation is my own, unaided work. It is being submitted for the degree of Master of Science in Engineering in the University of Cape Town. It has not been submitted before for any degree or examination in any other university.

Signature of Author .....

Cape Town

May 2009

Abstract

Passive Coherent Location (PCL) radar has proved to be feasible in a number of experimental systems, but the lack of comprehensive, published flight trials detracts somewhat from serious consideration of these PCL systems for operational applications, such as Air Traffic Control (ATC). The carrying out of flight trials is, in any case, difficult and very expensive.

This dissertation presents a method for accurately predicting the performance of a bistatic passive coherent location radar with the effects of the environment taken into account. The effect of the environement on a propagating electromagnetic wave is obtained from the Advanced Refractive Effects Prediction System (AREPS) model. The resulting performance predictions, in the form of spatial signal-to-noise ratio (SNR), signal-to-interference ratio (SIR) and signal-to-noise-plus-interference ratio (SNIR) maps, provide a powerful planning tool for the application of systems such as ATC. Furthermore, the spatial coverage maps, based on the bistatic radar equation, can be related to a particular probability of detection and false alarm as well as to a required dynamic range of the receiver ADC. Overall, the method provides a visual, as well as a quantitative measure of radar coverage with region-specific atmospheric and terrain effects taken into account.

The method proposed in this dissertation offers a marked improvement over traditional performance prediction methods based on the bistatic radar equation within a free space or flat terrain environment.

It is understood that the direct path signal of the illuminating transmitter is the cause of some severe limitations within a PCL system. In the interest of suppressing the strong direct signal before the ADC and to complement the development of the prediction method, an antenna pattern was synthesised and applied to an array of folded dipoles in order to place a null in the direction of the strong transmitter. The synthesised antenna pattern and its improvement on the performance of the PCL system was then evaluated using the proposed prediction method presented in this dissertation.

To my Family.

Acknowledgements

First and foremost I would like to thank my supervisor Professor Michael Inggs for getting me interested in PCL (Passive Coherent Location) radar, his valued insight and all the opportunities and support he has provided me with.

I would also like to thank Dr Yoann Paichard. His input and guidance was invaluable to the completion of this dissertation.

I am grateful to the South African National Defence Force for their financial support through the SANDF Ledger Project.

I would also like to acknowledge my co-workers in the RRSG (Radar Remote Sensing Group); firstly for their hard work associated with PCL and secondly for the assistance I have received from all quarters concerning many different aspects whilst working on my dissertation.

As part of the RRSG, I would also like to thank our colleagues at University College London for interesting us originally in the PCL work and for their valuable correspondence.

Finally, I would like to thank my immediate family and close friends for their support, patience, continuous motivation and general awesomeness.

Contents

List of Figures

List of Tables

List of Symbols

P_d	—	Probability of detection
P_{fa}	—	Probability of false alarm
F	—	Propagation factor
$\|E_0\|$	—	Electric field strength under free-space conditions
$\|E\|$	—	Electric field strength
L_{fs}	—	Free space path loss
L	—	Total real propagation loss
δf_d	—	Doppler Resolution
T_{int}	—	Integration Time
T_{MAX}	—	Maximum value of the coherent processing integration interval
c_0	—	Speed of light
f_0	—	Signal frequency
λ	—	Wavelength $\left(\frac{c_0}{f_0}\right)$
A_R	—	Radial component of the target acceleration
G_p	—	Processing gain
B	—	Transmitted RF bandwidth
f_d	—	Doppler shift
v	—	Target velocity
P_R	—	Bistatic power of target echo measured at the receiver
N_0	—	White Gaussian noise
P_D	—	Power of direct signal measured at the receiver
P_T	—	Transmitter power output
a	—	Transmitter-to-receiver path (Used as subscript)
b	—	Transmitter-to-target path (Used as subscript)
c	—	Target-to-receiver path (Used as subscript)
R_a, R_b , R_c	—	Range along paths a, b and c respectively
F_a, F_b, F_c	—	Propagation factor along paths a, b and c respectively
G_{Ta}, G_{Tb}	—	Transmit antenna gain along paths a and b respectively
G_{Ra}, G_{Rc}	—	Receiver antenna gain along paths a and c respectively

σ_B — Bistatic radar target cross section (RCS)
T_S — System noise temperature, $(T_s = T_a + T_e)$
T_a — Antenna noise temperature of the receiver
T_e — Equivalent noise temperature of the receiver
B_n — Noise bandwidth
k — Boltzmann's constant, $(1.38 \times 10^{-23}\ ^{J}/_{K})$
F_n — Receiver noise figure
L_a — Transmitter-to-receiver path loss data
L_b — Transmitter-to-target path loss data
L_c — Target-to-receiver path loss data
L_{bc} — Round-trip propagation loss, $(L_b L_c)$
Z_{in} — Input Impedance
θ — Angle of elevation
ϕ — Angle of azimuth
AF — Array factor
k — Wave number
d_x — Inter-element spacing
β — Progressive element phase shift
γ — Array azimuth offset from South

Nomenclature

ADC Analog to Digital Converter

AF Array Factor

APM Advanced Propagation Model

AREPS Advanced Refractive Effects Prediction Systems

ATC Air Traffic Control

ATC Air Traffic Control

COTS Commercial off-the-shelf

CPT Cape Town

CSV Comma Seperated Value

DPI Direct Path Interference

DTED Digital Terrain Elevation Data

EM Electromagnetic

ERP Effective Radiated Power

FEKO Electromagnetic software modelling tool. German acronym loosly translated to Field Computation for Objects of Arbitrary Shape

FERS Flexible and Extensible Radar and Sonar

FM Frequency Modulation

HPBW Half Power Beamwidth

ICASA Independent Communications Authority of South Africa

INTL International

ITU International Telecommunications Authority

JHB Johannesburg

LOS Line-of-Sight

MIMO Mulitple-input multiple-output

PCL Passive Coherent Location

PE Port Elizabeth

PL Propagation Loss

PPM Performance Prediciton Method

RCS Radar Cross Section

RF Radio Frequency

RRSG Radar Remote Sensing Group

Rx Receiver

SIR Signal-to-Interference Ratio

SNIR Signal-to-Noise-plus-Interference Ratio

SNR Signal-to-Noise Ratio

SRTM Shuttle Radar Topography Mission

TPO Transmitter Power Output

Tx Transmitter

UCT University of Cape Town

USRP Universal Software Radio Peripheral

UTM Universal Transverse Mercator

Chapter 1

Introduction

This dissertation presents a method for accurately predicting the performance of a bistatic passive coherent location (PCL) radar with the effects of the environment taken into account. The performance predictions, in the form of spatial coverage maps, provide a visual and quantitative means for determining radar detection range and required receiver dynamic range within a particular environment. These predictions in the form signal-to-noise and signal-to-interference maps are derived from bistatic radar range equation. The method proposed in this dissertation offers a marked improvement over traditional performance prediction methods based on the bistatic radar equation within a free space or flat terrain environment. Furthermore, methods of improving the performance of a PCL system via antenna pattern synthesis techniques are investigated.

This chapter will begin with a brief yet comprehensive overview of the field of PCL. The overview itself will begin with a general description of PCL configurations before touching upon the evolution of bistatic radar and associated technologies. Subsequent to this, is a discussion of some advantages and disadvantages of current state of PCL. Next, existing models for performance prediction are presented. The overview finishes with a look at existing PCL receivers, focusing in particular on the direct path interference cancellation techniques used to improve radar performance.

Following the overview of PCL, the objectives of this dissertation are given and motivated. Finally, an overview of the work reported in this dissertation is given.

1.1 Overview of Passive Coherent Location

The defining property of bistatic and, more generally, multistatic radar, is the fact that the transmitter and receiver sites are not co-located. A special case of a multistatic radar is a passive coherent location system, which is the case where the transmitters are non-cooperative. These transmitters usually form

part of terrestrial broadcast systems such as television and FM radio and are commonly referred to as illuminators of opportunity and thus effectively make such a system passive.

A bistatic PCL radar configuration is defined as a radar that has one transmission and one reception site [7] separated by a considerable distance which is comparable to the target distances [8]. Figure 1.1 illustrates a bistatic radar configuration.

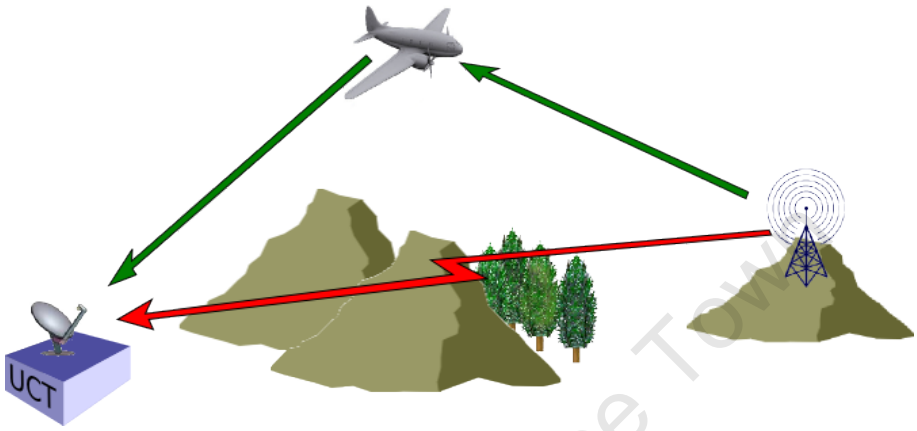

Figure 1.1: Bistatic PCL radar configuration.

A bistatic configuration is a subset of the the more general multistatic configuration which employs multiple transmit and receiving sites. In current literature netted radars and in some cases multiple-input multiple-output (MIMO) radars [9] are described as multistatic. Figure 1.2 illustrates a general multistatic PCL radar configuration with two receivers and two transmitters. Multistatic radar is in a sense an extension of the bistatic radar configuration.

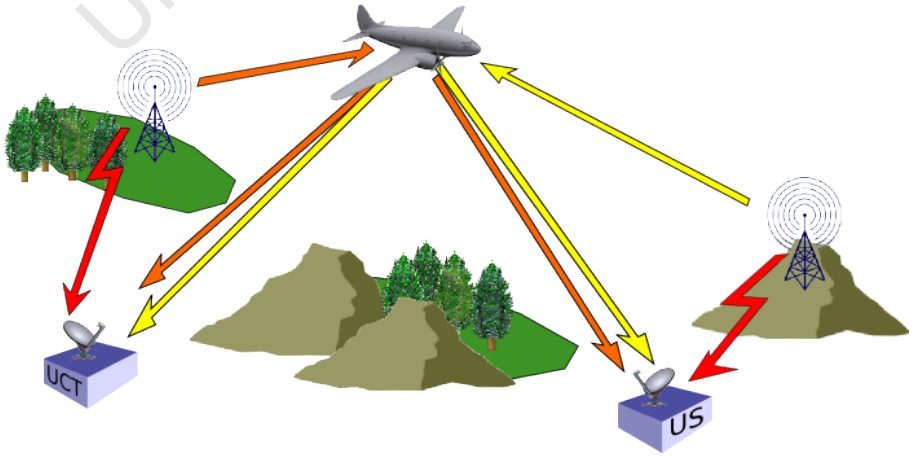

Figure 1.2: Multistatic PCL radar configuration.

The receiver node of a PCL system is required to operate as a matched filter. This means that the transmitted signal must be available through a separate,

dedicated reference antenna [2]. The idea of capturing the reference signal and comparing it to, or correlating it with, the target echo signal makes the PCL receiver coherent [10].

As shown in Figures 1.1 and 1.2 the direct signal, in addition to the echo signal, is incident on the receiver. In a bistatic and multistatic PCL radar, the direct signal can seriously limit the system performance and thus is a major factor to consider in the design of a PCL radar.

For target location information PCL radars estimate range, Doppler and possibly angle-of-arrival (AOA) [10]. Implementing a PCL radar system within a multistatic configuration would allow for techniques of multilateration for the determination of target location and could achieve target location accuracies comparable to conventional radars [2].

1.1.1 The Evolution of Bistatic and Multistatic Radar

Various early forms of radar devices were developed between around 1904 and 1925 [11]. These early radars were developed and tested nearly simultaneously and totally independently by the United States, United Kingdom, France, the Soviet Union, Japan, Germany and Italy [7] and were based on a bistatic configuration. The first radar, however, was developed and demonstrated in 1904 by a German engineer, Christian Hulsmeyer [7]. His device, uniquely named the *telemobiloscope*, was able to detect ships at ranges up to 3 km. Thereafter, the development of the duplexer, which allowed transmitting and receiving through the same antenna (i.e. monostatic radar) [1], resulted in bistatic and multistatic radar having a checkered career with an apparent resurgence cycle of about 15 to 20 years [8].

The latest notable resurgence occurred around 1986 with a study undertaken by Griffiths and Long of bistatic radar based on television transmissions [12]. This latest resurgence can be attributed to vast increase ambient radio signals, particularly television and FM radio, and the technological advances in digital signal processors and processing [1]. The work done by Griffiths and Long was the beginning of a renewed interest in the field of passive radar.

Throughout the twenty-two years since 1986, interest in passive radar has progressively grown, with the current resurgence cycle seemingly nowhere near its end. Willis's book [7] was one of the first thorough treatments of bistatic radar. Thereafter, Howland's early work in television based [13] and later work in FM radio based [2] bistatic passive radar showed promising results. His FM based experimental radar system achieved ranges in excess of 150 km from the receiver. In addition, target acquisition and tracking using passive radar was demonstrated [14, 15]. Developments of PCL radar have

also been seen in industry [16, 10]. For instance, the well-known and commercially available Silent Sentry 2 (SS2) is reported to achieve ranges of up to 220 km [16]. In addition, the Thales and Raytheon joint venture ThalesRaytheonSystems has developed a FM passive radar, Home Alerter 100, for applications of homeland security[1].

The current focus in the field PCL radar is the development of multistatic or netted radar systems. Given one or more transmitters, multiple receiver nodes that cooperate within a common reference frame of time and space is the underlying principle of netted radar [17]. Synchronising these nodes to a common reference frame can be achieved using the timing signal obtained from a GPS constellation and is a technique being investigated by Sandenbergh [17].

Another current interest is in the simulation of complex radar systems and can be attributed to the exponential rise of computing power available to engineers. To this end a signal level simulator called FERS (Flexible, Extensible Radar and Sonar), supporting a wide variety of radar systems and focusing particularly on multistatic and netted radar, has been developed by Brooker [18]. Simulation can provide an invaluable tool to radar researchers, engineers and operators by easily reducing the difficultly and costs associated with testing new radar technologies and approaches [18].

At this stage, however, no studies regarding prediction of bistatic and multistatic radar performance have been done given a set of region specific environmental parameters such as terrain and atmospheric conditions. Ultimately, the proposed prediction method together with the FERS simulator are effective tools that can be used to predict the performance - in terms of coverage - of complex radar systems and confirm the viability of PCL radar.

Lastly, an emerging and seemingly promising technology is that of MIMO radar which shares many, but not all, the principles of netted PCL radar. Noncoherent processing is done to exploit a target's spatial variations to obtain a diversity gain for a target detection and for estimation of various parameters, such as angle of arrival and Doppler [9]. For a target location, it is shown that coherent processing can provide a resolution far exceeding that supported by a radar's waveforms [9].

1.1.2 Advantages and Disadvantages of PCL

The use of bistatic or multistatic PCL radar has not always been advantageous in the past. In 1977, Skolnik [19] stated that bistatic radar was of marginal value, yet well used for special purposes. At that point he asserted

[1] http://www.thalesgroup.com/eurosatory2008/standthales3.htm, checked April 2009

that bistatic radar would not be widely deployed in the near future. This statement was later discussed by Willis in his book [7], published in 1991. In his discussion, Willis conceded that bistatic radar indeed possessed some insufficiency's. These were: Excessive complexity, high costs, degraded performance in terms of coverage as well as degraded performance in terms of low resolution and accuracy.

Advantages

The observations made by Willis and Skolnik held true for some time, though the rapid advancements over almost two decades have lessened the severity of these disadvantages. For instance:

- Much of the system complexity in terms of the design and implementation of bistatic or multistatic PCL receivers has been eliminated by increased capability of digital signal processing as well as by availability of commercial off-the-shelf (COTS) receiver parts [16].
- The costs associated with the development of a PCL system are inherently low [2, 16]. Thus the implementation of an experimental PCL system demonstrator is relatively affordable.
  - Receiver parts are available COTS.
  - No moving parts in the receiver necessary.
- Good coverage can be achieved with a multistatic (netted) PCL radar system. This is made possible by efficient processing and synchronisation between nodes [17].
- Resolution and accuracy comparable to conventional radars can be achieved by [2]:
  - Exploiting excellent Doppler information, due extended integration times possible.
  - Using a multistatic or netted radar configuration. This has the advantage of providing frequency and spatial diversity.
- FM radio based bistatic radars is simultaneously unambiguous in both range and Doppler. This useful property makes them ideal for detecting long-range high-speed targets. [2]

Some more commonly encountered advantages to PCL in a bistatic or multistatic configuration are listed below.

- Reduced operational and maintenance costs owing to the use of non-cooperative transmitter.
- The receiver is passive and thus it is less vulnerable to electronic countermeasures (ECM) [1]. Namely, the fact that the PCL receiver is not transmitting makes it covert and thus difficult to detect.
- PCL offers a counter to stealth technology that is primarily designed to defeat monostatic radar [1].

Disadvantages

The disadvantages associated with a bistatic or multistatic PCL radar have not changed much with time. To a large extent a monostatic mindset [7] is a major limitation to advancements in bistatic and multistatic radar.

- The use of a non-cooperative transmitter allows no control over:
  - The transmitted waveform. This includes waveform type, bandwidth and power. In particular, the range resolution of FM-based PCL is generally worse than achieved in conventional systems owing to the low and variable station bandwidth [20].
  - The location of the transmitter. This puts the broadcast transmitter at risk of an Attack Reconnaissance Helicopter (ARH) attack, compromising the entire PCL system when operating as a military radar. Furthermore, Low Probability of Intercept (LPI) techniques commonly used to improve the survivability of conventional radars cannot be applied to broadcast non-cooperative transmitters [21].
- Direct path interference from the illuminating transmitter can saturate the PCL receiver. This is a particular problem when there is direct line-of-sight (LOS) from transmitter to receiver. In this case the PCL receiver must take measures to attenuate the transmitting signal by Doppler filtering, spatial nulling or by terrain masking [7].
- Geometric complexity [7]. It is difficult to comprehend how the terrain of a certain location of interest can vary appreciably. As a result the computation of spatial coverage and consequently the performance of a PCL system is non-trivial. In comparison, the performance of a monostatic radar is easier to characterise as the shadow regions are easily identified.

- The costs associated with the development of a PCL system required to conform to military specifications can increase rapidly[21]. Such a system may require multiple nodes (a multistatic system) to ensure complete radar coverage. In addition, the use of an array antenna and adaptive cancellation processing for the suppression of interfering signals has the implication that the receiving system is not as simple nor as cheap as might originally have been supposed [22].

1.1.3 Modelling of Predicted Performance

A major factor in PCL is the choice of transmitted waveform, location of the transmitter and the location of the PCL receiver system. These must be chosen so as to maximise the coverage of a particular bistatic radar configuration. Furthermore, since the radar is passive, the location of the transmitter and the form of transmission to be exploited are no longer under the control of the radar designer. Thus it would seem that the scope for radar design and optimisation is severely limited [1].

However, bistatic PCL performance predictions can be done for any bistatic configurations in free space. One such prediction is shown in Figure 1.3. This prediction, shown in Cherniakov's book on bistatic radar [1], is of a FM based passive bistatic radar and is a result of Griffiths and Baker's original paper [22] investigating potential detection range and PCL performance of realistic systems. The figure shows the detection range and coverage in free space in terms of signal-to-noise ratio (SNR) and is in the form of the well-known ovals of Cassini [7].

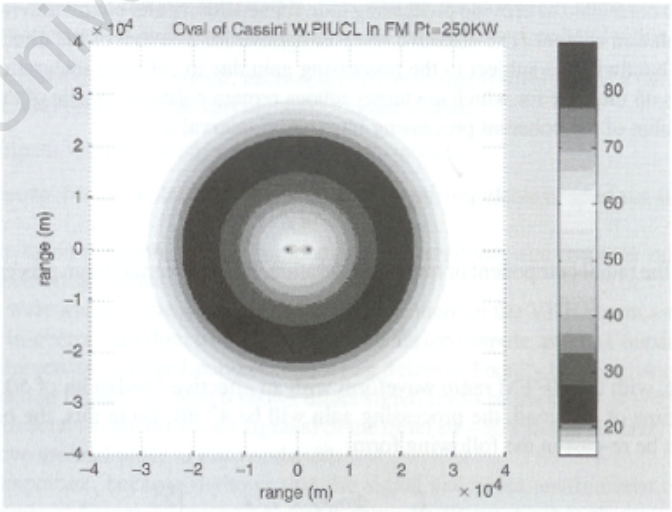

Figure 1.3: Detection range for a transmitter at Wrotham in South-East England and a receiver at UCL [1].

The minimum required SNR, as illustrated in Figure 1.3, could be related to a specific probability of detection, P_d, and probability of false alarm, P_{fa} [8].

These probabilities would be specified by the system requirements as derived from a customer's needs; however are currently not well-defined for passive bistatic systems in open literature and offer an avenue for future work. An SNR of $15\,\mathrm{dB}$ is generally accepted as a good benchmark for bistatic radar and PCL utilising broadcast FM radio signals [22, 2]. With an SNR specified around 15 dB and a target RCS set at 10 dB Tobias et al [23] determined a $P_d = 0.9999$ and $P_{fa} = 10^{-4}$ for a passive bistatic radar at low frequencies for their simulations.

A common problem in bistatic PCL systems is that the radar receiver must detect very low power target echoes in the presence of a very strong and continuous broadcast signal [1]. This could be said to be the greatest limiting factor in PCL systems, where direct-path interference (DPI) can in some cases be up to 90 dB greater than the echo [2]. A measure of the severity of this effect is the signal-to-interference ratio (SIR) and describes the required dynamic range of the receiver, in particular the dynamic range of the ADC. A commonly accepted level of SIR of a receiver is between $-60\,\mathrm{dB}$ and $-70\,\mathrm{dB}$.

Figure 1.4 shows the predicted signal-to-interference ratio (SIR) for a specific FM based bistatic radar in free space. In this case the receiver has a particular antenna pattern that is taken into account, thus providing a non-uniform coverage pattern as seen in the figure.

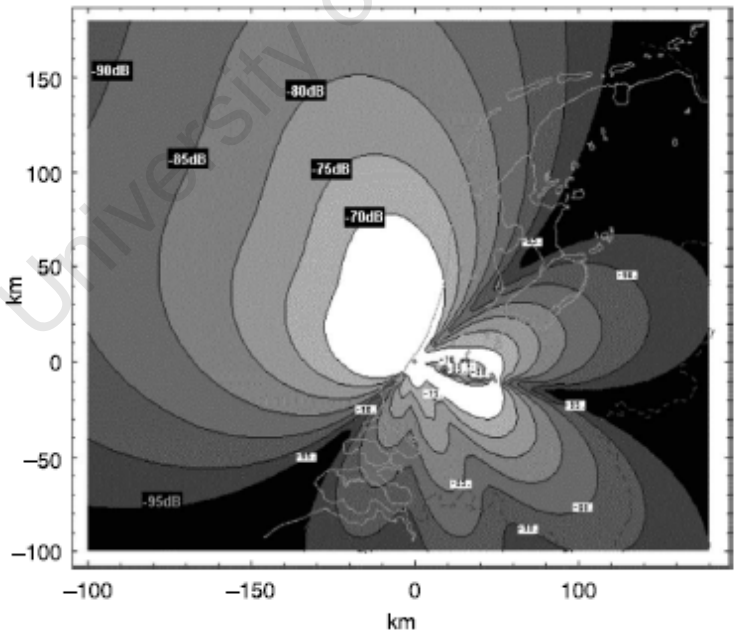

Figure 1.4: Predicted signal-to-interference ratio (dB) [2].

Using spatial maps of SNR and SIR data gives a good indication of the expected performance of a particular bistatic radar configuration and aids in identifying critical factors. As such, this method of visually representing the coverage of a bistatic PCL system provides a good figure of merit or tool to

determine the performance.

However, one major drawback to the aforementioned methods is that they are performed in free space with environmental effects not taken into account. The greatest environmental effect, of course, is that of terrain. The fact that the transmitter-to-target and target-to-receiver paths may not always be line-of-sight (LOS) is a significant aspect to consider. In addition, other significant propagation effects are multipath, diffraction, refraction and atmospheric absorption and cannot be disregarded. In the case of the Western Cape region the effect of the environment - in particular that of the mountainous terrain - on EM wave propagation is an important factor to take into account.

The ability to model and subsequently predict the possible detection range and coverage feasibility, by producing spatial SNR, SIR as well as SNIR (signal-to-noise-plus-interference) maps while taking the environmental propagation effects into account, provides an improved method for determining the performance of a bistatic PCL radar. It also allows for the identification of optimum receiver sites in order to maximise coverage and would in essence provide a powerful planning tool for an Air Traffic Control system.

1.1.4 Receiver System Designs

As was noted in the previous section, a strong DPI received in the target antenna correlates perfectly with the reference signal and can produce range and Doppler sidelobes that are several orders of magnitude greater than that of the wanted echo [2]. This makes receiver system design particularly important in the field of PCL.

Much work has been done concerning the cancellation of DPI. Software cancellation, namely, the cancellation implemented in the digital domain occurs last in the target echo receiver chain as indicated in Figure 1.5 and has been the subject of much attention. However, software cancellation cannot increase the target information in the quantised data obtained from an ADC with a limited dynamic range. Thus, used alone, software cancellation won't improve the performance of the passive radar significantly [24]. As such, Wan [24] stresses the importance of DPI cancellation prior to ADC for improvement of passive radar performance.

There are generally two effective techniques that enable DPI cancellation before the ADC as shown in Figure 1.5. One technique is to introduce a type of RF canceller and the other is to suppress the interference in an antenna pattern null using pattern synthesis techniques. The ability to synthesise the receiver antenna pattern has the advantage of being able to point the main beam in the region of interest while suppressing interfering signals from ar-

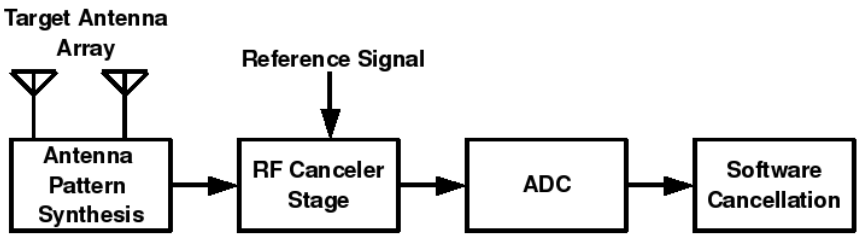

Figure 1.5: Target echo receiver chain.

bitrary directions in nulls.

Dynetics [10] reports the effective implementation of a PCL system and suppression of the DPI using a RF canceller. Their RF canceller was able, with manual adjustments, to attenuate the DPI by 20 dB. To eliminate clutter returns with zero Doppler shift, they delayed the reference signal, appropriately adjusted its gain and phase, and subtracted it from the target signal. The result was the elimination of all signals with zero Doppler shift. This technique proved quite effective and allowed detection of the desired aircraft targets as long as their Doppler shifts are non-zero. Real experiments done by Wan et al [24] with their RF cancellation stage gave a suppression of DPI of over 30 dB.

In terms of the target antenna front-end as illustrated in Figure 1.5, a common method to suppress the direct signal has been the use of adaptive antennas, namely the steering of nulls in the direction of the illuminating transmitter. Other less sophisticated - yet often successful - methods involve simply shielding the target antenna from the transmitter or using directive antenna elements focused in a particular direction.

For instance, Sahr and Lind, in their work on the Manatash Ridge radar designed for upper atmosphere radio science, isolated the receiver from the direct signal by physically displacing the target antenna from the transmitter by approximately 100 km, past an intervening mountain range [25].

In his work on TV based bistatic radar [14], Howland used two directive eight-element Yagi-Uda antennas to achieve an unambiguous measurement range of approximately $\pm 56^{\circ}$ about boresight. In this case the direct signal simply fell outside the main beam and on the pattern sidelobes of lower gain. Later, Howland used a receiver that comprised of two vertically-polarised half-wave dipoles over a mesh backplane for his investigation into FM based bistatic radar [2]. This yielded a radar that surveyed a sector approximately 120° in the azimuth. In this case, in order to suppress the DPI, the target antenna was physically oriented so as to try and place the transmitter in a null in the antenna pattern.

Dynetics [10] ultimately also made use of Yagi-Uda antenna for their target

antenna and similar to Howland [14] ensured that the direct signal fell outside the main beam. In their work they attempted, when possible, to place nulls in the direction of the transmitter.

The Silent Sentry 2 system employs a linear phased antenna array as their target antenna [16]. This allows them some control over their antenna array pattern and as such enables them to form nulls in the direction of the illuminating transmitter to suppress the DPI.

It is apparent that much work has been done regarding the investigation of RF cancellers and, in contrast, less regarding the shaping of antenna array patterns to suppress DPI. The opinion of Wan [24] and Zoeller of Dynetics [10] is that interference cancellation cannot be solely achieved by antenna synthesis techniques. However, arraying of antennas can offer an improvement of DPI suppression before the ADC. Namely, inefficient use of the target antennas could be detrimental, whereas effective implementation of an antenna array can offer performance improvement. Thus, the antenna front-end and the methods of antenna pattern synthesis are important aspects that must not be disregarded.

1.2 Objectives and Motivation

The objectives of this dissertation are to:

- Investigate the broadcasting platforms of the Western Cape in order to:
  - Identify transmitters that may be used as illuminators of opportunity.
  - Identify broadcast signals suited for use by a PCL system.
- Determine a method for predicting the performance of a PCL system in terms of detection range and required dynamic range with real-world environmental effects taken into account. The predictions are to be done using:
  - Signal-to-noise ratio (SNR) spatial coverage maps.
  - Signal-to-interference (SIR) spatial coverage maps.
  - Signal-to-noise-plus-interference (SNIR) spatial coverage maps.
- Investigate methods of antenna array synthesis to improve the predicted performance of a PCL system.
- Conclude on work done and discuss possible future research.

Before the development of any PCL system, a good knowledge of the available transmitters and signals of the specified region is required. Therefore, the characterisation of the broadcasting platforms within the Western Cape is an important starting point for this dissertation.

PCL has proved to be feasible in a number of experimental systems, but the lack of comprehensive, published flight trials detracts somewhat from serious consideration of these PCL systems for operational applications, such as Air Traffic Control (ATC). The carrying out of flight trials is, in any case, difficult and very expensive. Hence, an improved method of performance prediction for a PCL system, that accounts for the effects of the environment, is proposed in this dissertation. These performance predictions, in the format of spatial signal-to-noise ratio (SNR), signal-to-interference ratio (SIR) and signal-to-noise-plus-interference ratio (SNIR) maps, provide a powerful planning tool for the application of systems such as ATC and would offer an extension to the work reviewed in Section 1.1.3.

It is clear from the discussions in Sections 1.1.3 and 1.1.4 that the direct path signal is the cause of some severe limitations within a PCL system. In the interest of suppressing this strong direct signal before the ADC, antenna pattern synthesis techniques will be investigated in order to place a null in the direction strong transmitters. The synthesised antenna pattern and its improvement on the performance of the PCL system can then evaluated using the proposed prediction tool. Provided reasonable performance the array will be set up and its radiation pattern tested.

In general, the widespread acceptance of the PCL technology requires much more confidence from the user community. For example, in terms of predicting and measuring coverage, modern ATC radar systems (expensive on spectrum usage and cost) leverage a heritage going back to the 1939-1945 War. Comprehensive coverage studies of operational bistatic, multistatic and PCL systems have not been widely published, if at all available.

1.3 Overview of dissertation

Chapter 1 provides a brief overview of the field of PCL. It includes a discussion of PCL configurations, the evolution of bistatic radar and associated technologies as well as some advantages and disadvantages of the current state of PCL. Existing PCL receivers are reviewed in this Chapter, focusing on interference cancellation techniques and models for performance prediction.

Following the overview of PCL, the objectives of this dissertation are given and motivated. Finally, the current section provides an overview of the work

done, essentially giving a summary for each chapter.

Before the development of any PCL system, a good knowledge of the available transmitters and signals of the specified region is required. As such, a preliminary study into the properties of the broadcast transmitters and signals of the Western Cape, with the effects of the environment taken into account, was done and is reported in **Chapter 2**.

The purpose of this chapter is to identify and characterise the regional broadcast transmitters and their associated signals so as to determine the feasibility for their use as illuminators of opportunity. In particular, one transmitter is sought for the later application and investigation of an improved performance prediction method proposed in this dissertation and introduced in Chapter 3.

Chapter 2 begins with a review of some important environmental effects. Thereafter, the electromagnetic (EM) propagation modelling tools, APM and AREPS[2], are introduced and discussed. A central topic of this chapter and dissertation is the use of APM and AREPS to allow accurate modelling of EM waves propagating within the environment of the Western Cape.

Next, the signal and transmitter properties of possible illuminators of opportunity are studied. This involves a comparison and discussion of the signal strength received at UCT, for the free space, measured and simulated case. The study ultimately identifies the Villiersdorp transmitter as the best-case illuminator of opportunity. It's location, which is out of line-of-sight due to some mountainous terrain, is seen to provide additional attenuation of the direct signal and thus additional suppression of the DPI. The Villiersdorp transmitter will be used throughout this dissertation as the illuminator of opportunity for all ensuing case studies.

Chapter 3 presents the proposed method of predicting bistatic PCL performance, while accounting for environmental effects. The performance prediction, in the form of spatial signal-to-noise ratio (SNR), signal-to-interference ratio (SIR) and also signal-to-noise-plus-interference ratio (SNIR) coverage maps, provide a visual means for determining radar detection range and required dynamic range of the receiver. Using this method, expected coverage at different altitudes with specified transmitter and receiver properties is determined and compared with the conventional prediction method employing the ovals of Cassini. The method, which is essentially an extension to the work of Griffiths and Baker [22], provides the user with a means to compare the coverage of potential illuminators of opportunity quickly and easily.

The coverage maps produced here are based on an interpolation of propaga-

[2]Advanced Propagation Model (APM) and Advanced Refractive Effects Prediction System (AREPS)

tion loss data generated by APM and AREPS. Namely, realistic propagation loss is utilised to predict the loss along any path from a transmitter to a target and onwards to a receiver. This is achieved by taking into account the propagation factor, F, which is a quantity that commonly contains the effects of refraction, diffraction, multipath as well as atmospheric attenuation dealt with in the previous chapter.

To model the loss from a moving target to a receiver is difficult, since radar coverage prediction requires this to be done for all possible target positions, to the receiver. By appealing to theorem of reciprocity [4], the target to receiver loss is modelled in the reverse direction. It is thus possible to map the two way loss to each pixel of the area being assessed in one set of calculations, the results of which can be held as a lookup table for simulation or coverage assessment. The method's accuracy will degrade slightly in the case of targets lying in shadow regions subject to knife-edge diffraction.

This chapter begins by discussing the SNR, SIR and SNIR equations, derived from the well-known bistatic radar equation, for the purpose of coverage prediction. This is followed by a discussion of a conventional model of bistatic coverage, the ovals of Cassini. The proposed method of determining expected bistatic PCL radar coverage, while accounting for environmental effects, is then developed. Throughout this chapter a omnidirectional target antenna pattern with a gain of 5 dB is used.

The SNR coverage maps show an expected coverage, for given environment and system parameters, of around 75 km and 150 km at an altitude of 1600 m and 5000 m, respectively. These realistic detection ranges were, as expected, much less than the 250 km detection range predicted using the conventional model. These differences emphasised the importance of the propagation factors, F.

The SIR (and SNIR) coverage maps indicated the required dynamic range within a certain coverage region. An improvement, of around 25 dB, in the SIR coverage maps and subsequently the required dynamic range was seen by the increase of direct path loss resulting from the terrain and atmosphere effects. The required dynamic range can be further improved by reducing the DPI in the target antenna.

In general, this method can be used to compare various arrangements of receivers and transmitters in any bistatic configuration and will aid in the choice of optimum non-cooperative transmitter and receiver location. In essence, it offers improved performance prediction capability over the conventional prediction method.

Chapter 4 will present the modified coverage of expected detection range and required dynamic range in terms of SNR and SIR resulting from the target

antenna pattern synthesis. In particular, the Schelkunoff method is used to synthesise a pattern null in the direction of the illuminating transmitter to suppress the DPI in the target antenna of a PCL receiver. The case study introduced in the previous chapter is carried through here, in that an attempt to improve the coverage is made.

The chapter begins by listing necessary requirements for target antenna array.

Thereafter, target antenna array and its elements are simulated and discussed with the use of the sophisticated antenna and EM modelling tool, FEKO[3]. The name, FEKO, is derived from a German acronym which can be translated as "Field Computation for Objects of Arbitrary Shape".

First, folded dipoles, intended for the use as the elements of the target antenna array, are discussed. The choice of folded dipoles as elements of the array is found advantageous in that they are structurally stable and commercial available.

Next, the antenna pattern synthesis technique, the Schelkunoff Unit-Circle Method, is introduced and reviewed. With reference to the requirements, the target antenna array is designed using this technique and simulated in FEKO. The resulting four element array is investigated, with a particular focus on the subsequent azimuth radiation pattern. Applying a Schelkunoff excitation distribution to the four element array within FEKO results with a null in the expected direction.

Utilising the azimuth pattern with resulting from Schelkunoff distribution in the performance prediction method presented in Chapter 3, shows improved coverage in the sectors of interest. The decrease of coverage in other sectors was deemed acceptable for the application of the detection of aircraft in the direction of JHB. In general, the results suggest that coverage, in terms of possible detection range and required dynamic range, in a sector of airspace can be improved significantly with the application of antenna synthesis.

In **Chapter 5** the antenna array excitation determined in the previous chapter will be applied to real folded dipole antenna elements representing the target antenna. This is done for two reasons. Firstly, to verify the simulated pattern and to confirm that the application of the Schelkunoff method used in the previous chapter yields a physically realisable pattern. Secondly, to ascertain the predicted performance in terms of detection range and dynamic range resulting from the measured pattern. The bistatic configuration investigated here is a continuation of the case study dealt with in Chapter 3 and 4. The predicted performance determined here is compared with that of the simulated case determined in the previous chapter.

[3]www.feko.info, checked 6 February 2009.

This chapter begins with a description of the components that make up the target antenna array. Important characteristics of each of the components are noted and their configuration making up the receiver system is also discussed.

Thereafter, aspects concerning the measurement of the antenna array are dealt with. To begin with, a brief description of important measurement preliminaries are given. Namely, the setup of equipment as well as the proposed measurement procedure are described. Following the measurement procedure the measured pattern is presented and observations made.

The final results of this chapter suggest that Schelkunoff's Unit Circle Method is an effective technique for the purpose of null placement. Furthermore, this coupled with the good agreement of the simulated and measured patterns confirms that the application of Schelkunoff Method in Chapter 4 yields a physically realisable pattern.

The measured pattern was used as the receiver pattern within the performance prediction model. The results suggested a relatively similar decrease in expected coverage in terms of radar detection range, for an SNR of 15 dB. The decrease was slight from the results seen in Chapter 4, yet as s expected due to the slight discrepancy in the main lobe of the gain pattern. However, good coverage comparable to existing experimental systems was still predicted.

Chapter 6 and **Chapter 7** will provide and discuss the conclusion and future work of this dissertation respectively.

Chapter 2

Transmitter and Signal Environment Investigation of the Western Cape

Before the development of any PCL system, a good knowledge of the available transmitters and signals of the specified region is required. As such, a preliminary study into the properties of the broadcast transmitters and signals of the Western Cape, with the effects of the environment taken into account, was done and is presented here.

The purpose of this chapter is to identify and characterise the broadcast transmitters and their associated signals so as to determine the feasibility for their use as illuminators of opportunity. Consequently, a list of potential illuminating transmitters will be formulated and critically discussed. In particular, one transmitter is sought for the later application and investigation of an improved performance prediction method proposed in this dissertation and introduced in Chapter 3. In addition to this, the work presented in this chapter will lend itself well to the ultimate goal of implementing a PCL receiver at the University of Cape Town (UCT) in the future.

This chapter begins with a review of some important environmental effects. Thereafter, the EM propagation modelling tools, APM and AREPS, are introduced and discussed. A central topic of this chapter and indeed this dissertation will be the use of APM and AREPS to allow accurate modelling of EM waves propagating within the environment of the Western Cape. Next, the signal and transmitter properties of possible illuminators of opportunity are studied. This will involve comparing and discussing, the signal strength received at UCT, for the free space, measured and simulated case before the final conclusion of this chapter.

2.1 Environmental Effects on Propagating Waves

A propagating wave is subject to a variety of environmental effects that can alter its amplitude and phase [26]. These propagation effects generally result in a reduction of the received signal power, and thus limit the possible coverage range. This section serves as brief review and discussion of some important effects. The book by Barton [3] gives a good concise overview of the effect of the environment on a propagating wave and forms the basis of this section. The environmental effects of interest in this dissertation include:

- Multipath
- Diffraction
- Refraction
- Atmospheric absorption

2.1.1 Multipath

Multipath interference, is the most important non-free-space effect and can result in very considerable increase or decrease of the radar detection range compared with the free-space range [19]. The multipath effect is the modification of the expected free-space field at a particular point in space and is the result of a reflection of the propagating waves beneath the direct path [3]. The distances travelled to a particular point in space by the two waves (direct and ground reflection) are not equal and thus result in a phase difference. It is this phase difference that is primarily responsible for the multipath effect [19]. Additional phase difference is contributed by the reflection coefficient of the reflecting surface [19]. A list of different surface conditions is given in Barton [3]. The phase difference will cause the two waves to add constructively or in the usual case destructively.

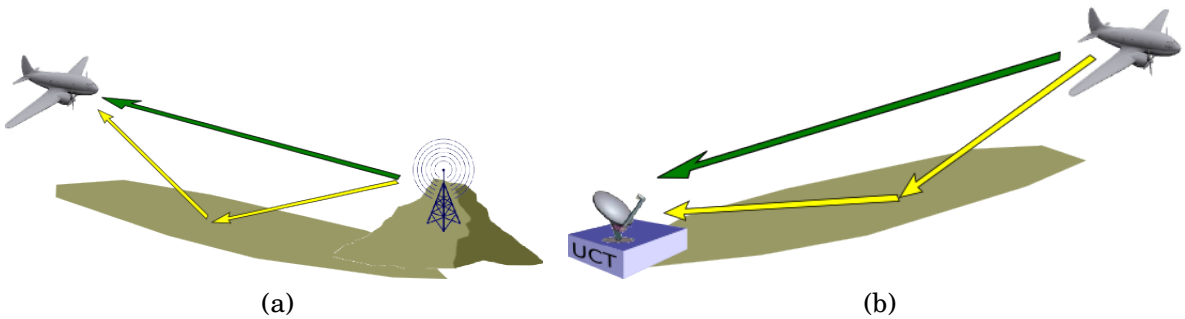

Figure 2.1: Direct propagation path and ground reflection path illustrating multipath effect between transmitter and receiver [26].

Figure 2.1 illustrates the basic concept of multipath for the transmitter-to-target (a) and target-to-receiver paths (b), for the illuminating and reflected wave respectively. These paths will not be the same, namely the propagating waves will travel over different terrain, and thus will possess different multipath effects. Furthermore, the multipath effect will continually change for a different target positions.

2.1.2 Diffraction

In terms of diffraction, energy tends to follow along the curved surface of an object, such as the earth. Namely, diffraction is the process by which the direction of the propagating wave is changed so that it spreads into the geometric shadow regions of an opaque obstacle or beyond the optical horizon of the earth. The ability of the propagating wave to do so is highly dependent upon frequency [27].

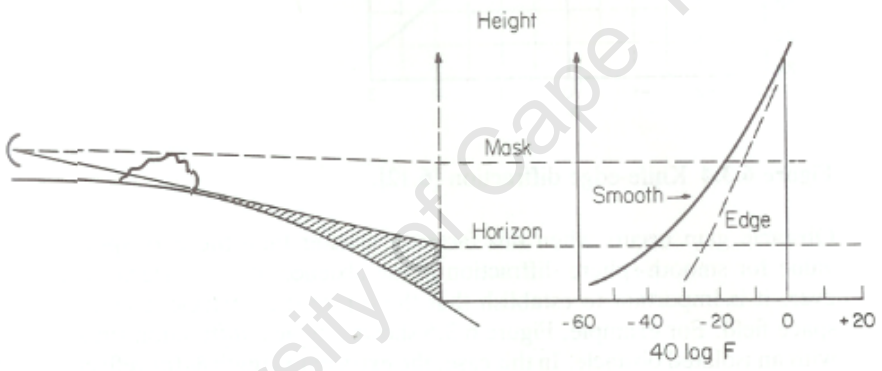

Figure 2.2: Comparison of diffraction effects [3].

Knife-edge diffraction is a special case where the diffraction is more pronounced, as a consequence of obstacles projecting well above the surface, as in the case of mountains and ridges. As illustrated in Figure 2.2, these will establish a horizon at a masking angle above that established by a smooth sphere. Below the mask angle, the factor F (described in Section 2.2), drops to zero more slowly than for the smooth sphere, enabling some radars to detect targets in shadow regions [3].

This capability, which is better for longer wavelengths has been exploited in existing radars and communication systems as *obstacle gain* [3], but is not an improvement to line-of-sight (LOS) propagation. The effect of knife-edge diffraction is of particular importance in the Western Cape, due to its mountainous terrain.

2.1.3 Refraction

The term refraction refers to the property of a medium to bend an electromagnetic wave as it passes through the medium [27]. Atmospheric refraction causes radar waves passing through the earth's atmosphere to bend downward, as seen in Figure 2.3, due to the changing refractive index of the troposphere and then by the ionosphere. In terms of radar this produces an error in the elevation angle, the ray having a somewhat larger angle than the direct geometrical path to the target [3].

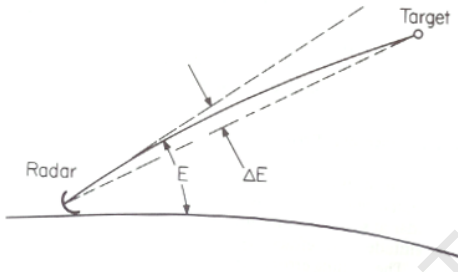

Figure 2.3: Ray path through the atmosphere [3].

For the troposphere which extends up to around 12 km [27], the usual region for most aircraft (commercial and military), three effects must be considered [3]:

Regular Refraction The gradual reduction in refractive index with altitude and causing elevation and range bias errors.

Tropospheric Fluctuations Random variations in the local refractive index and the cause of slow varying errors in all measured coordinates.

Ducting The result of steep gradients - usually found near the surface - in refractive index, creating low-loss propagation paths to low-altitude targets.

2.1.4 Atmospheric Absorption

Atmospheric attenuation or absorption is almost negligible at the lowest radar frequencies. It becomes more significant in the microwave bands and imposes severe limits on radar operation in the millimetre-wave bands [3]. For the application of FM based PCL radar, the attenuation rate in clear atmosphere is less than 0.012 dB/km and does not increase by much in the case of heavy rainfall (100mm/hr).

2.2 Propagation Loss Modelling Tools - AREPS and APM

The Advanced Propagation Model is a hybrid ray optics and parabolic equation propagation model, applicable to a range of frequencies from 2 MHz to 57 GHz. APM is the propagation model used within AREPS [27]. The goal in development of APM was to create an all-encompassing propagation model for the incorporation into the U.S. military's electromagnetic performance assessment systems. In addition to its use by the U.S. military and other U.S. government agencies, APM and AREPS are well-proven [28] and widely used by academic institutions and foreign agencies across the world [29].

The advantageous feature of the APM and AREPS software is their ability to compute the propagation factor, which is defined as the ratio of actual electric field strength created at a point in space to the field strength that would have been created by the same system operating in free space, with the beam of the transmitter directed towards the point in question [27, 3]. This ratio is represented by,

$$F = \frac{|E|}{|E_0|} \tag{2.1}$$

where $|E_0|$ is the magnitude of the electric field under free-space conditions, and $|E|$ is the magnitude of the field to be investigated at the same point.

The propagation factor, F, accounts for factors such as sea-surface reflectivity, atmospheric absorption and refraction, diffraction and multipath effects caused by terrain (discussed in the previous section). This factor is a useful quantity as it is an identifiable parameter in most radar range equations [27, 3, 7, 19]. The total real propagation loss would be found by combining the propagation factor, F, with the free space path loss, L_{fs}, as given by,

$$L = L_{fs} - 20\log_{10}(F) \tag{2.2}$$

By default, AREPS accepts the digital terrain elevation data (DTED) format. This elevation format was derived [1] from height maps obtained from the SRTM90 [2] database. The terrain data in used in this dissertation DTED level 1 format and corresponds roughly to 100 m of horizontal resolution.

Figure 2.4 shows the output given by AREPS. Shown is the propagation loss computed over a specified height and range for a particular azimuth bearing. In this case the height and range limits are 5000 m and 126 km respectively with the propagation path specified in the direction of the Menzies building at

[1] The conversion process is detailed in Appendix A

[2] http://srtm.csi.cgiar.org/, checked 27 July 2008

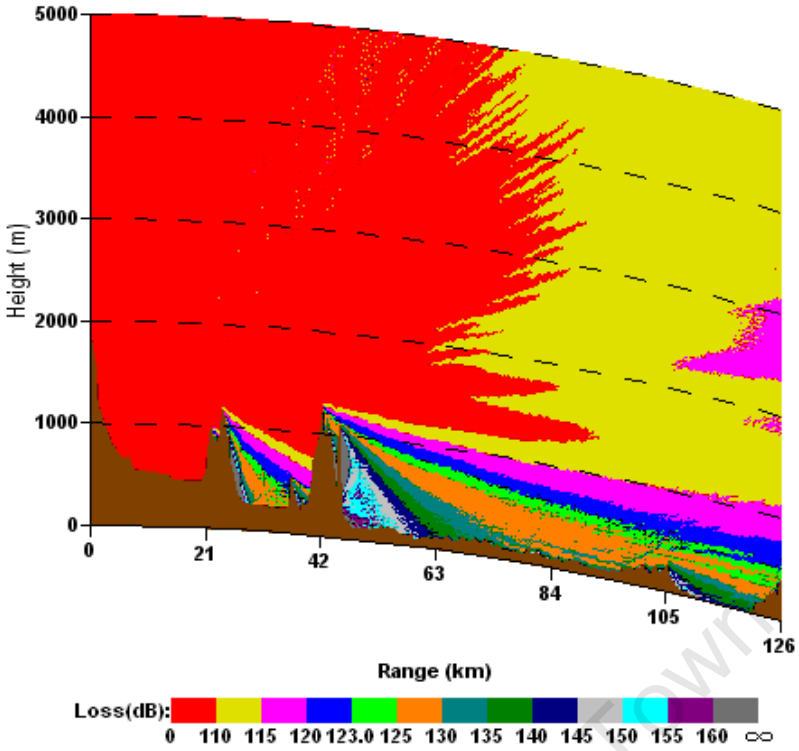

Figure 2.4: AREPS propagation loss over range and height above sea level in a particular azimuth direction.

UCT. In this figure the effects of knife-edge diffraction as discussed in Section 2.2 can clearly be seen.

Thus, given relevant regional terrain and atmospheric data AREPS and APM provide an effective tool to accurately compute the propagation loss associated with ones region of interest.

2.3 Properties of an Illuminator of Opportunity

There are numerous properties to consider when choosing an illuminator of opportunity. For instance, the transmitters are non-cooperative and as such their parameters such as location, power, signal waveform and beamwidth cannot be altered. In this section, signals that offer potential for use in a PCL radar system are investigated. Thereafter, properties of the illuminating transmitters emitting suitable signals are considered. The parameters of these transmitters stationed throughout the Cape region were kindly provided by Sentech [30] but can also be found in [6].

2.3.1 Signal Properties

The rapid growth in RF emissions for television (TV) and radio broadcasts as well as terrestrial (mobile and fixed) communications and space-based com-

munications, has resulted in in a wide range of signal types being available for exploitation by passive radar. Furthermore, many such transmissions are at VHF and UHF frequencies. This allows these parts of the spectrum not normally available for radar use, and at which stealth treatment of targets may be less effective, to be used [1]. In particular, at frequencies below 1 GHz, the materials used for a stealth target are less effective and the shaping is less influential at reducing the RCS owing to comparable size of the signal wavelength to the target structures [21].

In this dissertation as in the majority of other research [1], the signal emissions of the commercial broadcast transmitters are of interest, due to their high powers, attractive locations and density of deployment. For instance, in the region surrounding Cape Town there are over 200 different TV and FM radio signals emanating from 25 known broadcast transmitters.

Table 2.1: Frequency assignments in South Africa [6].

Broadcasts	Frequency Band [MHz]	Band Number	Number of Channels	Channel Width
VHF/FM Sound	87.5-108	Band II	204	100 kHz
VHF Television	174-238 and 246-254	Band III	9	8 MHz
UHF Television	470-854	Band IV and V	48	8 MHz

The Independent Communications Authority of South Africa (ICASA)[3] facilitates and controls frequency assignments within South Africa. It has ensured that the frequency plans and levels of spectrum usage in South Africa are based on and are consistent with internationally accepted practises designated by the International Telecommunications Authority (ITU) [6]. As such the frequency bands assigned for FM radio and TV, given in Table 2.1, are similar to those found globally.

In terms of the signal waveform proposed for use throughout this dissertation, the FM radio emissions are chosen over the television emissions. Despite the appeal of the pulse-like waveform structure of TV emissions, it was found that the waveform is not suitable for radar usage in a conventional radar matched filtering approach [2] (Howland reporting on Griffiths [12]). In a TV based bistatic radar target location and tracking is possible but becomes a difficult task [1, 14]. In contrast, FM broadcast signals have properties that make them attractive radar waveforms [10] and are the most common signals used in PCL radars to-date [1].

As is shown in Table 2.1, a FM radio broadcast occupies 100 kHz of bandwidth. A 100 kHz signal would translate to a range resolution of 1500 m as given by the approximation $c/2B$ [2]. In reality, the actual bandwidth value de-

[3]Website: www.icasa.org.za

pends upon program content and audio volume. Consequently, the bandwidth and thus the performance of the radar are a function of time [1].

The typical 3 dB modulation bandwidth observed by Zoeller of Dynetics [10] for the music genres rock, pop and country is about 60 kHz. A modulation bandwidth of 55 kHz is in some cases said to be typical [1], which agrees relatively well with that of Zoeller. Furthermore, research has shown fast-tempo jazz to have a small bandwidth of about 24.4 kHz [1]. Typical values of FM radio bandwidth provide a usable yet somewhat mediocre range resolution between 1500 m and 2500 m. In the case of jazz the range resolution is about 6000 m which is relatively poor.

Figure 2.5 shows the measured FM signal bandwidth for the 5FM radio station emitted by the broadcast transmitter located on the Constantiaberg mountain overlooking Cape Town. The transmission content comprises primarily of rock and pop. As such, the 3 dB modulation bandwidth measured is about 60 kHz, which is in close agreement with that of Dynetics [10].

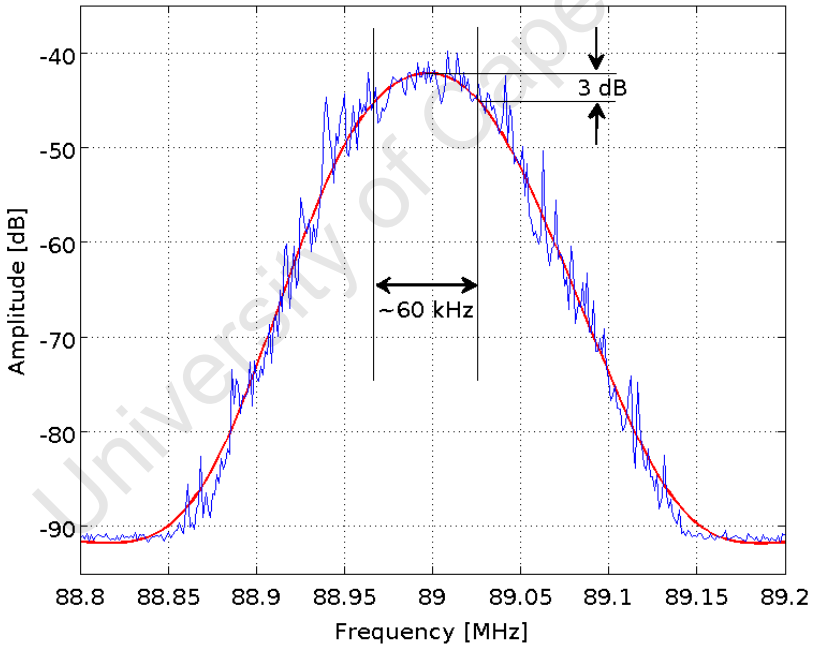

Figure 2.5: Measured FM signal bandwidth of the radio station 5FM at 89 MHz.

However, the suitability of a signal for target location is governed by more than its bandwidth. Of more importance is the ability of the radar receiver to unambiguously locate the target [2]. Commercial FM broadcast signals are generally said to be random phase-modulated waveforms [10] with noise-like characteristics [2]. As such, their ambiguity function is approximated by the ideal “thumbtack” ambiguity function, which is an attractive feature of using FM signals over TV [10].

This attractive feature is a result of the excellent Doppler accuracy achieved owing to the extended integration times possible with FM signals. In some cases Doppler can be two to three orders of magnitude more accurate than conventional microwave radar [2]. The Doppler resolution can be calculated by,

$$\delta f_d = \frac{1}{T_{int}} \tag{2.3}$$

where T_{int} is the integration time. A rule of thumb for the maximum value of the coherent processing integration interval is,

$$T_{MAX} = \left(\frac{\lambda}{A_R}\right)^{1/2} \tag{2.4}$$

where A_R is the radial component of the target acceleration [1]. For instance, in the case of a commercial aircraft possessing low acceleration, an integration time of 1 second would be reasonable. This coherent processing integration interval also provides a processing gain [1] governed by,

$$G_p = T_{MAX} B \tag{2.5}$$

and together with a signal bandwidth B of 60 kHz, as shown in Figure 2.5, would provide a processing gain of 48 dB.

The limits on the range and Doppler resolutions can be evaluated by measuring the transmitted waveform and computing the 'self-ambiguity', a method covered in the book edited by Cherniakov [1]. The range and Doppler resolutions are initially computed by matched filtering the directly received transmitter signal. It is called the 'self-ambiguity function' as the relative positions of the target, transmitter and receiver are not taken into account. The 'self-ambiguity' enables the best achievable range and Doppler resolutions to be evaluated and the time-varying properties to be investigated. This method is currently being used by a colleague to further characterise the transmitters and signal waveforms of the Cape region.

Lastly, a practical issue concerning the Western Cape region is that of duplicate carrier frequencies. The region requires that there be more lower power transmitters to fill the various gaps in the coverage caused by the mountainous terrain as apposed to few high power transmitters for regions of flatter terrain. Consequently, out of the seemingly many available frequencies, as shown in Figure 2.6, only a select few are useful for the application of a PCL radar system. Using a frequency of which there is a duplicate in the vicinity can cause mutual interference.

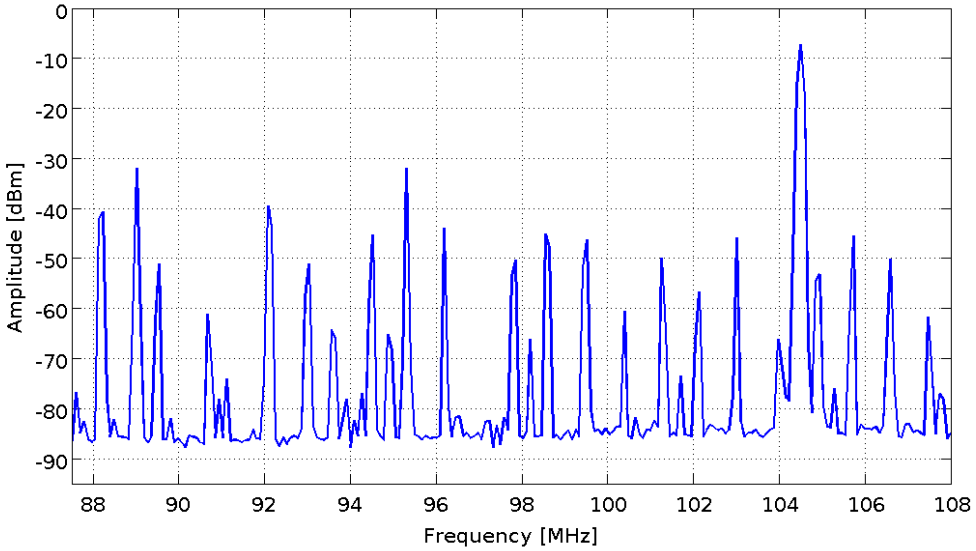

Figure 2.6: Spectrum of the FM broadcast signal band measured from UCT in Cape Town.

2.3.2 Transmitter Properties

Major factors that influence the choice of illuminating transmitter for an effective implementation of a PCL receiver located at UCT are specified below:

- Location of the transmitter.
- Flight Routes of commercial aircraft in the region.
- Effective radiated power (ERP) of the transmitter.
- Beamwidth of transmitting antenna.
- Line-of-Sight between transmitter and PCL receiver.
- Geometry for bistatic Doppler.

Aside from the signal waveform requirements and properties, the choice of an illuminator of opportunity can become a convoluted process as it depends on the combination and interaction of all the factors listed above. For instance, the location of the transmitter would certainly have an effect on the line-of-sight to the receiver and the target.

In this dissertation, the focus will be on the potential detection of commercial aircraft (the targets) en route with the Cape Town International (CPT INTL) Airport for the possible purpose of ATC. For this reason, common flight routes, of aircraft within the Western Cape, are important. As a further example of the interdependency's of the aforementioned factors, the illuminating transmitters are required to possess reasonable coverage of these routes.

Transmitter Locations

Taking into consideration the discussion of signal waveforms in Section 2.3.1 above and disregarding transmitters of lower transmit power, 6 transmitters were identified as having potential for use as illuminating transmitters. Figure 2.7 shows the locations of the transmitters, more or less uniformly spaced, within the Cape region; it also shows the locations of the CPT INTL Airport and UCT - the proposed site of the PCL receiver. The distances and bearings to these locations as measured from the receiver site at UCT are given in Table 2.2.

The geographical projection used in Figure 2.7 is Universal Transverse Mercator (UTM) and will be used throughout this dissertation. The UTM system divides the earth into 60 zones, each 6 degrees of longitude wide. A square grid is superimposed on each zone and aligned so that the vertical grid lines are parallel to the central meridian. The grid used in this projection is metric and can be assumed to be Cartesian within each zone, where each zone is never more than 674 km wide. The fact that projection can be assumed Cartesian makes range and bearing calculations simpler.

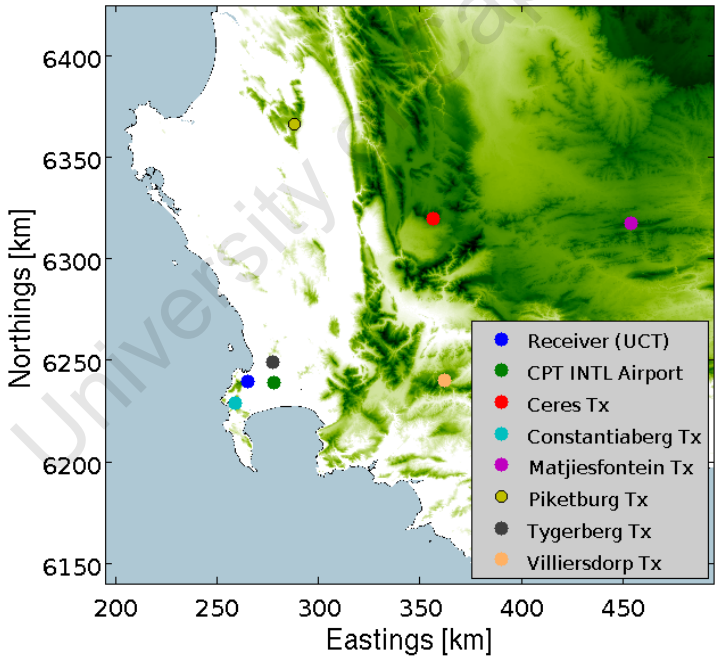

Figure 2.7: Location of the PCL receiver and airport as well as the locations potential illuminators of opportunity within the Western Cape.

Correct siting of the PCL receiver is critical to system performance [10]. Thus, the proposed siting of a PCL receiver on the roof of the Menzies building at UCT was not without consideration. The site, while convenient, has good elevation in addition to a wide field of view in an easterly direction. Furthermore, this field of view contains the location of the airport as well as the major domestic flight paths (as shown in Figure 2.8). Inversely, given a PCL

receiver siting, the selection of an illuminating transmitter, with consideration towards its location, is equally important.

Table 2.2: Distances and Bearings from UCT to the Airport and Potential Illuminating Transmitters.

Location Name	Distance [km]	Bearing Referenced to True North [°]
Airport	12.8	92.4
Constantiaberg	12.6	210.8
Ceres	121.3	48.7
Matjiesfontein	204.1	67.6
Piketberg	129.0	10.3
Tygerberg	15.6	52.3
Villiersdorp	96.8	89.6

Flight Routes of Commercial Aircraft

Figure 2.8 shows the major flight routes of aircraft en route with CPT INTL Airport. Other flight routes, in the northerly and westerly directions, exist but are used mostly by international flights and thus less frequently. Of interest, and shown in Figure 2.8, are the major domestic flight paths of aircraft arriving and departing at CPT INTL Airport.

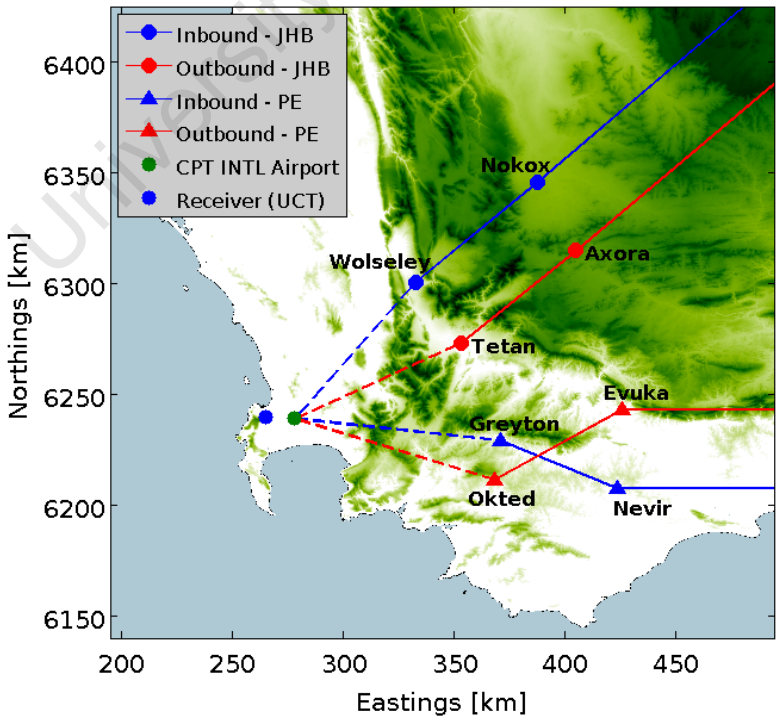

Figure 2.8: Flight paths of aircraft during approach and departure from Cape Town International Airport.

Two major routes in and out of the Cape Town airspace were identified using aeronautical charts [31]. These are in the general directions of Johannesburg (JHB) and Port Elizabeth (PE) and can be seen in the figure, where the inbound and outbound air traffic for both the JHB and PE routes are blue and red respectively. The routes are designated with waypoints where the circular markers in the figure indicate the JHB routes and the triangular markers the PE routes.

The dashed lines indicate the fact that aircraft will be under approach control for that distance. For instance, an aircraft inbound from JHB will pass directly over the two waypoints (Nokox and Wolseley) illustrated by the blue markers; after passing over the second waypoint the control tower of the airport will assign the incoming aircraft a specific runway and approach path. Similarly, outbound aircraft will be given instructions as on how to reach their first waypoint. The path taken by aircraft over distance indicated by the dashed line will vary with every aircraft approach and departure.

Effective Radiated Power of the Transmitters

As was mentioned in Section 2.3.1, the mountainous terrain - clearly visible in Figures 2.7 and 2.8 - has led to the necessity for multiple transmitters located in a fashion to cover the greatest area. This may be advantageous for a multistatic or netted radar configuration, however, it has the consequence that the signals emitted from these transmitter are of relatively lower power than those that would have been emitted across regions of more level terrain. The transmit powers are lowered, in this case, in order to avoid mutual interference between closely spaced stations operating on the same frequency [6].

Table 2.3 shows some parameters of the 6 potential illuminators of opportunity identified. These 6 transmitters possess the highest effective radiated power (ERP) out of all the transmitters in the Cape region and are relatively similar in terms of ERP level, with the possible exception of the Tygerberg transmitter.

Antenna Beamwidth

With the ERP known, the interaction between the factors antenna beamwidth and flight paths of commercial aircraft is of interest. Since the focus of here is on ATC, of particular interest is a transmitter that illuminates the airspace around the airport as well as the various designated flight corridors.

The values for antenna beamwidth are given in Table 2.3 and illustrated with the common flight routes in Figure 2.9.

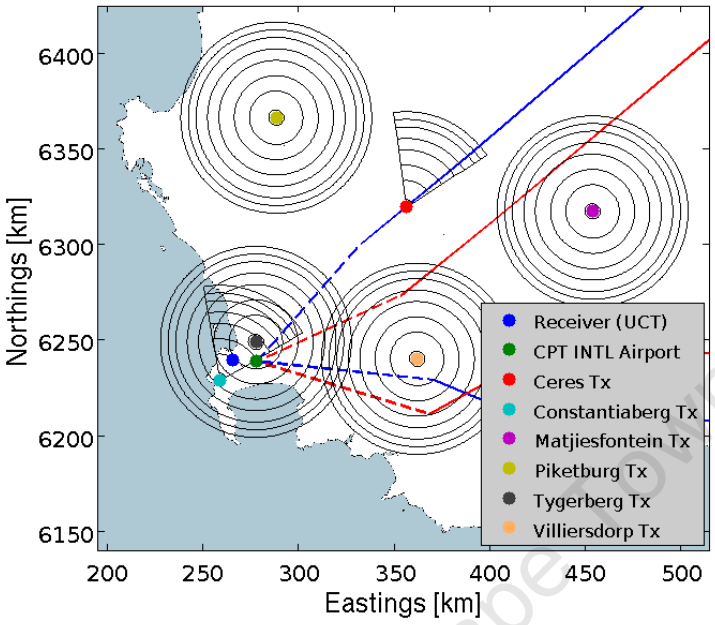

(a)

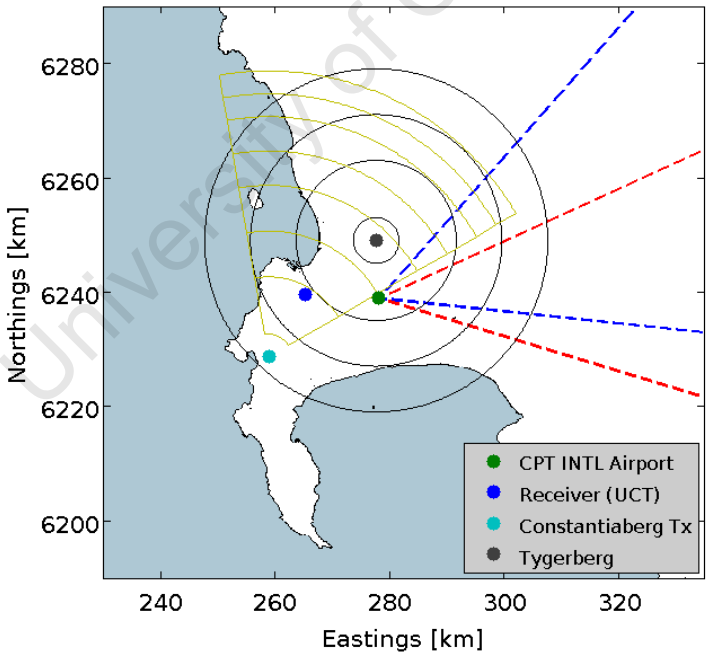

(b)

Figure 2.9: Beamwidth and transmitter power output for potential illuminators of opportunity within the Western Cape.

Table 2.3: Transmitter beamwidth, power and gain for potential illuminators of opportunity.

Number	Transmitter Name	Power [dBm]	Antenna Gain [dBm]	ERP [dBm]	Antenna Beam	
					Direction [°]	Width [°]
1	Constantiaberg	60	10	70	25	70
2	Ceres	57	16	73	25	65
3	Matjiesfontein	60	10	70	0	360
4	Piketberg	60	10	70	0	360
5	Tygerberg	57	4	61	0	360
6	Villiersdorp	60	10	70	0	360

Figure 2.9 (a) shows that in addition to being far away (Table 2.2), the Piketberg, Ceres and Matjiesfontein transmitters possess minimal coverage of the major flight routes of interest. A good coverage of the PE flight routes as well as a reasonable coverage of the JHB flight routes is shown for the Villiersdorp transmitter.

An enlargement of the area around the receiver is given in Figure 2.9 (b). This figure also illustrates the specified antenna beamwidths of the Constantiaberg and Tygerberg transmitters. The Constantiaberg transmitter has a directive beam which covers mostly inbound JHB air traffic. The Tygerberg transmitter, however, with its omnidirectional radiation pattern, offers the best coverage of the airspace surrounding the CPT INTL Airport.

Regardless of the airspace coverage, both transmitters are in close proximity to the PCL receiver, which may be cause for concern in terms of direct path interference. The detrimental effects caused by the DPI could potentially be reduced by terrain obstructing the line-of-sight between the transmitter and receiver and is dealt with next.

Line-of-Sight

The issue of line-of-sight relates back to the choice of transmitter (and receiver) location. By choosing a illuminating transmitter which is located just over the horizon or behind elevated ground, a situation may be achieved where the direct signal is somewhat reduced. This will reduce the detrimental effects caused by the DPI, however, the direct signal must be strong enough to be measured by the reference antenna for correlation purposes, where the reference antenna is usually in close proximity with the target antenna array. The propagation path of the echo signal should not be obstructed, namely the signal paths from the transmitter to the target followed by the reflected signal path from target to the receiver should line-of-sight as much as possible.

From the previous sections, Tygerberg and Villiersdorp transmitters offered

the best coverage of the flight corridors and possessed good ERP values. The terrain profiles from these two transmitters to the PCL receiver located at UCT are given in Figure 2.10.

A significant difference in the terrain between the transmitter and receiver for both cases is apparent. It is clearly seen that the Tygerberg transmitter is in full view of the PCL receiver as well as in close proximity (15.6 km). To suppress DPI from the Tygerberg transmitter would require a very deep null in the direction of that transmitter.

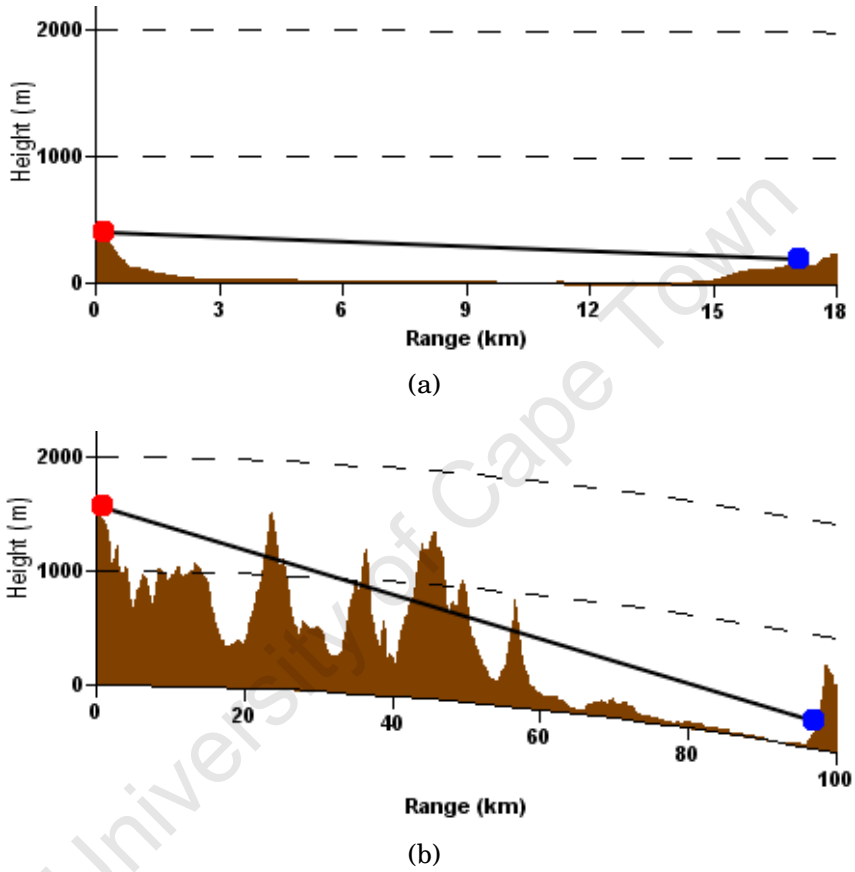

Figure 2.10: Terrain profiles between the receiver site at UCT and the (a) Tygerberg and (b) Villiersdorp transmitters.

In contrast, the Villiersdorp transmitter is not line-of-sight with the PCL receiver and is also a further distance of 96.8 km. Using this transmitter as illuminator of opportunity could offer some advantageous characteristics in terms of DPI reduction using obstructing terrain.

Geometry for bistatic Doppler

Knowing the flight routes taken by the aircraft allows for an estimation of the expected Doppler. Doppler is an effect seen on the signal itself, but is discussed here since it is inherently dependent on the choice of the illuminating transmitter and the resulting PCL system geometry.

Here, the Doppler expected as a result of using the Villiersdorp and Tygerberg transmitters for an aircraft flying the JHB and PE routes is investigated. The Doppler shift of such an aircraft is governed by,

$$f_d = \frac{v}{\lambda}\left(\cos\theta_1 + \cos\theta_2\right) \tag{2.6}$$

where v is the velocity, λ is the signal wavelength and the angles θ_1 and θ_2 are shown in Figure 2.11 as derived from [7].

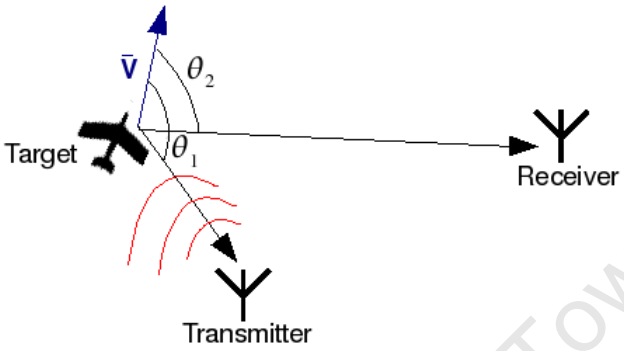

Figure 2.11: Geometry of Bistatic Doppler.

Figures 2.12 and 2.13 show the estimated Doppler, normalised by the factor (v/λ), of flights en route with Johannesburg and Port Elizabeth respectively. It is apparent from these figures that the Tygerberg transmitter exhibits the best Doppler properties over all flight routes.

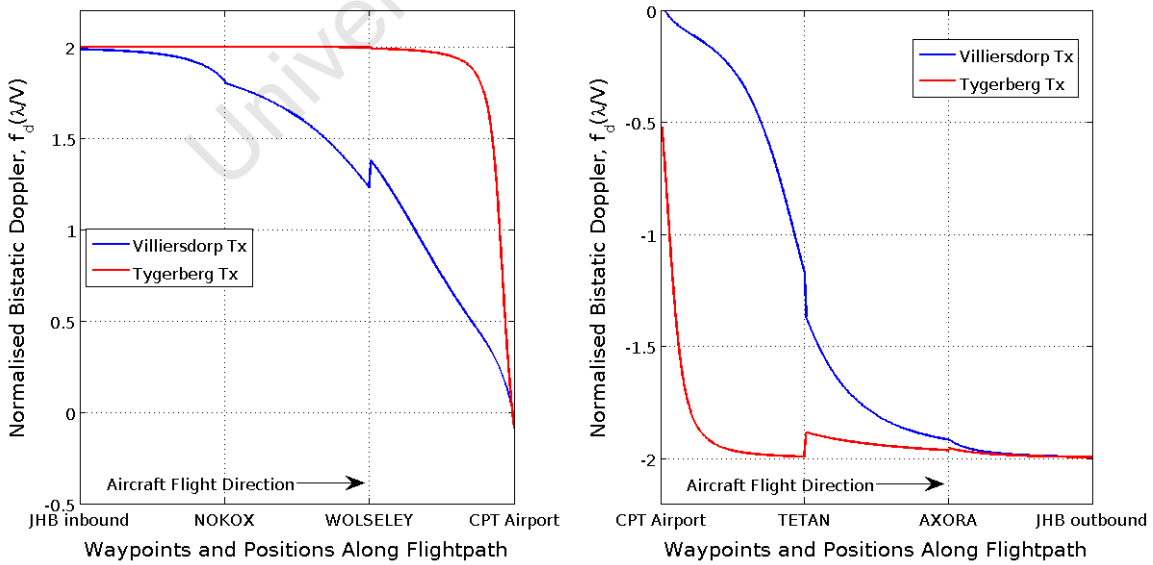

(a) Inbound (b) Outbound

Figure 2.12: Normalised Doppler estimation for (a) inbound and (b) outbound flights en route with JHB.

The Villiersdorp transmitter falls short as the aircraft near the airport. For

aircraft travelling further away from the airport, however, the expected Doppler as a result from using the Villiersdorp transmitter becomes comparable with that of the Tygerberg transmitter. An example of this can be seen in Figure 2.13 (a), where the Doppler of an aircraft inbound from PE is almost identical for both the Tygerberg and Villiersdorp transmitters up until the Greyton Waypoint. Thereafter, as the aircraft nears the airport the the Villiersdorp Doppler falls to zero - a consequence of flying near and parallel to the bistatic baseline.

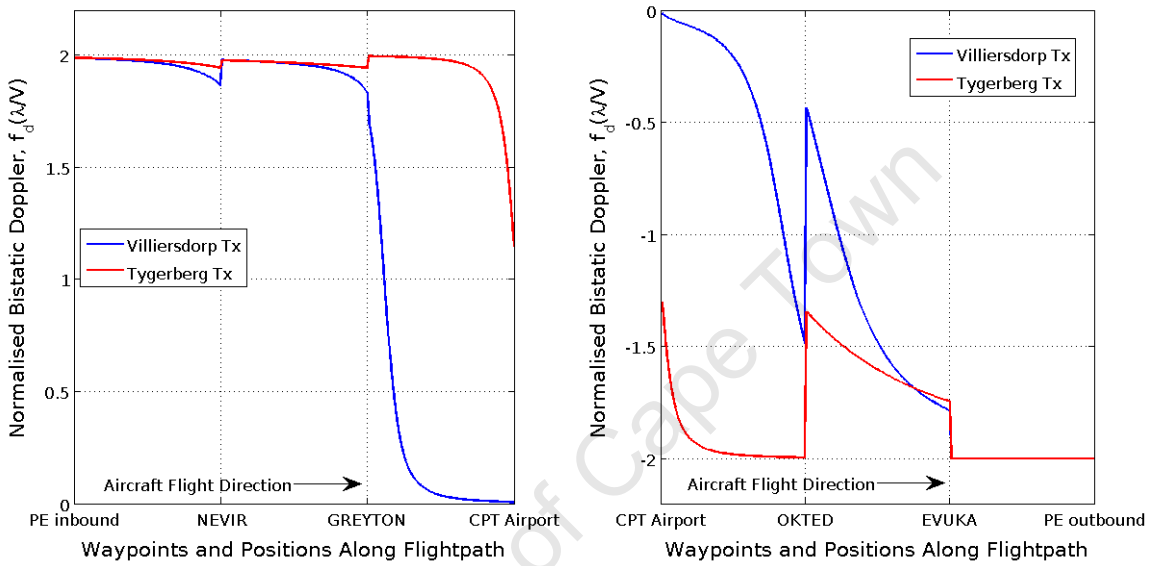

(a) Inbound (b) Outbound

Figure 2.13: Normalised Doppler estimation for (a) inbound and (b) outbound flights en route with PE.

As was mentioned above, aircraft are under approach control near the airport. This will vary the flight paths and subsequently the estimated Doppler of aircraft in close vicinity to the airport. Namely, this has the consequence that the Doppler due to the Villiersdorp transmitter may indeed improve for specific aircraft approach and departure paths.

2.4 Expected Signal Strength

In the preceding section the Tygerberg and Villiersdorp transmitters were identified as potential illuminators of opportunity for a PCL receiver located at UCT. In this section the expected signal strengths of two FM radio stations, one for each transmitter, are investigated. This will be done to illustrate the significant effect the environment - especially terrain - has on the received signal strength and in so doing, reinforce the requirement for AREPS and APM to accurately model realistic propagation loss.

Parameters specific to each transmitter are listed in Table 2.4.

Table 2.4: Parameters of the Villiersdorp and Tygerberg transmitters.

Transmitter Parameters	Transmitter	
	Tygerberg	Villiersdorp
ERP [dBm]	61	70
Frequency f_0 [MHz]	88.2	96.5
Radio Transmission Name	5FM Radio	FM Radio
Polarisation	Vertical	Vertical
Distance to Receiver R [km]	15.6	96.8

These parameters together with the receiver gain, G_r, can be used to predict the signal strength received under free space conditions with the use of the well-know Friis equation (2.7). In addition, by replacing the last term of equation (2.7) with the propagation loss computed by AREPS, the realistic signal strength received at UCT can be determined.

$$P_r(dB) = G_r(dB) + P_t(dB) + 10\log\left(\frac{\lambda^2}{4\pi}\right) - 10\log\left(4\pi R^2\right) \tag{2.7}$$

Table 2.5 shows the different values of the signal strength received at UCT for a receiver gain, $G_r = 8\,$dB. In addition to the propagation loss and signal strength obtained for the free space and simulated cases shown in the table is the signal strength physically measured at UCT.

Table 2.5: Signal strength expected and received at UCT from the Tygerberg and Villiersdorp transmitters.

Transmitter Name	Free Space		Simulated (AREPS)		Measured
	Propagation Loss [dB]	Signal Strength [dBm]	Propagation Loss [dB]	Signal Strength [dBm]	Signal Strength [dBm]
Tygerberg	94.9	-26.2	91.9	-23.3	-33.7
Villiersdorp	110.7	-33.9	143.1	-66.3	-71.5

First we note the difference in the propagation loss for the free space and simulated cases, where this difference is known as propagation factor as discussed in Section 2.2 and given in equation (2.2). For the Tygerberg transmitter, the propagation factor is $+3$ dB and for the Villiersdorp this factor is $-32.4\,$dB. This difference in propagation factor is significant and illustrates major effect that the environment can have on a propagating signal. In the case of the Villiersdorp transmitter the large 32.4 dB discrepancy is due to the severe obstruction of LOS illustrated in Figure 2.10 (b).

A discrepancy is apparent between the simulated and measured signal strengths for both transmitters. In both cases the measured signal is less than the

expected due to simulation. The discrepancy is 5.2 dB for Villiersdorp and 10.4 dB for Tygerberg. The discrepancy can in part be attributed to system losses incurred in the measurement equipment (antenna, transmission line and connectors). These losses were not factored into equation (2.7). The differences between the two discrepancies points towards a small variable error in the AREPS model and is expected since the AREPS model is itself based on model of terrain and atmosphere.

However, this error is deemed acceptable since it is small compared to the significant variation of the propagation factor, modelled by AREPS, for changing environments. This is clearly seen for the case of the Tygerberg transmitter and justifies the use of AREPS as a EM wave propagation modelling tool in this dissertation. In addition, the advantage of using AREPS propagation loss over that of free space propagation loss is clear.

2.5 Conclusion

This chapter introduced and discussed a variety of environmental effects. Of the effects discussed, the effects of multipath, diffraction and shadowing, caused by varying terrain, on a propagating signal were identified as the most prominent.

A means to model these effects, with the use of the tools AREPS and APM, was presented. These tools will be used in later chapters to compute realistic propagation loss for the use within proposed performance prediction method.

After the discussion of detrimental environmental effects, the broadcast transmitters and their associated signals were investigated. Two broadcast transmitters exhibited good characteristics for use as illuminators of opportunity for the case where the PCL receiver is located at UCT. Out of these two transmitters, the Villiersdorp transmitter presented the best-case characteristics. It's location, which is out of line-of-sight due to some mountainous terrain, provided additional attenuation of the direct signal and thus additional suppression of the DPI. The signal is, however, still at a measurable level for the reference antenna. Further suppression of DPI in the target antenna could be achieved by steering a null in the direction of the transmitter.

After the investigation completed in this chapter, the Villiersdorp transmitter will be used to introduce the improved method of performance prediction proposed in Chapter 3. The method is designed to provide the user with a means to compare the effectiveness of potential illuminators of opportunity with relative speed and ease, by essentially automating the process undergone in this chapter.

Chapter 3

Bistatic PCL System Performance Prediction Method

In this chapter a method[1] of predicting bistatic PCL performance, while accounting for environmental effects, is presented. The performance prediction, in the form of spatial signal-to-noise ratio (SNR), signal-to-interference ratio (SIR) and also signal-to-noise-plus-interference ratio (SNIR) coverage maps, provide a visual means for determining radar detection range and required dynamic range of the receiver. Using this method, expected coverage at different altitudes with specified transmitter and receiver properties is determined and compared with the conventional prediction method calculated in free space, as described in Section 1.1.3. The method, which is essentially an extension to the work of Griffiths and Baker [22], provides the user with a means to compare the coverage of potential illuminators of opportunity quickly and easily.

The coverage maps produced here are based on an interpolation of propagation loss data generated by APM and AREPS. Namely, realistic propagation loss is utilised to predict the loss along any path from a transmitter to a target and onwards to a receiver. As discussed in the Section 2.1 and 2.2 this is achieved by taking into account the propagation factor, F, which is a quantity that commonly contains the effects of refraction, diffraction, multipath as well as atmospheric attenuation.

To model the loss from a moving target to a receiver is difficult, since radar coverage prediction requires this to be done for all possible target positions, to the receiver. By appealing to theorem of reciprocity, the target to receiver loss is modelled in the reverse direction. It is thus possible to map the two way loss to each pixel of the area being assessed in one set of calculations, the results of which can be held as a lookup table for simulation or coverage assessment. The method's accuracy will degrade slightly in the case of targets

[1] See Appendix B for detailed explanation on how to perform performance predictions.

lying in shadow regions subject to knife-edge diffraction.

This chapter begins by discussing the SNR, SIR and SNIR equations, derived from the well-known bistatic radar equation, for the purpose of coverage prediction. This is followed by a discussion of a conventional model of bistatic coverage, the ovals of Cassini. The Villiersdorp transmitter will be used, here, as a case study.

The proposed method of determining expected bistatic PCL radar coverage, while accounting for environmental effects, is then developed. Once again, the Villiersdorp transmitter will be used as a case study to illustrate the method. Observations are made and differences between the coverage maps produced by conventional methods and those produced by processing AREPS data are then discussed. Finally, some conclusion are drawn.

3.1 Representation of Bistatic Coverage

The detection range and required dynamic range of a bistatic radar can be represented by the spatial SNR, SIR and SNIR coverage maps.

The work here is based on the bistatic radar configuration illustrated in Figure 3.1. The three propagation paths; transmitter-to-receiver, transmitter-to-target and target-to-receiver are represented by the letters a, b and c respectively and will be used as subscripts to describe path-specific variables.

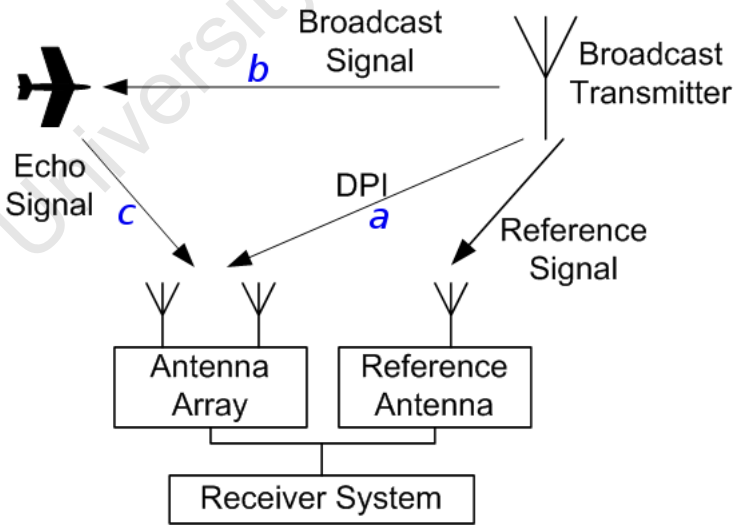

Figure 3.1: Bistatic Radar Configuration

As shown in Chapter 1, radar detection performance is best described by the probability of detection, P_d, and the probability of false alarm, P_{fa}. It can be shown that these two quantities define a minimum signal-to-noise ratio (SNR) [8]. Consequently, a more realistic detection range is determined by inserting the predicted propagation loss into the bistatic SNR radar equation.

The bistatic SNR equation is derived from the bistatic radar equation [7] and is given as,

$$SNR = \frac{P_R}{N_o} = \frac{P_T G_{Tb} G_{Rc} \lambda^2 \sigma_B \left(F_b F_c\right)^2}{k T_s B_n \left(4\pi\right)^3 \left(R_b R_c\right)^2} \tag{3.1}$$

Furthermore, one of the greatest limitations to a passive bistatic radar and especially PCL, is the interference of the direct signal (DPI) in the detection channel as discussed in Section 2.3.1 and 2.3.2. Plotting spatial maps of SIR and SNIR provides an effective means of determining the required dynamic range of ones receiver system. The bistatic SIR equation is represented by,

$$SIR = \frac{P_R}{P_D} = \frac{P_T G_{Tb} G_{Rc} \lambda^2 \sigma_B \left(F_b F_c\right)^2}{\left(4\pi\right)^3 \left(R_b R_c\right)^2} \frac{\left(4\pi R_a\right)^2}{P_T G_{Ta} G_{Ra} \lambda^2 F_a^2} = \frac{G_{Tb} G_{Rc} \sigma_B \left(F_b F_c\right)^2 R_a^2}{G_{Ta} G_{Ra} 4\pi F_a^2 \left(R_b R_c\right)^2} \tag{3.2}$$

The SNIR equation describes the power of the target echo signal received over the sum of the noise and interference and is given by the equation,

$$SNIR = \frac{P_R}{\left(N_0 + P_D\right)} = \frac{P_T G_{Tb} G_{Rc} \lambda^2 \sigma_B \left(F_b F_c\right)^2}{\left(4\pi\right)^3 \left(R_b R_c\right)^2 \left(k T_s B_n + \frac{P_T G_{Ta} G_{Ra} \lambda^2 F_a^2}{\left(4\pi R_a\right)^2}\right)} \tag{3.3}$$

Equations (3.1) through (3.3) share the common variables,

P_R	=	Bistatic power of target echo measured at the receiver
N_0	=	White Gaussian noise
P_D	=	Power of direct signal measured at the receiver
P_T	=	Transmitter power output
R_a, R_b , R_c	=	Range along paths a, b and c respectively
F_a, F_b, F_c	=	Propagation factor along paths a, b and c respectively
G_{Ta}, G_{Tb}	=	Transmit antenna gain along paths a and b respectively
G_{Ra}, G_{Rc}	=	Receiver antenna gain along paths a and c respectively
σ_B	=	Bistatic radar target cross section (RCS)
T_S	=	System noise temperature
B_n	=	Noise bandwidth
k	=	Boltzmann's constant $(1.38 \times 10^{-23\ J/K})$
λ	=	Wavelength.

It is evident that the values of the gains G, the propagation factors F and the ranges R corresponding to both path b and path c vary with target position.

Variations in target radar cross section as a function of angle of incidence and re-radiation are not considered in this work. Not only is there not very much data available in the way of multistatic radar cross section measurements, the value is very dependent on exact knowledge of the target aspect angle.

3.2 Conventional Coverage Prediction Model

Conventional performance predictions can be made by using the equations (3.1) through (3.3) and disregarding - setting to unity - the propagation factors, F. In the simple case, where omnidirectional antennas are employed at both the transmitter and receiver, the resulting coverage map will be in form of ovals of Cassini. These conventional predictions, based on computations done in free space result in ovals of Cassini because, in this case, the equations have the mathematical form $K/\left(R_b R_c\right)^2$, where K is the variable representing the remaining variables of constant value for each equation. Namely,

$$K_{SNR} = \frac{P_T G_{Tb} G_{Rc} \lambda^2 \sigma_B}{k T_s B_n \left(4\pi\right)^3} \tag{3.4}$$

$$K_{SIR} = \frac{G_{Tb} G_{Rc} \sigma_B R_a^2}{G_{Ta} G_{Ra} 4\pi} \tag{3.5}$$

$$K_{SNIR} = \frac{P_T G_{Tb} G_{Rc} \lambda^2 \sigma_B}{\left(4\pi\right)^3 \left(k T_s B_n + \frac{P_T G_{Ta} G_{Ra} \lambda^2}{\left(4\pi R_a\right)^2}\right)} \tag{3.6}$$

The model can be improved by adding the antenna patterns to the calculation, without too much difficulty. This section is very similar to the work done by Griffiths, Baker and Howland [22, 2, 1], reviewed in Section 1.1.3, with the Figures 1.3 and 1.4 illustrating their work.

As a case study, real transmitter and receiver parameters are applied here, to represent a hypothetical PCL system. The transmitter used, is the Villiersdorp transmitter, discussed in the previous chapter. Its important parameters are summarised in Table 3.1[2].

Table 3.1: Parameters of the Villiersdorp transmitter.

Transmitter Power Output [dBm]	60
Frequency [MHz]	96.5
Radio transmission name	KFM
Polarisation	Vertical
Transmit antenna 3 dB beamwidth [°]	360
Transmit antenna gain $[dB]$	10
Distance from UCT receiver$[km]$	96.8
Bearing from UCT receiver [°]	89.6

The receiver, located at UCT, has a hypothetical omnidirectional receive antenna with a gain of $5\,$dB in the azimuth plane over an isotropic antenna. This would represent a directive dipole (or vertical collinear array of dipoles) creating the classic do-nut radiation pattern focusing its energy towards the

[2]See Appendix C.1.1 and Table C.1 for the complete set of configuration parameters used.

horizon. This is a simplified version of the antenna system that is planned, and discussed further in Chapter 4. In this case, both the transmit and receive antennas are omnidirectional, resulting in $G_{Ra} = G_{Rc} = 5\,\text{dB}$ and $G_{Ta} = G_{Tb} = 10\,\text{dB}$.

The bistatic RCS, σ_B, is considered isotropic and is set to $10\,\text{m}^2$ to represent a large commercial aircraft and the propagation factor, F, is set to unity. The noise bandwidth, B_n, is set to $1\,\text{Hz}$ to simulate an integration time of 1 second, which is based in turn on equation (2.4).

The factor kT_s is 4.002×10^{-19} W/Hz, where T_s is the sum of the antenna noise temperature and the equivalent noise temperature of the receiver, namely $T_s = T_a + T_e$. Here, $T_a = 290\,\text{K}$ and $T_e = 28710\,\text{K}$, where T_e is the noise temperature of a receiver with a noise figure of $F_n = 20\,\text{dB}$.

Applying these values to equations (3.1) through (3.3) it becomes apparent that results from the SIR and SNIR equations are almost identical, namely

$$\begin{aligned} SNIR &\backsimeq SIR \\ \frac{P_R}{(N_0 + P_D)} &\backsimeq \frac{P_R}{P_D} \end{aligned} \tag{3.7}$$

Calculating the values $N_0 = 4.002 \times 10^{-19}\,\text{W}$ and $P_D = 2.054 \times 10^{-7}\,\text{W}$ it is clear that $N_0 \ll P_D$. In this case, the white Gaussian noise, N_0, is 12 orders of magnitude smaller than P_D, meaning it is -120 dB below P_D and thus has a negligible effect. This illustrates the severe effect that the direct signal has on PCL.

For the remainder of this dissertation, only SNR and SIR coverage maps will be considered. SIR coverage maps are chosen over SNIR maps, as it is felt that the SNIR maps in their current form do not provide any additional information.

The resulting ovals of Cassini, presented in Figures 3.2 and 3.3, show the predicted performance in terms of spatial SNR and SIR coverage maps for the hypothetical PCL system. The UTM geographical projection used here, allows the spatial coverage maps, also in Cartesian form, to be overlayed onto a metric UTM grid.

Figure 3.2 shows a spatial coverage map in terms of SNR. For a required SNR of 15 dB (see Section 1.1.3), this method predicts a detection range of up to 250 km as can be seen in the figure, which in the light of existing systems is somewhat optimistic.

Figure 3.3 shows a spatial coverage map of SIR and illustrates quite effectively, that for a reasonable detection range, the echo signal can be up to 90 to 100 dB below the direct signal. This is consistent with predictions done by Wan and Howland [24, 2].

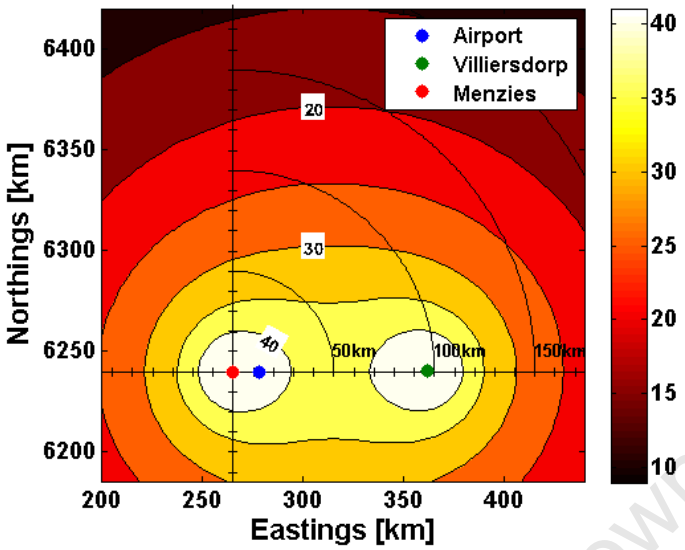

Figure 3.2: Conventional coverage prediction in terms of SNR in free space [dB].

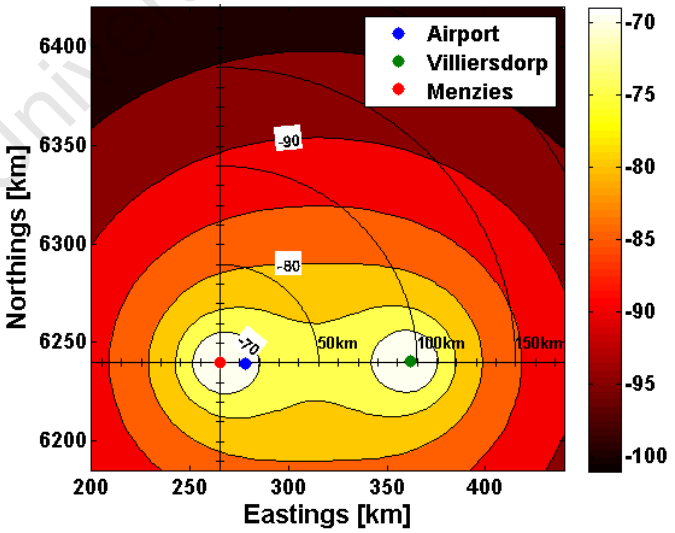

Figure 3.3: Conventional coverage prediction in terms of SIR in free space [dB].

It is evident that the coverage shown here is under ideal environmental circumstances, which does not mean it provides ideal results. The assumption that the propagation loss occurs in free space is a major limitation of the accuracy of this model. This particular limitation can be addressed by including the propagation factor, F, which accounts for the effects of the terrain and atmosphere, in the coverage computations.

3.3 Improved Coverage Prediction Model

An improved model for producing bistatic spatial SNR and SIR maps of predicted system performance by processing and interpolating realistic propagation loss data captured from APM and AREPS is presented here. This loss data includes the terrain and atmospheric effects, represented by the propagation factors, F, in equations (3.1) and (3.2).

3.3.1 Spatial Data Capture and Interpolation

In the general case, AREPS creates a height versus range propagation loss data set for a desired azimuth bearing [27] from a specific site. The propagation loss term that is extracted from this data set is solely dependent on the free-space propagation loss, $4\pi R^2$, and the propagation factor, F^2, and is given by,

$$L_{PL} = \frac{4\pi R^2}{F^2} \tag{3.8}$$

The propagation loss data extracted from AREPS is essentially 3D polar data, (r, ϕ, h). A cubic interpolation on this polar data, at an altitude of interest (h), is performed so as to achieve a regular grid of propagation loss data associated with one specific site, as illustrated in Figure 3.4. This interpolation is necessary so that propagation loss data from different sites can be combined over a common Cartesian grid. The combination of propagation loss data is important for the computation of the SNR and SIR coverage maps. Lastly, the resulting coverage maps, being in grid form, can easily be overlayed on a UTM grid as was done in Section 3.2.

More specifically, SNR coverage maps require the combination of the Cartesian propagation loss data for the two variable, target dependent paths (transmitter-to-target and target-to-receiver). In addition to the combined propagation loss along these two paths, SIR coverage maps must also factor in the propagation loss data for the unvarying transmitter-to-receiver path of a particular bistatic PCL system.

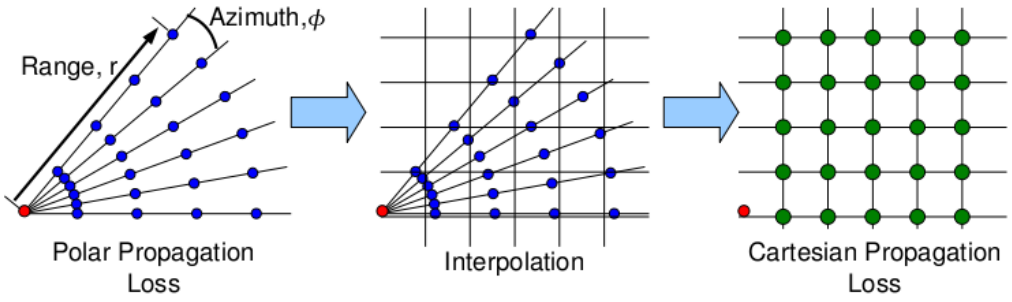

Figure 3.4: Illustration of Interpolation procedure at one particular height, h.

The procedure of capturing and interpolating the propagation loss data is best described by means of an example and thus the case study, involving the Villiersdorp transmitter as the illuminator of opportunity, introduced in Section 3.2, is also applied here.

Transmitter-to-Receiver Path (Path a)

Here the propagation loss as described by equation (3.8) along the path a is only necessary for the computation SIR coverage maps and resolved directly. Namely, L_{PL} at the exact position of receiver is found. In addition, the transmitter and receiver gains are included for the path under consideration. The complete transmitter-to-receiver path loss is governed by,

$$L_a = \frac{4\pi R_a^2}{F_a^2 G_{Ra} G_{Ta}} \tag{3.9}$$

This value does not vary with target position. Namely, L_a is a single, constant value for particular transmitter and receiver locations.

Transmitter-to-Target Path (Path b)

For this path, AREPS is used to calculate the propagation loss every 5° from $0^\circ - 355^\circ$ (72 bearings) for a range up to 300 km and an altitude up to 6000 m above mean sea level.

At this point, the altitude of interest is specified to be 1600 m to investigate the possible coverage of low flying aircraft and the effect of the terrain. Matlab is used to extract the AREPS propagation loss data represented by equation (3.8) for each bearing at the specified altitude.

The propagation loss data in this form is illustrated in Fig. 3.5 and shows 72 polar propagation loss data sets, one set for each bearing increment. Each data set contains propagation loss data at a finite number of range steps. The data in this form - before interpolation - can be likened to the leftmost

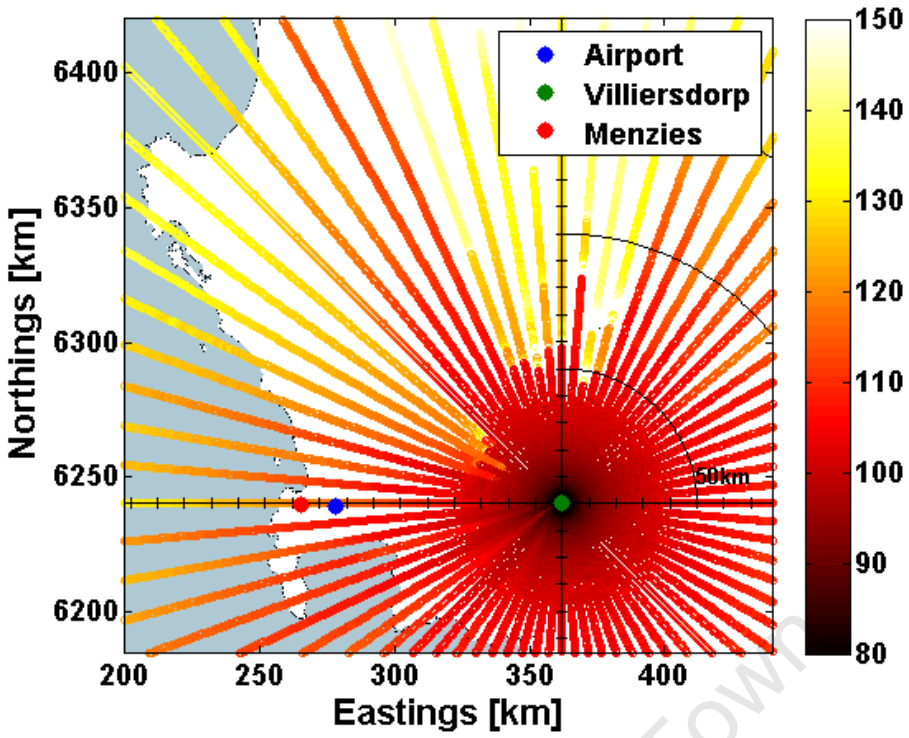

Figure 3.5: Polar propagation loss [dB] for the Villiersdorp transmitter at 1600m.

illustration in Figure 3.4. Gaps in the data are an indication of mountainous terrain at the specified altitude and range.

Every propagation loss data set is now weighted by the transmit antenna gain at the relevant azimuth bearings. In this case, the transmit antenna gain, G_{Tb}, is omnidirectional; thus the collective propagation loss data sets given by L_{PL} are decreased by 10 dB. The result is a loss term which represents the transmitter's combined polar propagation loss and gain and is given by $L_b(dB) = L_{PL}(dB) - G_{Tb}(dB)$, where L_b is the loss for the transmitter-to-target path (path b).

Next, a cubic interpolation is performed on the transmitter's combined polar propagation loss and gain data. This interpolation employs the Delaunay triangulation method and is done over a Cartesian grid encompassing the region of interest. The result is a grid of propagation loss data representing all possible transmitter-to-target paths within the region of interest. The loss data and transmitter-to-target paths are governed by the equation,

$$L_b = \frac{4\pi R_b^2}{F_b^2 G_{Tb}} \tag{3.10}$$

The points of the Cartesian grid are referenced to a UTM grid at was done in Section 3.2.

Target-to-Receiver (Path c)

Here it is assumed that the paths of propagation loss between the target and receiver are reciprocal. This assumption, which is fair for high altitudes, allows the receiver to be treated as a transmitter within AREPS. This assumption is currently necessary, since it is not computationally feasible to simulate the propagation loss from every possible target position to the receiver. Thus, to determine the target-to-receiver propagation loss, a transmitter is placed at the receiver location and using the same procedure as presented above, the propagation loss is computed at 5° increments for the entire azimuth.

The propagation loss data sets are now weighted by the omnidirectional receiver antenna pattern. This results in a target-to-receiver path loss given by $L_c(dB) = L_{PL}(dB) - G_{Rc}(dB)$.

The complete target-to-receiver path loss data is then interpolated over the same regular Cartesian grid as before. In this case the points on the grid are governed by,

$$L_c = \frac{4\pi R_c^2}{F_c^2 G_{Rc}} \tag{3.11}$$

Round-trip propagation loss (Path bc)

Both propagation loss grids, represented by equations (3.10) and (3.11), can be combined to form,

$$L_{bc} = L_b L_c = \frac{(4\pi)^2 (R_b R_c)^2}{(F_b F_c)^2 G_{Tb} G_{Rc}} \tag{3.12}$$

This can be done since both L_b and L_c have the same regular Cartesian grid. This combination results in a grid where each point represents the round-trip propagation loss L_{bc} as well as the gains for the transmit and receive antennas for a particular target position.

3.3.2 Computation of Bistatic Coverage Maps

Substituting the round-trip loss grid, L_{bc}, of equation (3.12) into equation (3.1) gives,

$$SNR = \frac{P_R}{N_o} = \frac{P_T \lambda^2 \sigma_B}{k T_s B_n (4\pi) L_{bc}} \tag{3.13}$$

Setting the remaining variables to the values specified in Section 3.2 a spatial SNR map is generated. This spatial SNR map is shown in Figure 3.6 and

indicates possible detection range and coverage feasibility at an altitude of 1600 m.

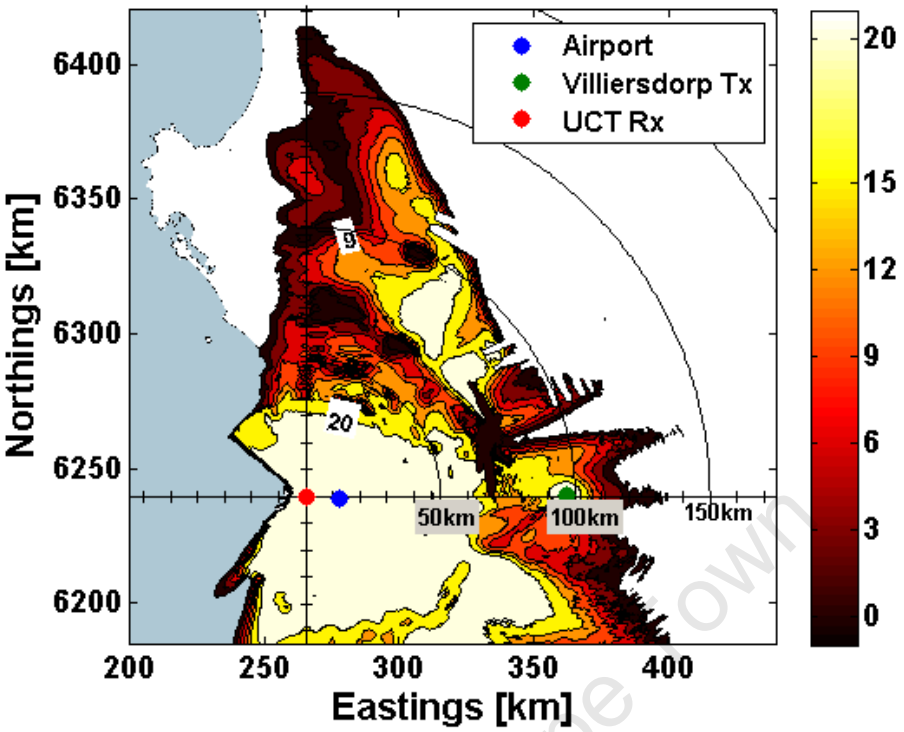

Figure 3.6: Spatial SNR map [dB] at 1600 m with omnidirectional receiver pattern.

In the case of the SIR the combined loss of equation (3.12) and the direct path loss of (3.9) are of interest. The SIR equation (3.3) can be represented as,

$$SIR = \frac{P_R}{P_D} = \frac{\sigma_B L_a}{L_{bc}} \tag{3.14}$$

As in the case of SNR, a spatial SIR map can be generated using equation (3.14). Figure 3.7 shows a SIR map for the parameters stated in Section 3.2. In general, Figures 3.2, 3.3, 3.6 and 3.7 use the same bistatic configuration parameters[3].

3.3.3 Observations

Looking at Figure 3.6 and Figure 3.2, it is evident that the simulated predicted coverage is much reduced compared to the conventional case. At an altitude of 1600 m above sea level, a detection range of around 75 km is predicted, a reduction of around 175 km from the conventional case. The reduction is not unexpected, yet important to note is the significant effect that environmental factors have on the bistatic SNR radar equation and radar detection range.

[3]See Appendix C.1.1 and Table C.1 for the complete set of configuration parameters used.

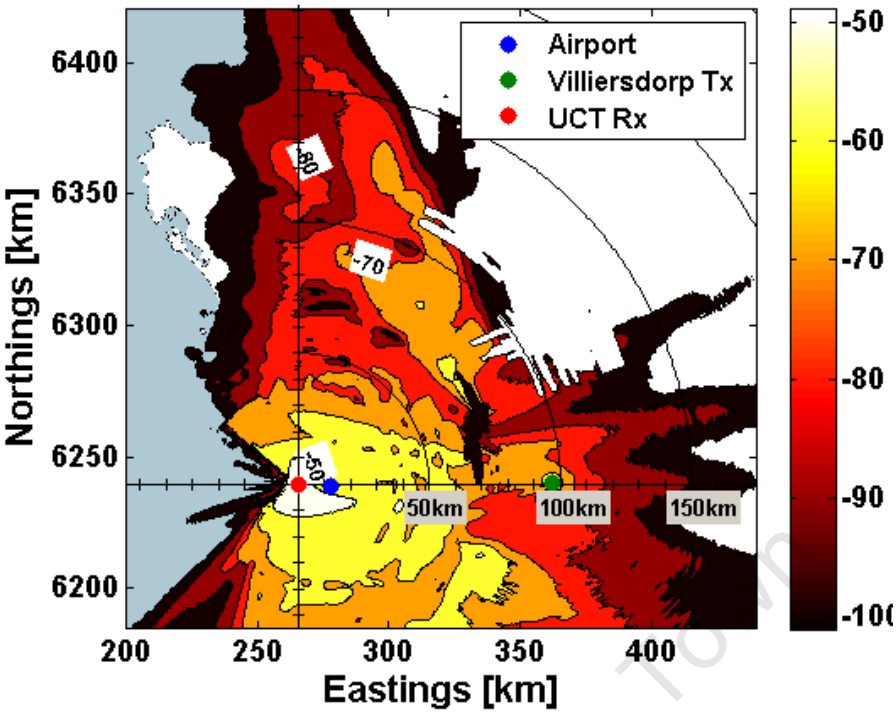

Figure 3.7: Spatial SIR map [dB] at 1600m with omnidirectional receiver pattern.

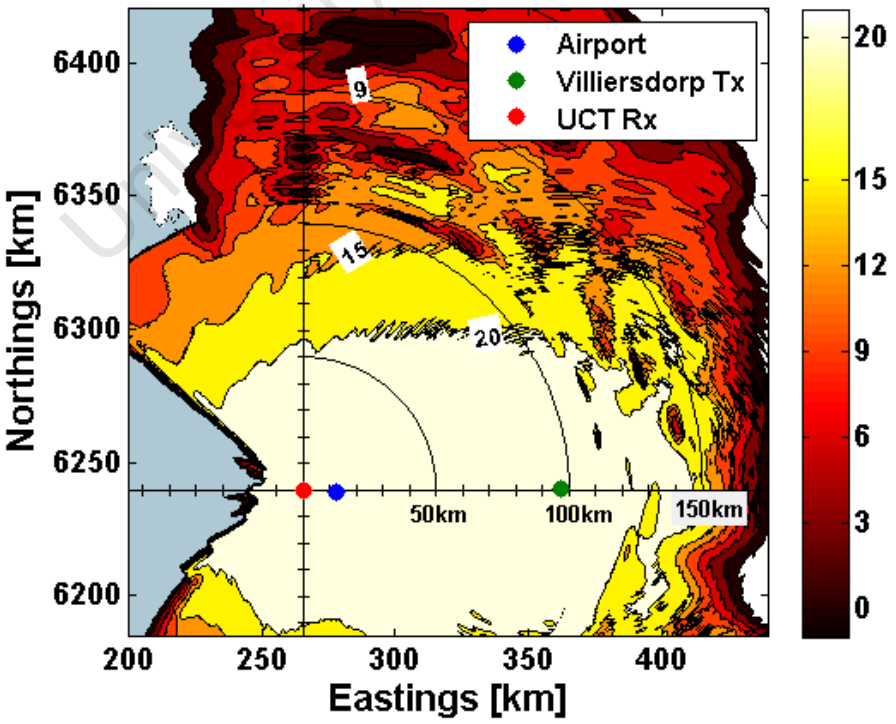

Figure 3.8: Spatial SNR map [dB] at 5000 m.

Figure 3.8[4] illustrates simulated predicted coverage of up to 150 km for an altitude of 5000 m. This shows, as expected, better coverage at higher altitudes. At higher altitudes the effects of the terrain on the propagation factor have lessened and the AREPS generated propagation loss data tends towards free-space-like propagation loss. Consequently, the coverage map can be likened to ovals of Cassini.

A significant difference is also observed between Figures 3.3 and 3.7. With reference to a commonly accepted SIR of -60 dB the maximum coverage achieved according to the conventional prediction method is less than 20 km surrounding the receiver and the transmitter as seen in Figure 3.3. With the addition of the environmental effects, the performance of the PCL system is predicted to improve. The improvement of required dynamic range is about 25 - 30 dB, consistent with the added propagation loss expected along the path of the direct signal (Table 2.5). As seen in Figure 3.7 the coverage in some cases extends as far as 100 km out from the receiver.

It is evident from equation (3.14) that to improve coverage described by the SIR, as shown in Figure 3.7, one must increase the direct path loss L_a. A common method of further increasing the direct path loss is to decrease the target antenna gain, G_{Ra}, in the direction of the transmitter by means of null forming.

3.4 Conclusions

This chapter introduced an improved method of generating SNR, SIR and SNIR coverage maps representing possible detection range and required receiver system dynamic range. This was done using APM and AREPS to compute realistic propagation loss, which incorporated the propagation factor. Significant differences between the conventional coverage maps - ovals of Cassini - and the coverage maps based on the AREPS propagation loss were presented. These differences emphasised the importance of the propagation factors, F, which take into account the effects of the terrain and atmosphere.

The SNR coverage maps showed an expected coverage, for given environment and system parameters, of around 75 km and 150 km at an altitude of 1600 m and 5000 m, respectively. These realistic detection ranges, were as expected, much less than the 250 km detection range predicted using the conventional model.

The SIR (and SNIR) coverage maps indicated the required dynamic range within a certain coverage region for a specific bistatic radar configuration. An improvement, of around 25 dB, in the SIR coverage maps and subsequently

[4]See Appendix C.1.2 and Table C.1 for the complete set of configuration parameters used.

the required dynamic range was seen by the increase of direct path loss resulting from the terrain and atmosphere effects. The required dynamic range can be further improved by introducing a receiver pattern null in the direction of the transmitter and will be investigated in Chapter 4.

This method can be used to compare various arrangements of receivers and transmitters in any bistatic configuration and will aid in the choice of optimum non-cooperative transmitter and receiver location.

A current shortcoming of this method is the assumption of reciprocity, which is a simplification, the effects of which must be investigated further. In addition, the RCS of the target is assumed to be isotropic and constant. In reality the bistatic RCS of the target is of interest, which requires knowledge of 3D shape of the target and the angles at which the EM waves are incident and reflected.

Despite this, the method presented here offers improved performance prediction capability over the conventional prediction method. Using this method, various configurations of receivers and illuminating transmitters can be tested, easily and quickly.

Chapter 4

Target Antenna Pattern Synthesis and Coverage Improvement

As concluded in Chapter 3, a high power direct path signal has an adverse effect on the performance of a PCL radar. By suppressing the direct path signal in a target antenna pattern null the performance and subsequent coverage of the PCL radar can be improved and forms the subject of this chapter. Here, the modified coverage of expected detection range and required dynamic range in terms of SNR and SIR resulting from the target antenna pattern synthesis is presented. In particular, the Schelkunoff method is used to synthesise a pattern null in the direction of the illuminating transmitter to suppress the DPI in the target antenna of a PCL receiver. The case study introduced in the previous chapter is carried through here.

The chapter begins by listing necessary requirements for target antenna array, such as direction of the null and the size of the array. This is followed by a discussion of the folded dipole, intended for the use as the elements of the target antenna array. Here, the various parameters of the antenna are characterised.

The sophisticated antenna and EM modelling tool, FEKO, based on the technique of Method of Moments (MoM), is used in this chapter to simulate the folded dipole element and later the target antenna array. The name, FEKO, is derived from a German acronym which can be translated as "Field Computation for Objects of Arbitrary Shape". The FEKO solver is based on the Method of Moments, which it uses to calculate Maxwell's equations.

Next, the antenna pattern synthesis technique, the Schelkunoff Unit-Circle Method, is introduced and reviewed. With reference to the requirements, the target antenna array is designed using this technique and simulated in FEKO. The resulting array is investigated, with a particular focus on the sub-

sequent azimuth radiation pattern.

Thereafter, the synthesised pattern, with a null in the direction of the transmitter, is applied to the performance prediction method introduced in Chapter 3. The consequent effect on the coverage of the PCL system is presented and discussed. Finally, conclusions are drawn.

4.1 Requirements

The core requirement is to reduce the direct path signal, the DPI, received in the target antenna. This can be done by means of an antenna array and null formation techniques. The Villiersdorp transmitter, is used here as the illuminating transmitter. Requirements for the target antenna are:

- Reduce DPI by means of antenna pattern null in the direction of Villiersdorp transmitter, which is at bearing of $89.6°$ (referenced to True North), while providing reasonable gain in the direction of existing flight paths.
- The antenna array must be linear and less than 5 m in length. This requirement is a result of limited space on the roof of the Menzies building at UCT coupled with the large wavelengths at FM frequencies. In the case of the Villiersdorp transmitter, the KFM radio station transmits at 96.5 MHz which translates to $\lambda = 3.11$ m.
- The antenna array must be low-cost and COTS where possible.

4.2 Elements of the Antenna Array

The antenna elements used for the array are folded dipoles, commercially available and manufactured by SpaceTV[1]. The folded dipole is also convenient as it is structurally more stable and more broadband [4] than the simple half-wave dipole. A model of the folded dipole, with the antenna port indicated as the red segment, is shown in Figure 4.1.

The simulated real and imaginary input impedance at the terminals of this antenna for all FM frequencies is shown in Figure 4.2. The input impedance of a folded dipole is usually in the order of four times larger than that of a simple linear dipole of similar dimensions (in the order of $Z_{in} \simeq 73 + j42.5\,\Omega$) [4], a property that can be seen in the figure.

The input impedance for the Villiersdorp transmission at 96.5 MHz is indicated on both curves and is measured to be $Z_{in} = 288.7 + j20.9\,\Omega$. This input impedance is relatively high compared to the characteristic impedance

[1] www.spacetv.co.za, checked 6 February 2009.

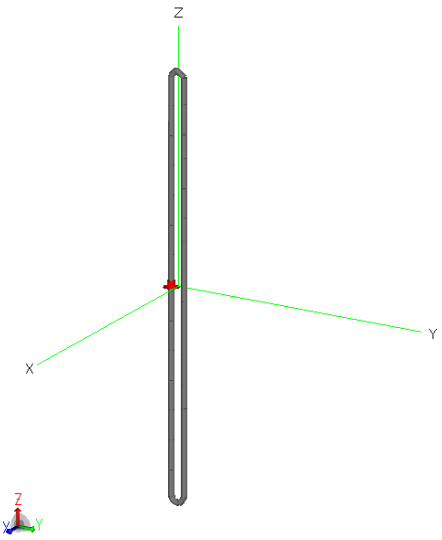

Figure 4.1: FEKO model of the folded dipole .

$Z_0 = 75\,\Omega$ of the RG 6 transmission lines usually associated with this antenna. Thus, a small matching network and balun, at the terminals of the folded dipole is employed by the manufacturer SpaceTV to transform the input impedance to a nominal $75\,\Omega$ value.

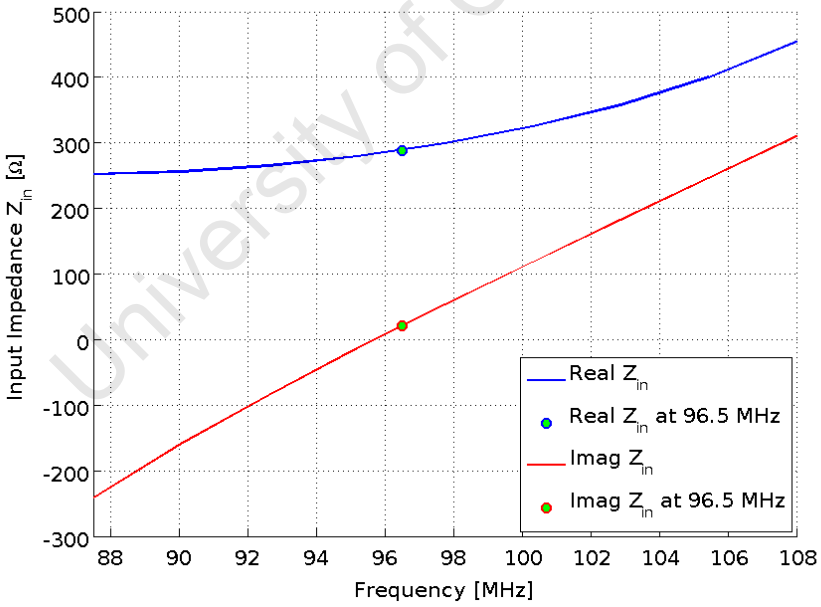

Figure 4.2: Simulated input impedance of the folded dipole.

For the ideal case, where the dipole is conjugately matched at 96.5 MHz to the transmission line and receiver system, maximum power can be received at that frequency. The simulated bandwidth of the folded dipole, under this condition can be seen in Figure 4.2. The bandwidth, measured as a reduction of 10 dB on a $|S_{11}|$ plot, is found to be 4.3 MHz (~ 4.5 % bandwidth), more or less centred around the frequency of interest, 96.5 MHz.

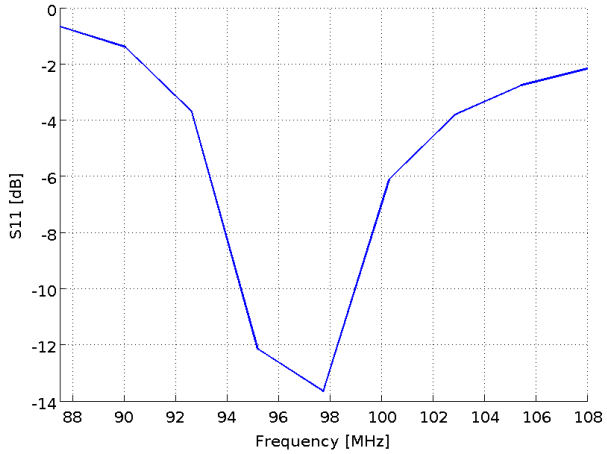

Figure 4.3: Simulated antenna bandwidth measured at -10 dB on a $|S11|$ plot.

Finally, the antenna radiation pattern is given in Figure 4.4. A small deviation in the antenna pattern is apparent and can be seen in Figure 4.4 (b). This deviation has an amplitude of around 0.15 dB making the resulting radiation pattern effectively omnidirectional in azimuth.

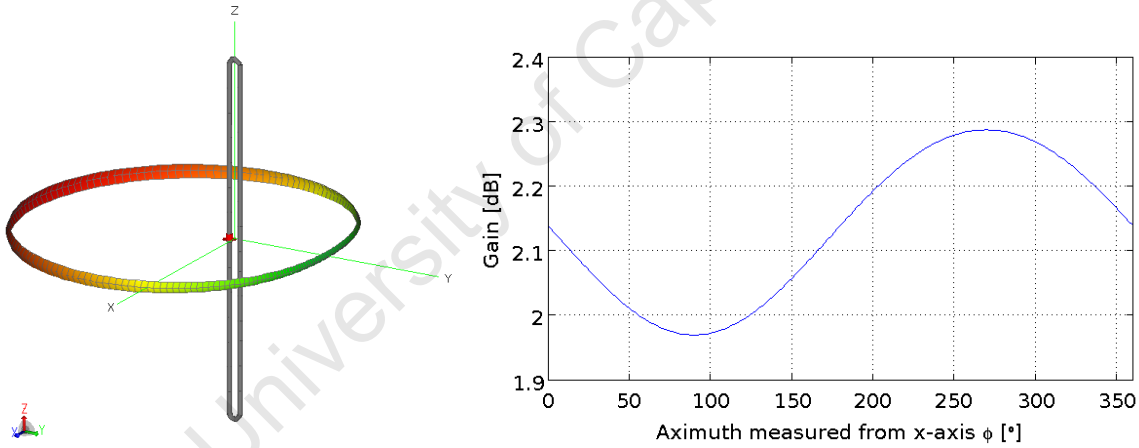

(a) (b)

Figure 4.4: Antenna radiation pattern of a single folded dipole.

As can be seen in Figure 4.4 (a) the deviation in the antenna pattern is because the one side of the folded dipole - the length of wire across from feed port - acts as a reflector. Consequently, more power is radiated (reflected) in the negative y-axis direction. This is further seen in Figure 4.4 (b) by noting that the negative y-axis direction is at an azimuth angle of $\phi = 270°$.

4.3 Target Antenna Pattern Synthesis

According to Balanis [4], antenna pattern synthesis can typically be classified into three major categories, namely:

1. Beam shaping
2. Narrow beam and low sidelobe forming
3. Null placement

The first category, beam shaping, requires that the antenna pattern exhibits a desired distribution in the entire visible region. This can be achieved by the Fourier and Woodward-Lawson methods discussed in Balanis [4].

The second category includes techniques that enable antenna patterns to be produced that have very narrow beams and low sidelobes. These can, for instance, be achieved by applying a binomial or Taylor [32] excitation distribution to the antenna array.

Null placement, the third category, requires that antenna patterns possess nulls in desired elevation θ and azimuth ϕ directions. This can be achieved by the Schelkunoff Unit-Circle Method, a technique covered in [4, 5], based on Schelkunoff's historical paper [33], and can be applied to a linear array of antenna elements.

A focus of this dissertation is to suppress the DPI in the target channel incident from the illuminating transmitter. Since, in the general case, the transmitters can be any direction relative to a potentially variable receiver location, it is of particular use to be able to manipulate the position of nulls in an antenna pattern. Thus, the Schelkunoff method will be the synthesis technique used here and aims to satisfy the first requirement listed in Section 4.1.

4.3.1 Review of Schelkunoff's Unit-Circle Method

Schelkunoff's Unit-Circle method consists of the manipulation of the zeros (nulls) of the array pattern to achieve a desired pattern for a linear array. This representation can be used to describe any uniformly spaced array [5]. To synthesise a particular pattern, this method requires information on the number of nulls and their locations [4] from which the number of elements and their excitations are derived.

Suppose an array has M elements, arranged along the x-axis (Figure 4.5). This arrangement of antennas would have an array factor (AF) governed by,

$$AF = \sum_{m=1}^{M} a_m e^{j(m-1)(kd_x \cos\phi \sin\theta + \beta)} = \sum_{m=1}^{M} a_m e^{j(m-1)\psi} \tag{4.1}$$

where k is the wavenumber and is equal to $2\pi/\lambda$, d_x is the inter-element spacing, the angle of azimuth is given by ϕ and the progressive element phase shift is given by β. By limiting the investigation to the azimuth plane, θ can be set

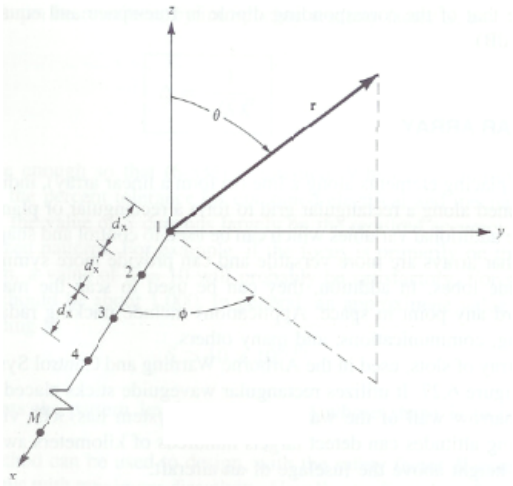

Figure 4.5: Linear array geometry [4].

to $90°$ in which case $\sin\theta = 1$. Considering that the array factor describes a linear array along the x-axis, the array pattern will be symmetrical about the x-axis.

Now following Balanis [4] and letting

$$z = x + jy = e^{j\psi} = e^{j(kd_x \cos\phi + \beta)} \tag{4.2}$$

equation (4.1) can be rewritten as

$$AF = \sum_{m=1}^{M} a_m z^{m-1} = a_1 + a_2 z + a_3 z^2 + \cdots + a_M z^{M-1} \tag{4.3}$$

This polynomial has $(M-1)$ roots and can be expressed as a product of $(M-1)$ linear terms and in terms of magnitude as

$$AF = a_m (z - z_1)(z - z_2)(z - z_3) \cdots (z - z_{M-1}) \tag{4.4}$$

$$|AF| = |a_n| |z - z_1| |z - z_2| |z - z_3| \cdots |z - z_{N-1}|) \tag{4.5}$$

respectively. Where $z_1, z_2, z_3 \ldots, z_{M-1}$ are the roots, which may be complex.

Looking again at equation (4.2), we note that $|z| = 1$ and thus z lies on a unit circle. However, the position of z on the unit circle is determined by its phase $\psi = kd_x \cos\phi + \beta$. The array pattern is symmetrical about the array axis as seen in Figure 4.5, consequently limiting the azimuth angle ϕ to the range $0°$ to $180°$. As ϕ increases, ψ decreases and z progresses in a clockwise rotation along the unit circle as shown in Figure 4.6 [5]. The arc traced out by z, along the unit circle, is referred to as the visible (realisable) region. The remaining part of the unit-circle is known as the invisible region. Allowing $\psi_s - \psi_f$, $2kd$,

to exceed 2π can cause more than one main beam (grating lobes) [5]. The overall extent of the visible region can be controlled by the spacing between the elements and its relative position on the unit circle by progressive phase excitation of the elements [4].

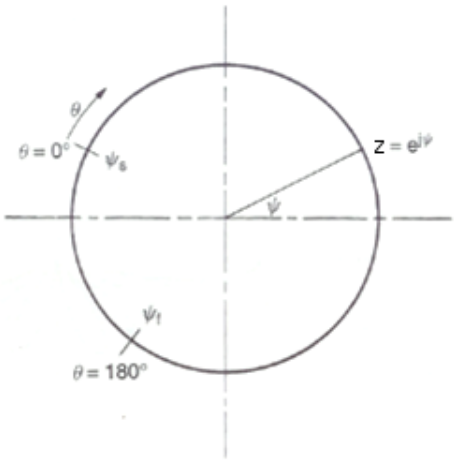

Figure 4.6: Unit circle in the z-plane [5].

Looking again at equation (4.5) it is clear that $|AF|$ is proportional to the product of distances between z and each of the zeros (roots). If all the roots are located in the visible region, then each one corresponds to a null in the pattern of $|AF|$ because as ϕ changes $z = e^{j\psi}$ changes and eventually passes through each of the $z'_m s$ [4].

Thus, it can be seen, that for a set of specified nulls in the azimuth plane and for an array of given size, the zeros (roots) on the unit-circle can be manipulated to either reduce sidelobes or to place pattern nulls. Sidelobes are reduced by moving the zeros on either side of it closer together. This has a trade-off effect in that either the main-lobe beamwidth increases or the other sidelobes rise [5].

Care must be taken when synthesising array using this method. By reducing the spacing between elements, zeros can be shifted from invisible space to visible space so as to narrow the beam and reduce sidelobes. As a consequence large sidelobes are created in invisible space that represent energy storage in the array. This stored energy reduces the bandwidth and efficiency of the array [5].

4.3.2 Antenna Array Design and Simulation

The target antenna array, designed and simulated with FEKO, is comprised of four folded dipole elements (discussed in Section 4.2) spaced 0.49 λ apart and is shown in Figure 4.7. Spacing between elements is chosen slightly less

than 0.5 λ to avoid grating lobes but large enough so as to reduce mutual coupling between the elements and energy stored in the array. A spacing of 0.49 λ for a carrier frequency of 96.5 MHz translates to a $d_x = 1.523$ m spacing between elements, which makes the array of four folded dipoles 4.570 m long and puts it within the limit of the 5 m requirement.

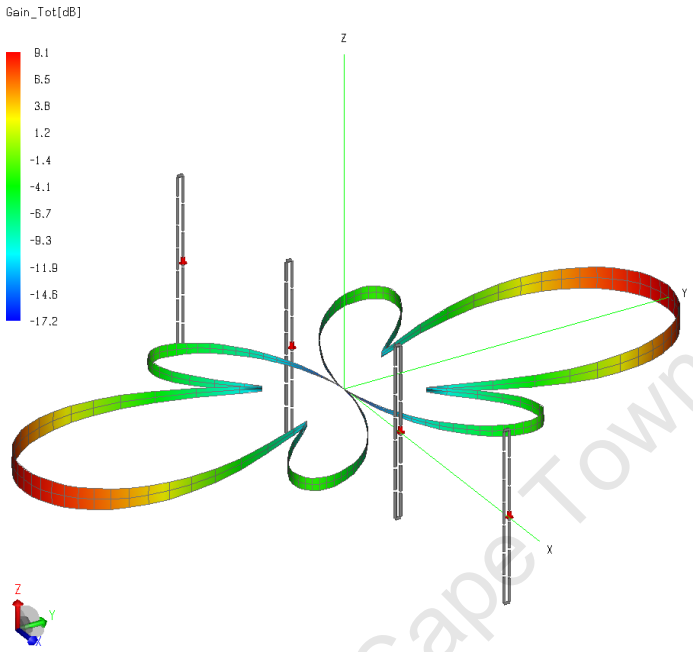

Figure 4.7: Receive antenna array, comprised of 4 folded dipole elements, with radiation pattern of a uniform amplitude and phase distribution.

Figure 4.7 also depicts the broadside radiation pattern resulting for a uniform amplitude and phase excitation distribution. Furthermore, the symmetry of the antenna pattern about the array axis, resulting from the linear nature of the array, is also apparent.

Figure 4.8 shows the orientation of antenna array, with element numbers, in the azimuth plane with respect to the cardinal points. Here, the antenna array patterns will be measured as angle of azimuth, ϕ, with respect to the array axis (x-axis). The array axis is measured as the angle γ from South.

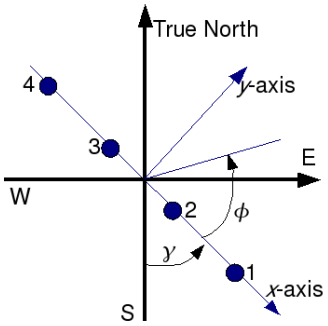

Figure 4.8: Orientation of antenna array in the azimuth plane.

Given the gain pattern of the array under a uniform distribution in addi-

tion to the requirement for reduced gain in the direction of the Villiersdorp transmitter and reasonable gain in the direction of existing flight paths, the antenna array will be orientated such that peak of the broadside pattern is in the direction of the flight route for aircraft inbound from JHB. This is done since the formation of the null in the direction of the Villiersdorp transmitter happens to be in the same direction as the flight routes associated with PE.

The chosen orientation can be seen in Figure 4.9, where inbound aircraft are incident on an angle of $\phi = 90°$ measured anti-clockwise from the axis of the array. The axis of the array itself will thus be orientated such that $\gamma = 40°$.

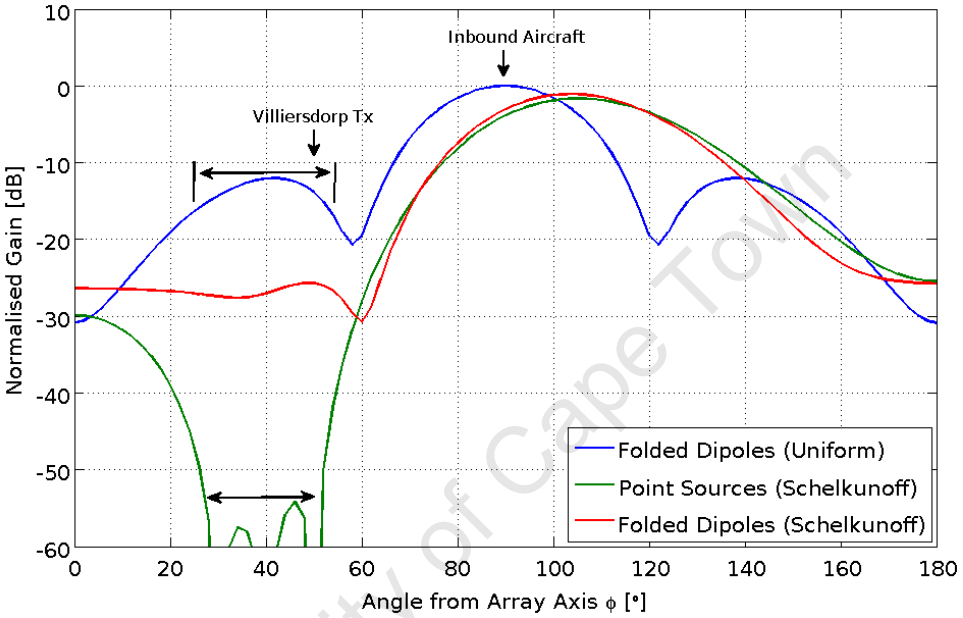

Figure 4.9: Normalised gain patterns of an array of folded dipoles (blue and red) and point sources (green).

This arrangement would place the Villiersdorp transmitter at an angle of $\phi \simeq 50°$ from the antenna array axis. At this point, a signal from Villiersdorp would be incident on a sidelobe (indicated in the figure by the top double arrow) of the gain pattern, at a level of -13.9 dB.

Schelkunoff's Unit-Circle method is used to specify nulls in such a way so as to reduce the indicated sidelobe in the pattern of the uniform distribution, as was explained in Section 4.3.1. The 4 antenna elements allow the specification of 3 nulls, which are placed at ϕ equal to $30°$, $40°$ and $50°$ to reduce the sidelobe. These nulls correspond to roots of the Schelkunoff polynomial, equation (4.3). Thus substituting the aforementioned values for k, d_x and ϕ with a progressive phase shift of $\beta = 0°$ results in 3 roots:

$$\begin{aligned} z_1 &= 1\angle 152.8° = -0.889 + j0.457 \\ z_2 &= 1\angle 135.1° = -0.708 + j0.706 \\ z_3 &= 1\angle 113.4° = -0.397 + j0.918 \end{aligned} \tag{4.6}$$

Substituting the complex representation of these roots (4.6) into equation (4.4), with a_m set to unity, the complex coefficients $a_1, a_2 \ldots a_M$ of equation (4.3) can be determined. These coefficients, being complex, provide the sought amplitude and phase distribution of the array and are given in Table 4.1.

Table 4.1: Amplitude and phase distribution of an array using Schelkunoff's method.

Number	Amplitude [V]	Amplitude [dB]	Phase [°]
Element 1	1	0.00	138.7
Element 2	2.88	9.19	92.5
Element 3	2.88	9.19	46.2
Element 4	1	0.00	0

Applying the resulting amplitudes and phases to an array of point sources, results in a radiation pattern depicted in Figure 4.9 with the green curve. It can be observed that the combination of the three nulls, in theory, produces one wide null, as indicated by the bottom double arrow. This wide null is positioned to cover the range of angles corresponding to sidelobe in question.

Applying the distribution, computed by Schelkunoff's method, to the array of folded dipoles (with $\gamma = 30°$) results in a gain pattern illustrated by the red curve in Figure 4.9. The reduction of the sidelobe apparent in the uniform distribution can be clearly seen. The gain in the direction of Villiersdorp, is reduced from -13.9 dB to -25.7, an improvement of 11.8 dB.

However, this improved effect is compromised by the reduction in the peak of the main lobe by 3 dB in the direction of the JHB flight route and is seemingly a trade-off alluded to in Section 4.3.1. This 3 dB compromise results in an effective sidelobe level of -22.7 dB.

By orientating the array such that $\gamma = 30°$, ϕ equals to $100°$ is in the direction of the inbound aircraft from JHB and the direct signal is further reduced in a null at $\phi = 60°$ of the array radiation pattern. In this case the direct signal will be reduced down to -29.6 dB from the peak in the target antenna pattern, as shown in Figure 4.10. This would result in a notable effective improvement over the uniform distribution by 15.7 dB.

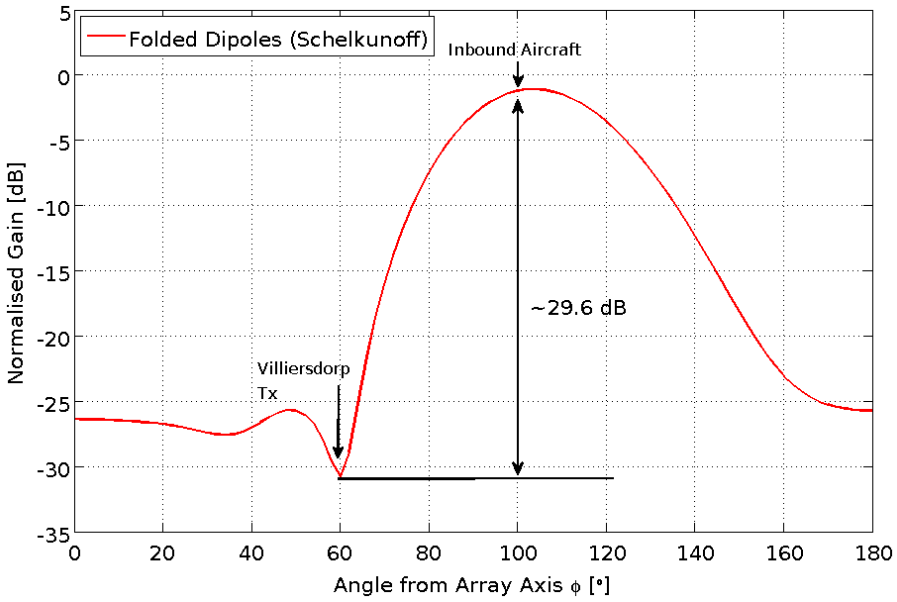

Figure 4.10: Normalised gain pattern of an array of folded dipoles with excitation distribution determined by Schelkunoff's method.

4.4 Predicted Coverage with Synthesised Target Antenna Array Pattern

Figure 4.11 [2] shows the the resulting spatial SNR map at an altitude of 1600 m after the application of the Schelkunoff synthesis method to the target antenna and the consequent formation of the null in the direction of the Villiersdorp transmitter. Compared to Figure 3.6, the coverage shown here is much improved in the direction of aircraft en route with JHB. A PCL system in this configuration is predicted to achieve detection ranges of up to 100 km in the sector of interest for an SNR of 15 dB.

The effect of the null can be seen by the reduced level of SNR expected in the direction of the Villiersdorp transmitter. Furthermore, the coverage in the southern direction is reduced, though for the application of the detection of commercial aircraft en route with JHB this shortcoming is deemed acceptable.

Figure 4.12 [3] shows an overall improvement of the coverage feasibility, in terms of required dynamic range, compared to Figure 3.7, with no apparent drawbacks. The coverage data presented here as a spatial SIR map showed an improvement in the order of 30 dB in the JHB route direction. For an commonly accepted SIR of -60 dB a coverage range in some cases up to 130 km can be expected.

In this case, there is no predicted decrease in performance in the southern

[2] See Appendix C.1.3 and Table C.1 for the complete set of configuration parameters used.
[3] See Appendix C.1.3 and Table C.1 for the complete set of configuration parameters used.

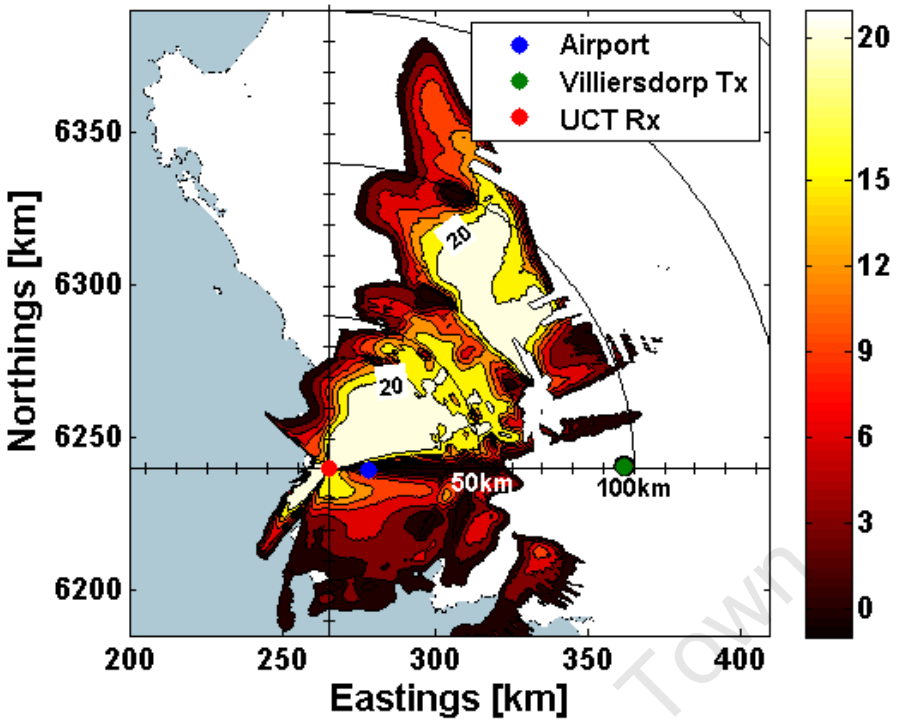

Figure 4.11: Spatial SNR map [dB] at 1600m with synthesised receiver pattern.

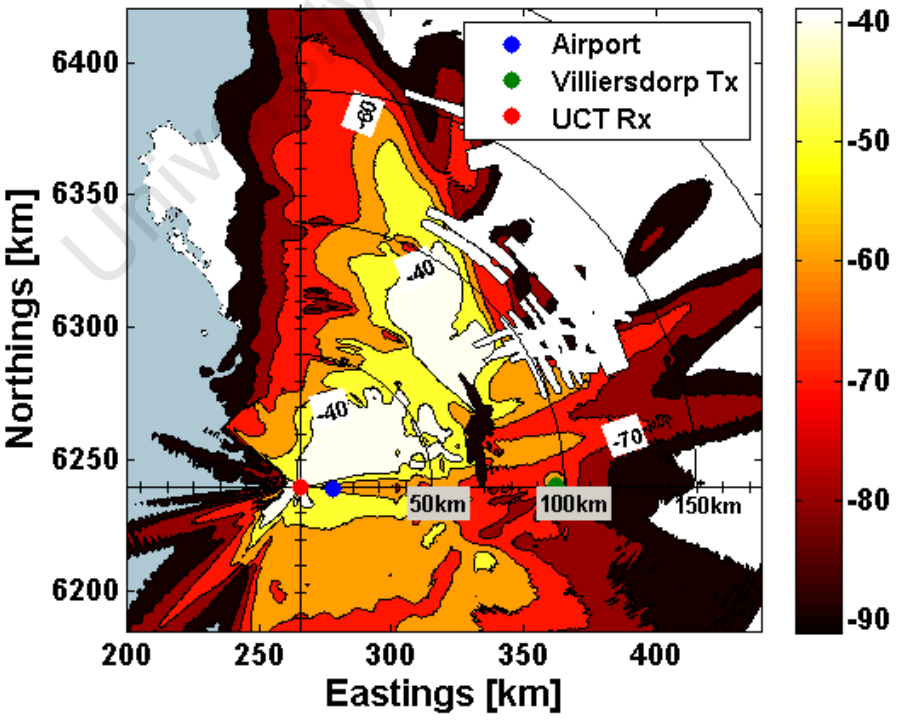

Figure 4.12: Spatial SIR map [dB] at 1600m with synthesised receiver pattern.

direction as was seen for the SNR coverage. However, the required dynamic range in this direction is not improved either, with the level of SIR remaining relatively similar to that seen in Figure 3.7.

The spatial SNR coverage map at an altitude of 5000 m is shown in Figure 4.13 [4] . The figure also shows the flight paths discussed in Chapter 2. Here, the predicted detection range is up to 150 km, a 50 km increase in detection range from 1600 m (Figure 4.11). This further illustrates the significant effect of the environment - especially terrain. Compared to Figure 3.8, the figure shown here has a smaller possible detection region. This can, as before, be attributed to the lack of coverage to the south.

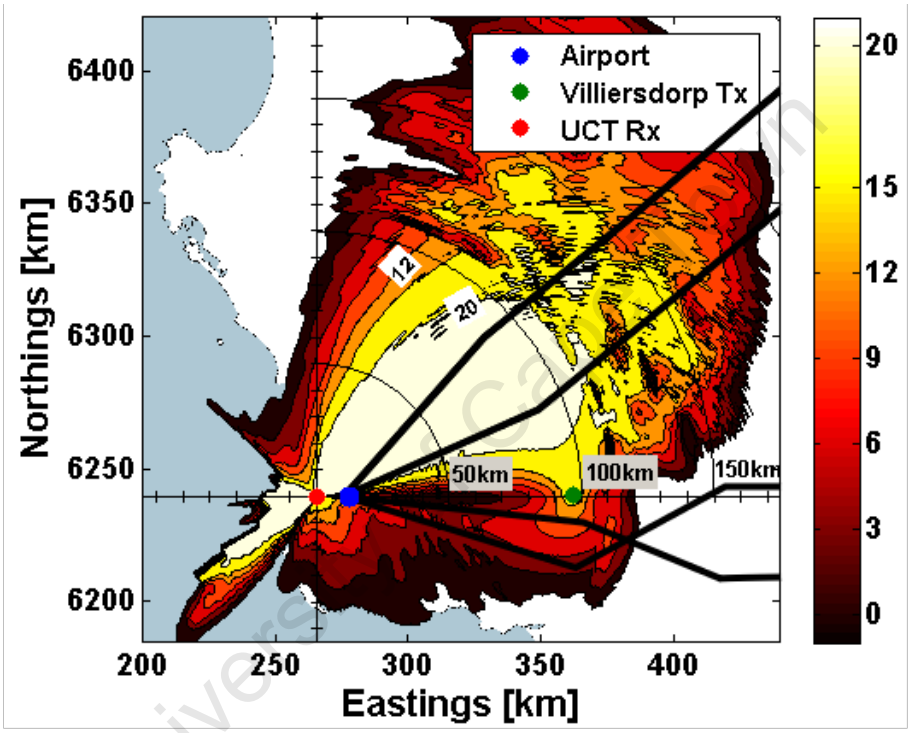

Figure 4.13: Spatial SNR map [dB] at 5000 m with synthesised receiver pattern.

4.5 Conclusion

The Schelkunoff Unit-Circle Method was used in this chapter to illustrate the coverage improvement that can be achieved by synthesising antenna patterns and in particular by forming a target antenna pattern null in the direction of the Villiersdorp transmitter.

The target antenna array and its elements were simulated and discussed with the use of FEKO. The choice of folded dipoles as elements of the array was advantageous in that they are structurally stable and commercial available. The

[4] See Appendix C.1.4 and Table C.1 for the complete set of configuration parameters used.

array, comprising of four folded dipole elements, was also simulated in FEKO. Applying a Schelkunoff excitation distribution to the array saw an effective sidelobe level in the direction of the Villiersdorp transmitter of -22.7 dB for a normalised gain pattern. By changing the orientation of the array slightly the direct signal can be reduce down to -29.7 dB from the peak of the main lobe (in the direction of the JHB flight route). The Schelkunoff distribution used here offered a 15.7 dB improvement, in terms of reduction of sidelobes, over the uniform excitation distribution.

Utilising the azimuth pattern resulting from Schelkunoff distribution in the performance prediction method presented in Chapter 3, showed improved coverage in the sectors of interest as seen in Figures 4.11 through 4.13. The decrease of coverage in other sectors was deemed acceptable for the application of the detection of aircraft in the direction of JHB. In general, the figures, which show possible detection range and required dynamic range, suggest that coverage in a sector of airspace can be improved significantly with the application of antenna synthesis.

Chapter 5

Antenna Array Implementation

In Chapter 4 an element excitation distribution was determined and applied to a model of an array of folded dipoles within FEKO in order to null a strong direct signal. In this chapter this excitation distribution is applied to real folded dipole antenna elements representing the target antenna. This is done for two reasons. Firstly, to verify the simulated pattern and to confirm that the application of the Schelkunoff method used in the previous chapter yields a physically realisable pattern. Secondly, to ascertain the predicted performance in terms of detection range and dynamic range resulting from the measured pattern. The bistatic configuration investigated here is a continuation of the case study dealt with in Chapter 3 and 4. The predicted performance determined here is compared with that of the simulated case determined in the previous chapter.

This chapter begins with a description of the components that make up the target antenna array. Important characteristics of each of the components are noted and their configuration making up the receiver system is also discussed.

Thereafter, aspects concerning the measurement of the antenna array are dealt with. To begin with, a brief description of important measurement preliminaries are given. Namely, the setup of equipment as well as the proposed measurement procedure are described. Following the measurement procedure the measured pattern is presented and observations made.

The bistatic radar detection range and dynamic range in terms of SNR and SIR resulting from the measured pattern are determined and compared with results of Chapter 4. Finally, conclusions are drawn.

5.1 Antenna Array Setup

5.1.1 Target Antenna Array

Figure 5.1 illustrates the four channels leading from each antenna element of the target antenna array into a combiner element. The signal captured by each of the antenna elements is weighted and shifted in phase according to the excitation distribution detailed in Table 4.1. Summing these altered signals would yield a specific radiation pattern of the target antenna array as was seen in Figure 4.9.

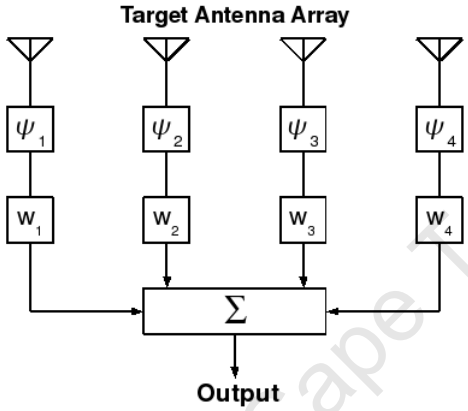

Figure 5.1: Target Antenna Array Receiver

5.1.2 Components[1]

The target antenna array as shown in Figure 5.1 was assembled from commercial off-the-shelf products. The antenna elements were purchased from SpaceTV and the transmission line, RG 6 cable, was sourced from Ellies[2]. In terms of the weighting, Tee attenuators were built to manipulate the amplitude distribution of the array. Lastly, the combiner element used to sum the four channels was also sourced from Ellies. The entire receiver system has a nominal impedance of 75 Ω.

The phase and attenuation of each of the four channels was measured with an Agilent E5071B network analyser.

To begin with the S_{11} parameter of the four antennas was measured, the results of which can be seen in Figure 5.2. The antennas are specified to have a nominal input impedance of $75\ \Omega$. As can be seen in Figure 5.2 (a) the log-magnitude responses of all four elements are well below the -10 dB level for the entire FM band, suggesting good radiation characteristics within the

[1] See Appendix D for further details on components described in this section.
[2] www.ellies.co.za , checked 15 December 2008

band. In addition, the phase response in (b) is relatively linear in the FM band. No significant phase differences between the four antennas were observed. Overall, the folded dipole elements provide good S_{11} characteristics.

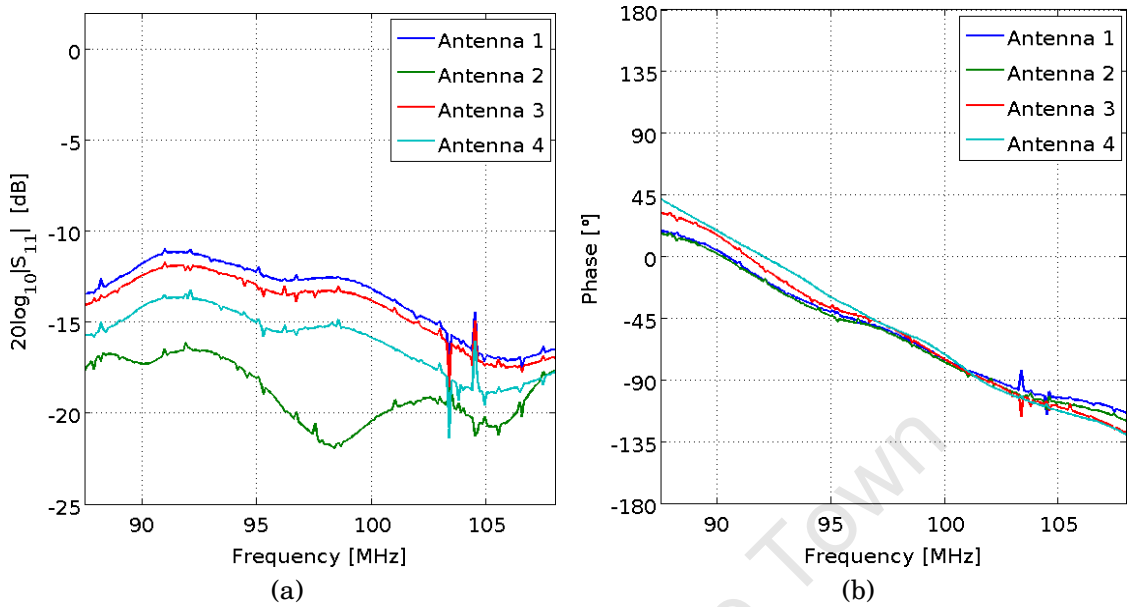

Figure 5.2: Measured log magnitude (a) and the phase (b) of the S_{11} parameter at the input terminals of the folded dipole antennas.

Here, each channel is described as being comprised of transmission lines and all other components found between an antenna port and a combiner port for the particular channel.

Channels 1 and 4 contained an attenuator each, representing the weightings w_1 and w_4 in Figure 5.1. Namely, instead of amplifying the amplitude in channels 2 and 3 as suggested in Table 4.1 the signal amplitude in channels 1 and 4 is attenuated. Subsequently, weightings w_2 and w_3 are kept at unity. Tee attenuators were built and added to channels 1 and 4 for the purpose of applying the amplitude distribution to the target array.

The relative phase shift between channels indicated in Figure 5.1 as the components ψ_1 through ψ_4 was achieved by the addition of varying lengths of transmission lines.

After assembling all the channels, the S_{21} of each channel, including all the aforementioned components, was measured using the network analyser. Of interest was the relative attenuation and phase shift between each channel. The final values recorded can be seen in Table 5.1 with the phase distribution normalised to channel 4.

Lastly, the combiner sourced from Ellies was characterised. Table 5.2 summarises the levels of insertion loss and isolation measured at 96.5 MHz, which are mostly consistent throughout the entire FM band (Appendix D.4). The

Table 5.1: Relative attenuation and phase shift measured between receiver channels. Phase distribution is referenced to channel 4. Discrepancy between measured and calculated (Table 4.1) is shown in the final two columns.

	Measured		Discrepancy	
Channel Number	Relative Phase [°]	Relative Amplitude [dB]	Phase [°]	Amplitude [dB]
1	138.4	-9.53	- 0.3	- 0.34
2	93.3	0	+ 0.8	0
3	47.3	-0.02	+ 1.1	- 0.02
4	0	-9.33	0	- 0.14

overall characteristics of the combiner are good with the insertion loss consistent over all input ports and only 1 dB higher than the theoretical 6 dB insertion loss for an ideal passive 4 port combiner. In addition, the isolation between input ports is good averaging around 27.5 dB.

Table 5.2: Combiner characteristics at 96.5 MHz.

Insertion Loss [dB]				Isolation [dB]					
S-1	S-2	S-3	S-4	1-2	1-3	1-4	2-3	2-4	3-4
7.04	7.08	7.09	7.06	25.89	28.03	28.38	28.19	28.69	25.72

5.2 Array Pattern Measurement

5.2.1 Measurement Procedure

The aim of the measurement was to determine the azimuth radiation pattern of the target antenna array. The Tygerberg transmitter was utilised for the purpose of pattern measurement. This transmitter was the practical choice for the purpose of the pattern measurement since it is a high power transmitter and visible from the roof of Menzies with few physical obstructions.

In addition, the Tygerberg FM frequency used during the measurement is that of Good Hope Radio and is at 96.2 MHz, 300 kHz below that of the Villiersdorp transmitter frequency used throughout the case study. Namely, the use of the Good Hope frequency here - with no change to the excitation distribution and structure of the array design in the previous chapter - has no effect on the expected radiation pattern seen in Figure 4.10.

The target antenna array is rotated clockwise from an initial position in which the positive $x-$axis, along array axis, is pointing in the direction of the Tygerberg transmitter as indicated in Figure 5.3. Rotating the array clockwise in the direction of the red arrow essentially traces out the radiation pattern of the array associated with the azimuth angle ϕ measured anti-clockwise from

the positive $x-$ axis. As discussed in the previous chapter, the linear nature of the antenna array results in a symmetrical pattern around the array axis. For this reason the measurement is performed over $180°$.

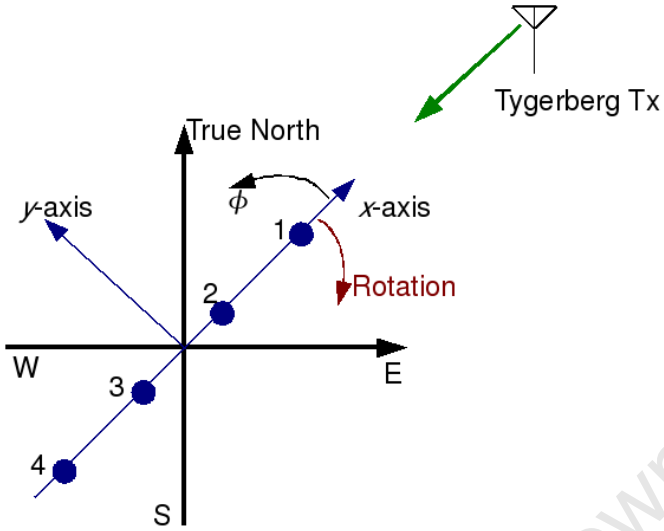

Figure 5.3: Measurement procedure. The array is rotated clockwise in the direction of the red arrow essentially tracing out the radiation pattern of the array described by the black arrow associated with the azimuth angle ϕ.

The output of the combiner as indicated in Figure 5.1 is fed through a matching pad into a (Agilent E4407B) spectrum analyser. The matching pad matches the 75 Ω receiver system output to the 50 Ω input of the spectrum analyser and has a specified 5.72 dB insertion loss in the FM band. The power of the Good Hope Radio signal contained in the 100 kHz band, centred around 96.2 MHz, is then measured using the spectrum analyser over the range $\phi = 0°$ to $\phi = 180°$ at every $10°$ step. Each measurement was done with a resolution bandwidth of 1 kHz and due to the frequent variation of the radio signal, an averaging factor of 100.

Figure 5.4 shows the physical measurement set up. As shown in the figure the antenna array was rotated in a clockwise direction, once again illustrated by the red arrow, around a central pivot point marked on the floor. Also seen the figure are the folded antenna element numbers as well as the array axes, where the positive y-axis is in the broadside direction of the array and the positive x-axis is in the direction indicated away from the first element along the axis of the array.

The picture of the array configuration indicated in Figure 5.4 is consistent with that shown in Figure 5.3. The picture shows the array in its final positions. Namely, the array was rotated from its initial position as shown in Figure 5.3 through 180° at 10° steps to the position shown in Figure 5.4.

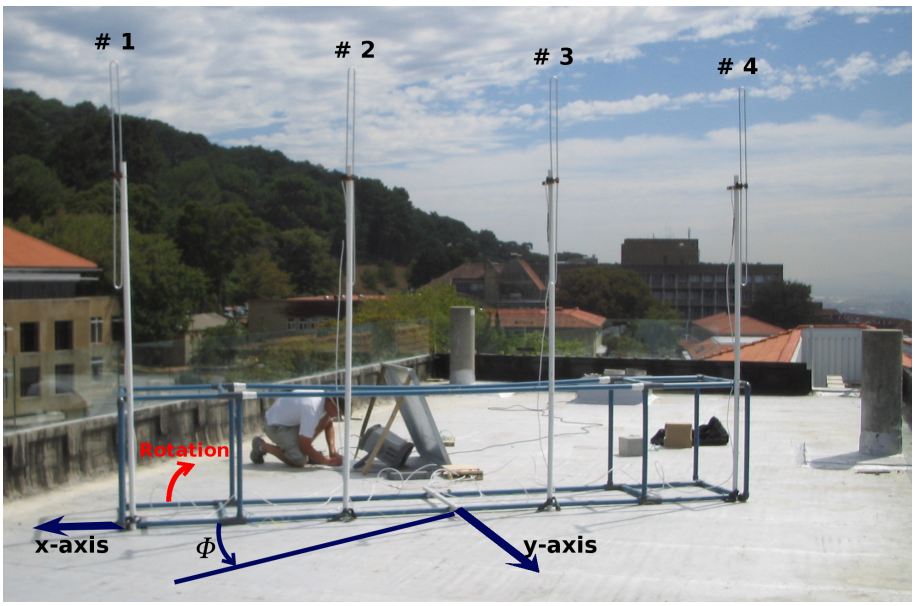

Figure 5.4: Measurement setup on the roof of the Menzies building. The array axes, element numbers, rotation angle and azimuth angle consistent with Figure 5.3 are also shown.

5.2.2 Results and Observations

Following the procedure detailed above, the power received by the array of folded dipoles with a Schelkunoff excitation distribution was measured. To illustrate the procedure, a particular measurement (at $\phi = 100°$) is shown in Figure 5.5. The band power of this particular signal was measured was around -42.4 dBm.

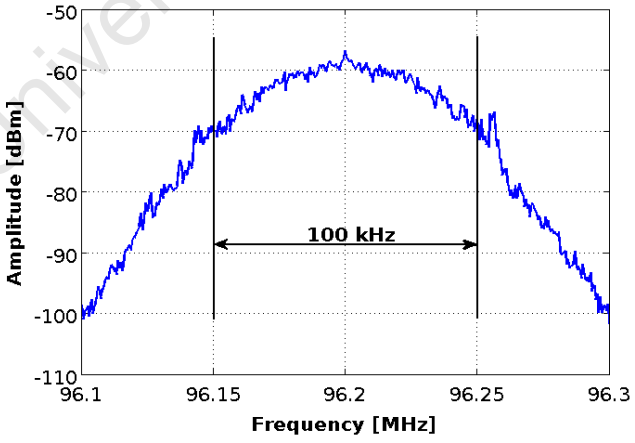

Figure 5.5: Measured power level (-42.4 dBm) in the 100 kHz bandwidth of the 96.2 MHz, Good Hope Radio signal emitted from Tygerberg incident at $\phi = 100°$.

As was seen in Figure 4.4 the pattern of the folded dipole has a mean value of 2.15 dBi in the azimuth plane, similar to the value of the widely accepted broadside gain of a half-wave dipole. The power measured by a single folded

dipole, also with a resolution bandwidth of 1 kHz and an averaging factor of 100, of Tygerberg's Good Hope Radio was -43.6 dBm. Due to the near omni-directional nature of a single folded dipole, the signal power measured can be said to be constant for all incident azimuth angles of ϕ. Namely, rotating the folded dipole in the azimuth plane sees no change to the measured power of -43.6 dBm.

By referencing the measured power of the folded dipole target array to the measured power of a single folded dipole the gain of the array is determined. Namely, the gain of the array over an isotropic radiator can be expressed as,

$$G_{arr}\,(dBi) = (P_{arr}\,(dBm) - P_{dip}\,(dBm)) + 2.15\,(dBi) \tag{5.1}$$

where G_{arr} is the gain of the target antenna array, P_{arr} and P_{dip} is the signal power measured by the target antenna array and the single folded dipole respectively. The factor 2.15 dBi is the mean gain of the folded dipole over an isotropic radiator in the azimuth plane.

As an example, the measurement at $\phi = 100°$ would result in the gain of the array, $G_{arr} = (-42.4 - (-43.6)) + 2.15 = 3.35$ dBi.

The measured radiation pattern as well as the simulated pattern are shown in Figure 5.6. The two patterns are in good agreement, however some deviations are noted below.

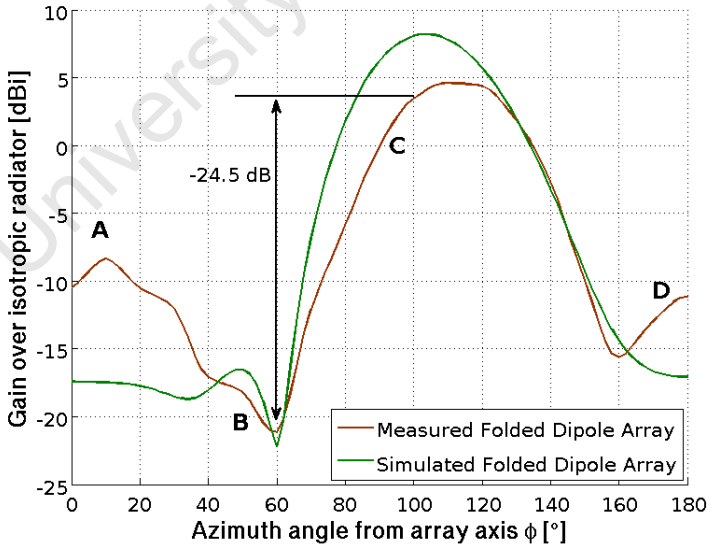

Figure 5.6: Comparison between measured and simulated azimuth pattern of the target array.

Looking at Figure 5.6, point C in the figure indicates a discrepancy in the gain of the main lobe of the pattern in the order of 5 - 7 dB. Another major difference is seen at points A and D, which are much higher than predicted in the FEKO simulation shown in the previous chapter.

The discrepancies can be partially attributed to multipath effects as well as to the insertion loss of the combiner, which were not factored into the simulation. The combiner would cause additional attenuation, or a decrease, in the measured power and subsequently the absolute gain pattern. In terms of multipath, the Menzies roof is positioned at the foot of Devil's Peak and thus horizontal multipath effects become more prevalent. Seeing that the gain pattern measurement is based on received power, it is likely that signal power reflected from the mountain would be incident on the main lobe of the antenna array in the case where the array axis is pointing towards the Tygerberg transmitter. This causes the measured power to increase, which translates to an increase of pattern gain for the particular azimuth direction in question.

The depth of the null at point B is of satisfactory depth. The ratio of the null to direction of aircraft en route with JHB is 24.5 dB. This level, which is 5.1 dB lower than the simulated 29.6 dB is deemed acceptable.

5.3 Predicted Coverage with Measured Target Antenna Array Pattern

The predicted coverage in terms of radar detection range and required dynamic range of the receiver is shown in this section. The investigation here follows a similar format to that of Section 4.4. In this case however the performance prediction is done using the measured radiation pattern of the folded dipole array.

Figure 5.7 [3] shows the radar detection range in terms of SNR at an altitude of 1600 m. For an SNR of 15 dB the PCL system has an expected range of 100 km in a North-Easterly direction. The coverage shown here is slightly less than the coverage predicted in Figure 4.11 in the direction of aircraft en route with JHB. There is however a slight increase in the coverage in the South-East direction. This is as expected due to the variations in the measured gain pattern apparent in Figure 5.6.

[3] See Appendix C.1.5 and Table C.1 for the complete set of configuration parameters used.

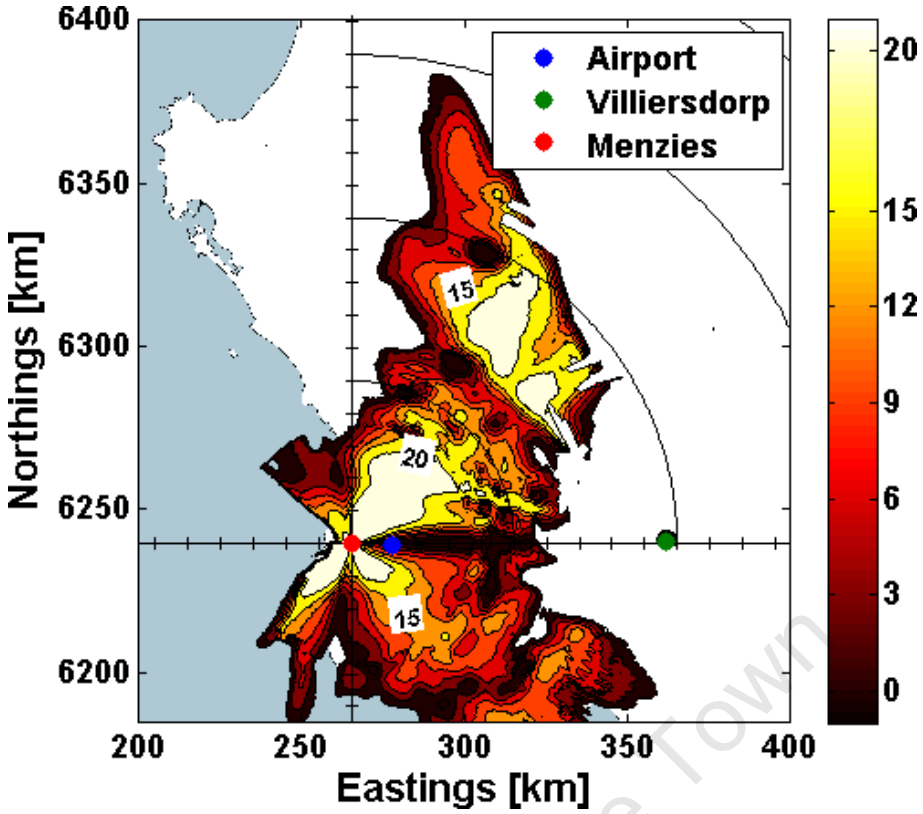

Figure 5.7: Spatial SNR map [dB] at an altitude of 1600 m using the measured target antenna array pattern.

The detection range at 5000 m is shown in Figure 5.8 [4]. Similar relationships can be seen between the this figure and Figure 4.13 as were seen for the case at 1600 m. Namely, the coverage for the case of the measured pattern is slightly less than that using the simulated antenna radiation pattern. However, looking at Figure 5.8, the detection range is still very good at around 130 km for an SNR of 15 dB.

Finally, Figure 5.9 [5] shows the predicted SIR indicating the required dynamic range of the receiver. For an aircraft at an altitude of 1600 m and a required dynamic range of - 60 dB, coverage of aircraft is in some cases expected to be up to 140 km.

The coverage shown here in terms of SNR and SIR is generally quite good and comparable to coverage achieved by existing experimental systems in the UK [2].

5.4 Conclusion

This chapter presented the measured gain pattern of a folded dipole array previously simulated in Chapter 4. This measured pattern was subsequently

[4] See Appendix C.1.6 and Table C.1 for the complete set of configuration parameters used.
[5] See Appendix C.1.5 and Table C.1 for the complete set of configuration parameters used.

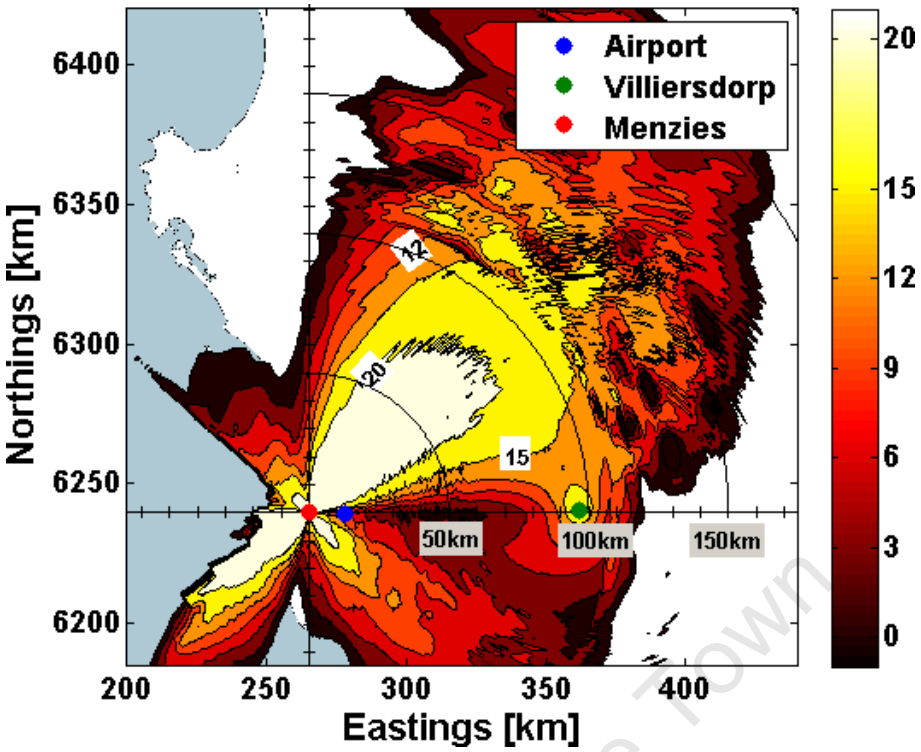

Figure 5.8: Spatial SNR map [dB] at an altitude of 5000 m using the measured target antenna array pattern.

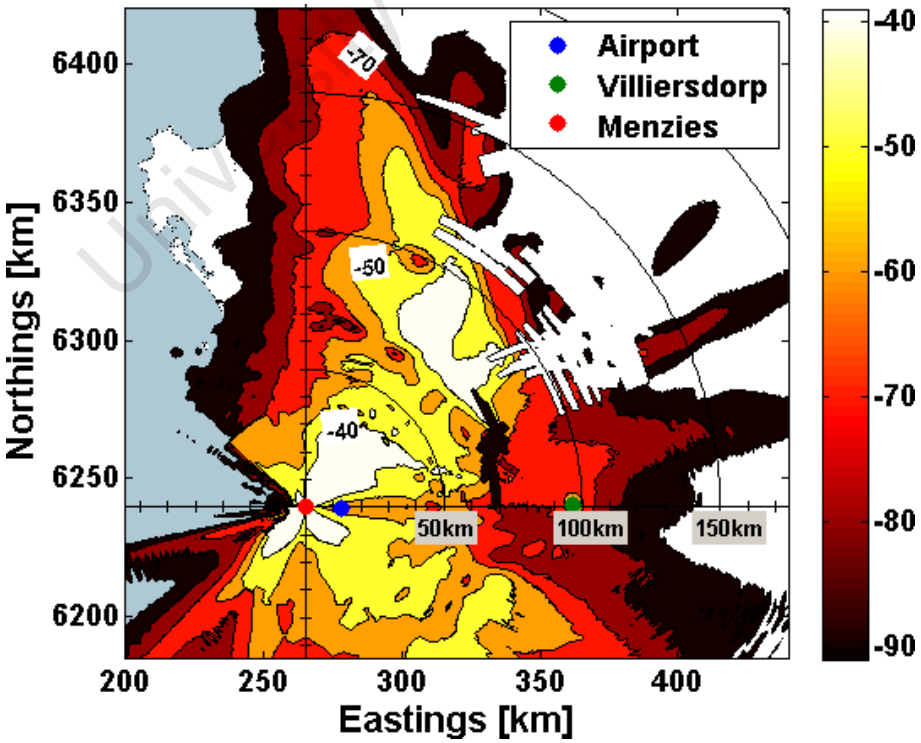

Figure 5.9: Spatial SIR map [dB] at an altitude of 1600 m using the measured target antenna array pattern.

used within the performance prediction model to compare the expected coverage of a simulated antenna array with that of a real antenna array.

The gain pattern measured on the roof of Menzies using commercial off-the-shelf antenna hardware seemed to be in good agreement with that simulated within FEKO previously. Some discrepancies were noted however. The discrepancies can be partially attributed to multipath effects as well as to the insertion loss of the combiner, which were not factored into the simulation. The combiner would cause additional attenuation, or a decrease in the measured gain pattern. In terms of multipath, the Menzies roof is positioned at the foot of Devil's Peak and thus horizontal multipath effects become more prevalent.

Regardless of these effects, the ratio of the null to the peak of the main lobe is at a satisfactory level of 24.5 dB. This result suggests that Schelkunoff's Unit-Circle Method is an effective technique for the purpose of null placement. Furthermore, this coupled with the good agreement of the simulated and measured patterns confirms that the application of Schelkunoff Method in Chapter 4 yields a physically realisable pattern.

The measured pattern was finally used as the receiver pattern within the performance prediction model. The results suggested a relatively similar decrease in expected coverage at an altitude of 1600 m and 5000 m in terms of radar detection range, for an SNR of 15 dB. The decrease was slight from the results seen in Chapter 4 and as expected due to the decrease in the main lobe of the gain pattern. However, good coverage comparable to existing experimental systems was still predicted up to around 100 to 130 km.

In terms of SIR, a required dynamic range of around -60 dB and for aircraft at an altitude 1600 m, coverage is expected to extend to about 140 km. This was again seen to be slightly less than its Chapter 4 counterpart. Nevertheless, the coverage in terms of SIR still remains quite good, due to the respectable 24.5 dB null to peak ratio.

Chapter 6

Conclusion

The method of bistatic PCL radar performance prediction proposed in this dissertation offers a marked improvement over conventional methods based on the bistatic radar equation within a free space or flat terrain environment. Furthermore, methods of improving the performance of a PCL system via antenna pattern synthesis techniques were presented.

The improved method discussed in this dissertation offers a greater accuracy of predicted performance by accounting for the effects of the environment on a propagating signal. The method makes use of realistic propagation loss data computed by the AREPS utility to provide performance predictions in the form of spatial Signal-to-Noise Ratio and Signal-to-Interference Ratio coverage maps. The coverage maps, based on the bistatic radar range equation, provide a visual means for determining radar detection range and coverage feasibility. These represent the probability of detection (and false alarm) of a target and required receiver dynamic range respectively.

A comprehensive preliminary study into the properties of the available broadcast transmitters and their associated signals of the Western Cape was completed in order to identify one transmitter with the best characteristics for an illuminator of opportunity. The terrain effects on the propagating signals were also considered using AREPS. Finally, the Villiersdorp transmitter was identified as acceptable for a PCL receiver located at the University of Cape Town.

Following the preliminaries, the improved bistatic performance prediction method was explained. The method involves the extraction and interpolation of accurate propagation loss data from AREPS and the subsequent computation of the coverage maps using the interpolated data in conjunction with the bistatic range equation. These realistic performance predictions were illustrated by means of a case study and developed throughout the dissertation, where the case study makes use of real parameters of the Villiersdorp transmitter and a receiver located at UCT.

Firstly, an omnidirectional target antenna was used at the PCL receiver site. Comparing the conventional performance prediction method, which utilises free space loss, and the improved performance prediction utilising AREPS propagation loss data, a vast difference in expected coverage was observed. In terms of radar detection range, the conventional method predicted coverage of up to 250 km for a target at an altitude of 1600 m, which in the light of existing experimental passive radars is very optimistic. However, the coverage predicted at the same altitude using realistic propagation loss was significantly reduced, in this case only extending to about 75 km. This result emphasises the major effect that terrain has on a propagating signal.

Furthermore, the limitation imposed on the PCL radar by the direct signal in the target channel was observed in the spatial SIR maps. Namely, for an omnidirectional target antenna the predicted coverage was poor and only up to a range of 50 km for a required receiver dynamic range of -60 dB.

To improve the coverage of the PCL system the direct path interference was suppressed in a target antenna pattern null - synthesised using the Schelkunoff Unit-Circle method. The null to main lobe ratio was simulated in FEKO to be 29.7 dB. The physically measured pattern agreed well with the simulated, but had a slightly lower null depth of 24.5 dB. Applying the measured pattern to the target antenna of the PCL receiver saw a vast improvement in coverage over the coverage expected with the omnidirectional target antenna. For the specified receiver dynamic range (-60 dB) the improvement was in the order of 90 km (total range of 140 km) for a target at 1600 m.

Comparing the resulting radar detection range of the synthesised target array with that of omnidirectional antenna saw the coverage described by the spatial SNR map increase to 130 km in the North-Easterly direction at the cost of coverage in the Southern direction and in the direction of the transmitter.

While suppressing the direct signal, the synthesised pattern also causes a decrease in radar detection range in certain sectors. However, due to its low-cost nature multiple PCL receivers can be employed to create a netted (multi-static) PCL radar in so doing increasing coverage of region as well as adding redundancy, an important property for any radar system.

Finally, the work done in this dissertation showed a simple yet effective method of producing realistic, environmentally dependent, coverage maps for a bistatic PCL radar. Furthermore, a technique of suppressing the significant limitation caused by the direct signal was discussed and presented. This prediction tool can be used to characterise the performance of any bistatic PCL configuration before final implementation.

Chapter 7

Future Work

The topic of PCL radar offers many different avenues for future work. Some of these avenues are currently being explored by colleagues within the Radar Remote Sensing Group (RRSG) at the University of Cape Town.

To begin with, the work in this dissertation emphasised the importance of factoring in environmental propagation effects in performance predictions of radar systems. An avenue to be investigated is the incorporation of the realistic AREPS propagation loss data in the Flexible and Extensible signal level Radar Simulator (FERS) [1] developed by Marc Brooker [18].

Currently, performance predictions of bistatic radar configurations using the method outlined in this work requires the use of two different platforms. Namely, to begin with AREPS computes the realistic propagation loss after which Matlab is used to compute the coverage predictions. This increases the time taken to investigate any one bistatic configuration. The method can be extended by automatically calling AREPS without the need to compute the propagation loss manually.

The performance prediction method presented here assumed a constant bistatic radar cross section. An avenue for future research is that of the multistatic RCS of a target. Little is published in open literature concerning the bistatic and more specifically the multistatic RCS of a target. Thus, research towards a better understanding of the behaviour of the RCS of a target in a multistatic radar configuration would be extremely beneficial to radar simulators and performance prediction utilities, such as the FERS simulator and the prediction method presented in this dissertation. Together with numerically modelled multistatic radar cross section estimates, these utilities will allow realistic investigations of multistatic PCL radar systems.

The work done here also opens up the possibility of performing receiver site optimisation. Namely, the method presented in this dissertation could be ex-

[1] http:www.sourceforge.org/projects/fers

tended to find the best possible receiver site in a specific region with varying mountainous terrain, for a given set of transmitters.

As discussed in this dissertation, the direct path signal in the target antenna channel is a major limiting factor of any bistatic PCL system. Methods to suppress this direct path signal were discussed in Chapter 1 and are important avenues to consider for future work. Some investigations are currently underway by members of the RRSG. For instance, adaptive filter techniques using the USRP (Universal Software Radio Peripheral) are being investigated for the purpose of direct path interference cancellation. Furthermore, techniques for analog and digital beamforming for a planar array [34, 35, 36] are also of interest and are currently being investigated as an extension of the work done here.

Appendix A

SRTM data to DTED conversion

This section will describe in detail how a conversion from SRTM () data format to DTED (Digital Terrain Elevation Data) data format can be achieved. AREPS, the EM propagation tool used in this dissertation, requires terrain data in the DTED format in order for it to calculate the propagation factor, F, accurately.

The format referred to as DTED is mainly used by the US military. The resolution and some metric approximations are given in the table below.

Table A.1: Resolution and metric approximations of DTED levels

DTED Level	Arc seconds in Latitude [″]	Approximate Metric Distance [m]
0	30	ca. 900
1	3	ca. 90
2	1	ca. 30

Conversion from SRTM to DTED

MICRODEM[1] is a freeware microcomputer mapping program written by Professor Peter Guth of the Oceanography Department, U.S. Naval Academy. The program MicroDEM is able to produce 1x1 degree tiles very easily by simply going through the following steps:

Load the program MicroDEM.

Unlike VTBuilder[2], another tool for viewing and processing many kinds of geospatial data, with MicroDEM you are required to unzip the SRTM data so that it is purely in .tif (GeoTiff) format. Click *File* ▷ *Open* ▷ *Open DEM*, then select the GeoTiff that you would like to convert to DTED and click OK.

[1] http://www.usna.edu/Users/oceano/pguth/website/microdem.htm checked April 2009
[2] http://www.vterrain.org/Doc/VTBuilder/overview.html checked April 2009

You should now see a SRTM GeoTiff tile of the area that you are interested in. By clicking Info some information concerning the particular GeoTiff tile should be displayed. Some important properties to note are:

DEM size: 6000x6000

Grid Space: 3x3″ (about 88.44x94.23m)

This information is given for a 5x5 degree tile.

From this tile we are able to export 1x1 degree DTED tiles of Level 1 format for the elevation data for AREPS. To get a better view of which tile you wish to convert set the grid to 1x1 degrees under the menu path *Modify* ▷ *Grid*; in the dialogue box enter a 1 in the space provide next to Lat/long grid interval(°).

Now, select *File* ▷ *Save DEM* ▷ *DTED*. You will now be presented with a DTED save parameters dialogue box. In this dialogue box all the necessary properties for conversion to DTED 1 are available. Check the Force 1°cell box. Once checked you are able to specify the bottom left Latitude and Longitude coordinate of the DTED tile to be created.

Also ensure that the DTED level is set to 1. This will create an elevation tile of resolution 3x3″ in DTED format. Click OK.

If these elevation tiles are to be used for AREPS you must use the following naming convention. When prompted to save the file, create a folder with name describing the longitudinal position of the bottom left corner such as e012, e023 or w019 etc. (note the 3 digits), where E and W represent east or west and the 012, 023 or 019 represents the whole degrees of longitude [27]. Now, within this folder you must save the actual DTED file as S19.DTX or N24.DTX where N24 and S19 represent the whole degrees of latitude. The file extension represents the DTED level [27]. In the case of this dissertation, the extension would be *.DT1.

Click OK when you have named the file and repeat the process for as many times as necessary. You can save multiple .DTX files of latitude under one folder of longitude.

Appendix B

PPM (Performance Prediction Method) Matlab Code Running Procedure

The procedure to produce SNR, SIR and SNIR coverage maps is explained here. This procedure can be divided into 3 major steps. The first involves producing the necessary raw polar propagation loss data using AREPS.

The second step explains the procedure of capturing the propagation loss data. In this step the data stored in the AREPS data files is extracted by a series of Matlab scripts. An interpolation over a regular grid is also done here.

The third step involves visualisation of results. This step explains the the available options for visualisation. Among these options are the mapping SNR, SIR and SNIR coverage as well as the plotting of propagation loss data over a given area.

This appendix is split into four section. Section B.1 deals with AREPS specific tasks. Section B.2 explains the folder structure used and necessary initialisations done by the PPM (Performance Prediction Method) code. Section B.3 explains the execution process of *PPMcompute.m*, PPM code. Finally, Section B.4 describes the visualisation of - most importantly - the SNR, SIR and SNIR data.

All the necessary data files can be found in the folder on the RRSG server or on the DVD provided with this dissertation, namely:

RRSG Server /rrsg/data/software/Performance Prediction Method

CD /software/Performance Prediction Method

B.1 Step 1 - AREPS

Here all the required steps to produce the necessary AREPS propagation data are explained. For completeness this explanation will begin with all the initialisation steps required after a new installation of AREPS. It is recommended that the reader go through Section B.1.1 to ensure that AREPS is setup correctly. Thereafter, the process of executing an AREPS project will be looked at.

B.1.1 AREPS Initialisation

Assuming you have a new installation of AREPS, some initial steps must be taken before execution.

Check your version of AREPS via *Help* ▷ *About AREPS*. The version of AREPS used during the completion of this dissertation was Version 3.6.02.42 May 10, 2007 and was run on a Windows XP OS.

AREPS requires (Digital Terrain Elevation Data) DTED elevation data. This is a specific elevation format. This terrain data can be found in the folder \Terrain data on the RRSG server or CD the location of which is given above. The elevation data contained in this folder covers a large sector of south western South Africa. See Appendix A for information on the DTED elevation format and on how to create more elevation data for additional regions. It is suggested that you copy this terrain data to your hard drive and place it in the ..\AREPS30\Data\Dted folder.

Next, we are going to import the necessary data associated with all the transmitters and receivers. This data has already been prepared and only needs to be imported. Select *Systems* ▷ *Database Utilities* ▷ *Open an Existing Database*. In the dialogue, browse to the folder ..\Areps\Databases on your the DVD or on the RRSG server and select PCL Database.

The raw propagation loss data computed by AREPS is not stored by default and needs to be enabled. To store this data for further computations within Matlab (Section B.3) select *Options* ▷ *Save Optional Data*. This opens the *AREPS Configuration - Save Optional Data Options* window. Check the *APM data in ASCII text format* and the *Terrain data in ASCII text format* tick box. The coverage display tick boxes can remain unchecked. Check the tick box that indicates that previously saved optional files for a particular project will be removed before a new execution.

Next, select *Options* ▷ *Program Flow*. This opens the *AREPS Configuration - Program Flow Options* window. In this window change the default earth quadrant to *Southeast* and the initialisation units to *Metric*.

Now, select *Options* ▷ *Terrain Data*. This opens the *AREPS Configuration - NGA (DTED/SRTM) Terrain Options* window. Change the *DTED level* to the available DTED elevation data level; in the case of this report level 1 was used. Check the *Assume empty fields are water* tick box. Also, enter zero latitude and longitude to bypass file editor defaults.

Finally, select *Options* ▷ *Default Project* ▷ *APM Parameters*. In the *AREPS Configuration - APM Parameters Options* window, select the options *Use parameters for all projects* and *Full coverage mode*. Everything else can be left as default.

B.1.2 AREPS Execution

You are now ready to run AREPS and create an AREPS Project.

Select *File* ▷ *New...* ▷ *Standard Project*. This will open an *Untitled AREPS Project* window. After specifying all the necessary information in this window you will be able to run AREPS and create an AREPS Project. Various details in this window can be checked and changed (should not be necessary) by right-clicking on the option name.

In the *Decision Aid* box select the *Communications (> 30 MHz)* radio button.

In the *Environment Specification* box select <Use DTED> from the Terrain drop-down menu. If you would like to perform your investigation a flat earth you can select <None> instead.

The *Graphic Display* box can be used to specify your area of interest by entering the minimum and maximum height and maximum range of your investigation. As an example, specify a height range of 0 to 6000 m above mean sea level and a maximum radial range up to 200 km.

In the System Specification box select the site for your investigation from the Platform/Site drop-down. For example, select Constantiaberg C1. Check that the Auto-populate box next to the Platform/Site drop-down is ticked. This will ensure that the geological latitude and longitude co-ordinates are automatically entered into the Project Geographic Area box below. All other tick-boxes in the Systems Specification box should remain unticked.

Now, choose an emitter from the Transmitter drop-down. All the possible emitters located at this site are listed in this drop-down menu. In the case where Constantiaberg C1 is the project site, only two emitters are available. To continue with the example, select the *const Rad5 89* as the emitter. This will have caused the Antenna height (m) AGL box to be updated with the height of the antenna of the *const Rad5 89* emitter. Ensure that the antenna height is given as height above ground level (AGL) and not height above mean sea level (MSL). As mentioned above, right-click on any value or unit in the

AREPS Project window to make any changes.

The choice of Comm receiver is not important for the purposes of this investigation. This is because, in terms of AREPS, we are only interested in the propagation loss from a Platform/Site by a Transmitter for a specific area of interest. Any platform can be chosen here.

Finally, the Project Geographic Area box must be populated. The Latitude and Longitude (Deg) should have been auto-populated and should show the position of the Platform/Site chosen above.

Upon execution, AREPS computes the propagation loss along a specified bearing. Additional computations are done by incrementing the bearing, namely by moving the bearing of interest in a clockwise direction. Thus, an area of interest can be described by specifying the First bearing ($^{\circ}True$) , the Bearing increment (Deg) and the Number of bearings.

Currently, the Matlab script is only capable of dealing with bearings divisible by 5. This means that the First bearing must be divisible by 5 and that the Bearing increment must be 5°.

The subsequent Number of bearings must be chosen to encompass the area of interest. For example, the Constantiaberg transmitter has a beamwidth of half-power beamwidth of 70° centred at 25°. This translates to an area of interest described by the bearing range 350° to 60° at 5° steps. Subsequently, the first bearing will be 350°, the bearing increment 5° and the number of bearings 15.

For the common case of an omnidirectional transmitter, the first bearing will be 0°, the bearing increment 5° and the number of bearings 72.

B.1.3 AREPS Data Format

Propagation loss data for each bearing is saved within one text file. There are two sections of interest in each text file. One section for the propagation loss data and another for the propagation factor. Subtracting the propagation factor from the propagation loss data provides one with free space propagation loss data, in essence giving one all the necessary propagation loss data.

The propagation data for both sections is further divided into loss data at finite heights. For each of these heights there is a set of finite range points. An example of data format can be seen by viewing the text files within a project folder .

B.2 PPMRoot (Performance Prediction Root) Folder Structure and Initialisations

The Matlab scripts necessary to create the coverage maps are contained in a directory named PPMRoot<yymmdd>, <yymmdd> corresponds to the latest updated version, for example PPMRoot090104. This directory will be referred to as the root directory. The directory and its sub-folders is shown in Figure B.1.

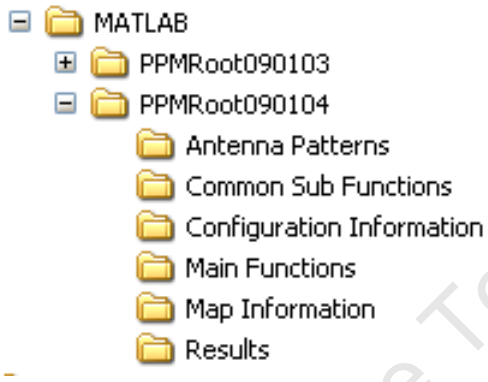

Figure B.1: Folder structure of the PPMRoot folder.

B.2.1 Configuration Information Folder

Some parameters need to be initialised before executing the PPMcompute script. The most important of these is the initialisation text file found in the folder *Configuration Information*. This file contains all the initialisation data necessary for PPM scripts to run correctly. The type of output data required is also set in this text file. The parameters contained in an initialisation text file are shown in B.1. As an example here, the parameters for a transmitter of opportunity at Constantiaberg and a receiver at UCT Menzies are given.

Transmitter Information

1 Transmitter Name This is the name given to the transmitter to identify in very general terms.

2 Tx Latitude $[d^{\circ}, m', s'', Hemi]$ This is the geographical latitude of the transmitter. It must written in a CSV format as indicated in the square brackets. The degrees, minutes and seconds are measured from the equator $0^{\circ}, 0', 0''$ to any one of the north or south poles $90^{\circ}, 0', 0''$. The variable $Hemi$ signifies the hemisphere of d, m, s value and can either be N or S (north and south respectively).

Table B.1: Initialisation Parameters for PPMcompute.m

Transmitter Information		
1	Tx Name	Constantiaberg
2	Tx Longitude $[d^{\circ}, m', s'', Hemi]$	34,3,15,S
3	Tx Latitude $[d^{\circ}, m', s'', Hemi]$	18,23,15,E
4	AREPS Tx Project Folder Name	ConstantiabergTx89
5	Frequency [MHz]	89
6	Power [W]	1000
7	Tx Beamwidth Start $[0^{\circ} - 359^{\circ}]$	350
8	Tx Beamwidth End $[0^{\circ} - 359^{\circ}]$	60
9	Gain Within Beamwidth [dB]	10
10	Gain Outside Beamwidth [dB]	-30
Receiver Information		
1	Rx Name	Menzies
2	Rx Longitude $[d^{\circ}, m', s'', Hemi]$	33,57,31.16,S
3	Rx Latitude $[d^{\circ}, m', s'', Hemi]$	18,27,36.36,E
4	AREPS Rx Project Folder Name	MenziesRx89
5	Antenna Pattern [*.mat file]	AntPat.mat
6	Rx Sector Start $[0^{\circ} - 359^{\circ}]$	350
7	Rx Sector End $[0^{\circ} - 359^{\circ}]$	60
8	Receiver Noise Figure, F_n [dB]	10
Additional Information		
1	PL Data Calculation Choice [y/n]	n
2	Free Space PL Calculation [y/n]	y
3	Altitude [m]	1600
4	SNR and SNIR Processing Bandwidth, B [Hz]	1
5	Target RCS $[m^2]$	10
6	Antenna Noise Temperature T_a [K]	290

3 Tx Longitude $[d^\circ, m', s'', Hemi]$ This is the geographical longitude of the transmitter. It must written in a CSV format as indicated in the square brackets. The degrees, minutes and seconds are measured from the meridian $0^\circ, 0', 0''$ to the international date line at $180^\circ, 0', 0''$ in an easterly or westerly direction. The variable $Hemi$ signifies the hemisphere of d, m, s value and can either be E or W (East and West respectively).

4 AREPS Tx Project Folder Name This is a string of characters that makes up the name of the folder that contains all the AREPS generated propagation loss data relevant to one transmitter (at the specified location). The words and numbers that make up this string of characters are usually chosen in such a way that they completely describe the project. An example here as shown in Table B.1, is ConstantiabergTx95.3, where the chosen characters imply that the transmitter used is at Constantiaberg and that the frequency used is 95.3 MHz.

5 Frequency [**MHz**] This is the FM radio frequency used for the investigation. It is given in MHz.

6 Power [**W**] This is the TPO (Transmitter Power Output). This is the amount of power used to emit the FM radio signal at the specified frequency.

7 Tx Beamwidth Start $[0^\circ - 359^\circ]$ This contains the value for the start of the HPBW (Half Power Beamwidth) for the transmitter pattern as given by the specifications by Sentech.

8 Tx Beamwidth End $[0^\circ - 359^\circ]$ This contains the value for the end of the HPBW (Half Power Beamwidth) for the transmitter pattern as given by the specifications by Sentech. The transmitter beamwidth is measured clockwise from **7 Tx Beamwidth** Start to **8 Tx Beamwidth End**.

9 Gain Within Beamwidth [**dB**] This is the gain within the HPBW of the transmitting antenna radiation pattern.

10 Gain Outside Beamwidth [**dB**] This is the gain outside the HPBW of the transmitting antenna radiation pattern.

Receiver Information

1 Receiver Name This is the name given to the receiver to identify it in general terms.

2 Rx Latitude $[d^\circ, m', s'']$ This is the geographical latitude of the receiver. See **2 Tx Latitude** for a description of variable format.

3 Rx Longitude $[d^\circ, m', s'']$ This is the geographical longitude of the receiver. See **3 Tx Longitude** for a description of variable format.

4 AREPS Rx Project Folder Name This is a string of characters that makes up the name of the folder that contains all the AREPS generated propagation loss data relevant to one receiver (at the specified location). See **4 AREPS Tx Project Folder Name** for more detail.

5 Antenna Pattern $[data\ file]$ The data file referenced here will contain information on the antenna radiation pattern of the receiver. This allows for receiver antenna patterns, simulated in modelling software such as FEKO, to be included in the bistatic coverage prediction. The data file must be in a *.mat (Matlab data file) format.

6 Rx Sector Start $[0^\circ - 359^\circ]$ This contains the azimuth value that describes the start of the sector of interest as seen from the receiver.

7 Rx Sector End $[0^\circ - 359^\circ]$ This contains the azimuth value that describes the end of the sector of interest as seen from the receiver. The sector of interest is measured clockwise from **6 Rx Sector Start** to **7 Rx Sector End**. The sector of interest is an important consideration. For the proper visualisation of the coverage results one must ensure that at least some of the transmitter beamwidth is covered by the sector of interest.

8 Receiver Noise Figure F_n [**dB**] The receiver noise figure specifies the noise added within the receiving system.

Additional Information

1 PL Data Calculation $[y/n]$ This allows the option of calculating the propagation loss (PL) data from the transmitter and receiver without taking into account the gain patterns of either the transmitter or the receiver. Processing time is saved by choosing not to (specify n) calculate the propagation loss and gain-free data.

2 Free Space PL Calculation $[y/n]$ This allows the option of calculating free space losses in addition to the usual AREPS terrain propagation losses. Processing time is saved by choosing not to (specify n) calculate free space losses.

3 Altitude [**m**] The altitude at which the investigation is performed. All the resulting data will be given for that altitude.

4 SNR Processing Bandwidth B [**Hz**] The processing bandwidth is linked with the integration time. Namely, by $T_i = 1/B_p$.

5 Target RCS $[\mathbf{m}^2]$ This is the target's bistatic Radar Cross Section (RCS).

6 Antenna Noise Temperature T_a **[K]** This is the noise temperature of the antenna and is usually kept at room temperature.

B.2.2 Antenna Patterns Folder

This folder contains any receiver/target antenna patterns that you would like to use within your performance prediction. These antenna patterns are saved as *.mat files. As an example, the antenna pattern specified in Table B.1 is AntPat.mat. This Matlab data file contains two variable; PhiAnt and GainAnt. The two variables must be named PhiAnt and GainAnt.

PhiAnt corresponds to the azimuth angle, ϕ, measured clockwise from True North. ϕ must be defined for the range $[0^\circ,\ 359^\circ]$ and must have corresponding gain (GainAnt) values for every ϕ point.

B.2.3 Map Information Folder

This folder contains three images of the Western Cape terrain, which are used as background for the spatial mapping of SNR, SIR and SNIR. The projection of these terrain images is UTM with the dimensions of the maps precisely known. Being UTM allows Cartesian data to be overlayed.

B.2.4 Main Functions Folder

This folder contains the main functions, which are stand-alone functions. They are not called by any other functions and are written to perform specific tasks. The functions contained in this folder are:

- BearingCalc.m
- TxRxAirportPos.m
- PPMcompute.m
- PPMplotter.m
- SNRdata.m

The two functions important to the this section are PPMcompute and PPMplotter. These two functions compute the SNR, SIR and SNIR coverage data and allow visualisation of the data by overlaying onto a Western Cape map respectively. To achieve this they call the Common Subfunctions (Section B.2.5). More in-depth descriptions of these functions can be obtained by typing *help*

function_name (example *help PPMcompute*) at the command line within Matlab, after path initialisation (Section B.2.7).

B.2.5 Common Subfunctions Folder

- BearingPadding.m
- DisplayInfo.m
- dmsh2deg.m
- FindPos.m
- geo2utm
- ImportMap.m
- RxTxPostion.m
- SampleGain.m
- SIRcalc.m
- SNIRcalc.m
- SNRcalc.m
- TheoFSPLcalc.m
- TxPat.m

More in-depth descriptions of these functions can be obtained by typing *help function_name* (example *help SNRcalc*) at the command line within Matlab, after path initialisation (Section B.2.7).

B.2.6 Results Folder

The Results folder would contain all the data computed by PPMcompute. In general, it will contain three different sets of propagation loss data; one associated with the receiver, one with the transmitter and one containing all the combined propagation loss data from both the transmitter and receiver.

One additional temporary data set will be saved as well, called *temp.mat*. This serves as a backup of sorts and contains the same data as the combined propagation loss data set.

All of the data files will be Matlab *.mat files. The data filenames, with reference to Section B.2.1, will be in the following format:

1. Receiver specific data:
   <Areps Rx Project Folder Name>_<Altitude>.mat. An example is *MenziesRx96.5_1600.mat*

2. Transmitter specific data:
   <Areps Tx Project Folder Name>_<Altitude>.mat. An example is *VilliersdorpTx96.5_1600.mat.*

3. Combined specific data:
   <Areps Tx Project Folder Name>_<Areps Rx Project Folder Name>
   _<Altitude>.mat.
   An example of this is *VilliersdorpTx96.5_MenziesRx96.5_1600.mat.*

The variables (data) contained in each of these *.mat files will depend on the specifications made in the Configuration Information (Section B.2.1).

When running PPMplotter.m you will prompted to select one (or more) of these data sets. The prompt will specify whether receiver, transmitter or combined specific data is required.

B.2.7 Path Initialisations

The paths to all the necessary functions, subfunction, maps, results and antenna patterns must be initialised before the execution of any of the main functions. This is done by running the IniPaths.m script found in the RootPPM directory. Running IniPaths.m will set the RootPPM directory in which it is found as the current working directory of Matlab.

Once the paths have been initialised PPMcompute.m and PPMplotter.m (provided available Results data in the case of PPMplotter.m) can be run by simply typing the script name in the Command Window.

B.3 Step 2 - Matlab PPMcompute script

This step will explain the execution process of *PPMcompute.m*. The name stands for the computation of the data necessary for performance prediction method. This Matlab script imports data generated by AREPS and extracts all the information necessary for the specified investigation. As emphasised in the dissertation, AREPS data contains the effects of the environment.

B.3.1 Execution of PPMcompute.m

Before the execution of the PPMcompute.m script the paths need to be initialised. This is done by the IniPaths.m found within the root directory (Sec-

tion B.2.7).

After typing PPMcompute in the Command Window, you will be prompted to select a configuration information text file. This text file will serve as input to the PPMcompute function. Thus it is important to ensure that the parameters are specified correctly within the configuration file.

Once the configuration file is selected, the parameters are printed out within the Command Window again for confirmation purposes.

You will be required to press return at this point to proceed. Once return is pressed, the script begins to extract the specified propagation loss data from the entire data set previously computed by AREPS (Section B.1).

In simple terms, the PPMcompute script searches for a particular altitude within a text file associated with a certain bearing. Once the required altitude is found, the associated propagation data over the finite range steps is extracted. The range steps and consequently the propagation data (along a particular bearing) are mapped to a Cartesian UTM grid for a certain altitude.

Continuing this process, results in a number of polar propagation data sets. This polar data is then interpolated of a regular Cartesian UTM grid.

A host of useful information is captured from the AREPS propagation data. For this reason, the data is saved to the hard drive, which also aids in freeing up memory. The results from PPMcompute are saved in the Results folder (see Section B.2.6 for more details about the saved data).

B.4 Step 3 - PPMplotter Script

This is the final step, and it involves the creation and visualisation of - most importantly - the SNR, SIR and SNIR data. Other data can also visualised, such as the propagation loss data from the transmitter and receiver sites. There are four main options available when running the PPMplotter.m script; these are:

1. Plot propagation loss data
2. Plot a SNR coverage map
3. Plot a SIR coverage map
4. Plot a SNIR coverage map

The flow of these options is illustrated in Figure B.2. Option 1 (*Plot Propagation Loss (PL)*) branches to the top of the figure and options 2 through 4 (*Plot SNR/SIR/SNIR Coverage*) branch to the bottom.

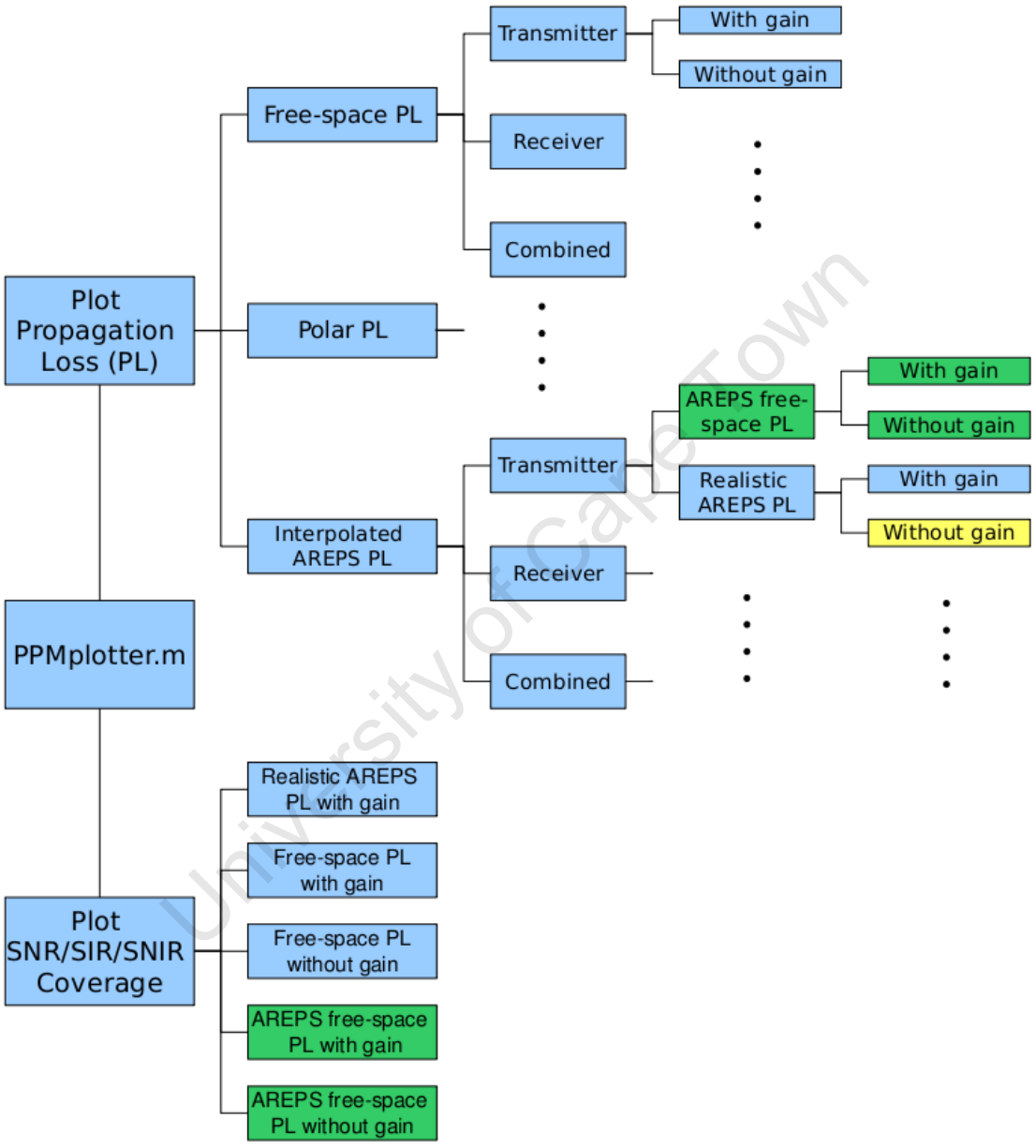

Figure B.2: Illustration of possible options within PPMplotter.m.

The processes indicated with a yellow block, require extra data computed by specifying '*y*' for the *PL Data Calculation* parameter detailed in Section B.2.1. The processes indicated with the green blocks, require extra data computed by specifying 'y' for the *Free-Space Data Calculation* parameter detailed in the same section.

All the processes indicated by the blue blocks can be performed under default conditions.

Appendix C

Dissertation-Specific Configuration Information

The configuration information detailed here relates to a bistatic PCL system which utilises the Villiersdorp transmitter as the illuminator of opportunity with the receiver located on the roof of the Menzies building at UCT. Investigations done in this dissertation were performed at different altitudes, with different antenna patterns, but in general shared many common parameter.

First the exceptions to the common parameters listed in Table C.1 are given. Thereafter, a section is dedicated to each configuration used in this dissertation. Namely, each following section contains information on data used for the exception for the investigation performed.

C.1 Exceptions

All the configurations used within this dissertation for illustration purposes use the configuration information shown in Table C.1 with two exceptions. These two exceptions are:

- The target antenna pattern (Number 5 of the Receiver Information section).
- The altitude of interest (Number 3 of the Additional Information section).

C.1.1 Configuration Information Set A

Antenna Pattern $[data\ file]$ An omnidirectional target antenna receiver pattern called, *Omni5dB.mat*, was used here.

Altitude $[m]$ The altitude of interest is *1600* m above sea level.

Remaining Parameters These are common to all configurations used in this dissertation and are listed in Table C.1.

C.1.2 Configuration Information Set B

Antenna Pattern $[data\ file]$ An omnidirectional target antenna receiver pattern called, *Omni5dB.mat*, was used here.

Altitude $[m]$ The altitude of interest is *5000* m above sea level.

Remaining Parameters These are common to all configurations used in this dissertation and are listed in Table C.1.

C.1.3 Configuration Information Set C

Antenna Pattern $[data\ file]$ An antenna array of folded dipoles was used here in order to suppress the DPI from the illuminating transmitter. This pattern was simulated with FEKO. The antenna pattern is saved in the Matlab data file named, *4eleFDArray.mat*.

Altitude $[m]$ The altitude of interest is *1600* m above sea level.

Remaining Parameters These are common to all configurations used in this dissertation and are listed in Table C.1.

C.1.4 Configuration Information Set D

Antenna Pattern $[data\ file]$ An antenna array of folded dipoles was used here in order to suppress the DPI from the illuminating transmitter. This pattern was simulated with FEKO. The antenna pattern is saved in the Matlab data file named, *4eleFDArray.mat*.

Altitude $[m]$ The altitude of interest is *5000* m above sea level.

Remaining Parameters These are common to all configurations used in this dissertation and are listed in Table C.1.

C.1.5 Configuration Information Set E

Antenna Pattern $[data\ file]$ An antenna array of folded dipoles was used here in order to suppress the DPI from the illuminating transmitter. This antenna pattern was the pattern measured on the roof of Menzies. The antenna pattern is saved in the Matlab data file named, *4FDSchelkMeasPat.mat*.

Altitude $[m]$ The altitude of interest is *1600* m above sea level.

Remaining Parameters These are common to all configurations used in this dissertation and are listed in Table C.1.

C.1.6 Configuration Information Set F

Antenna Pattern $[data\ file]$ An antenna array of folded dipoles was used here in order to suppress the DPI from the illuminating transmitter. This antenna pattern was the pattern measured on the roof of Menzies. The antenna pattern is saved in the Matlab data file named, *4FDSchelk-MeasPat.mat*.

Altitude $[m]$ The altitude of interest is *5000* m above sea level.

Remaining Parameters These are common to all configurations used in this dissertation and are listed in Table C.1.

Table C.1: Common Configuration Parameters for PPMcompute.m for the Villiersdorp-Menzies case

Transmitter Information		
1	Tx Name	Villiersdorp
2	Tx Longitude $[d^{\circ}, m', s'', Hemi]$	33,58,9,S
3	Tx Latitude $[d^{\circ}, m', s'', Hemi]$	19,30,25,E
4	AREPS Tx Project Folder Name	VilliersdorpTx96.5
5	Frequency [MHz]	96.5
6	Power [W]	1000
7	Tx Beamwidth Start $[0^{\circ} - 359^{\circ}]$	0
8	Tx Beamwidth End $[0^{\circ} - 359^{\circ}]$	359
9	Gain Within Beamwidth [dB]	10
10	Gain Outside Beamwidth [dB]	-30
Receiver Information		
1	Rx Name	Menzies
2	Rx Longitude $[d^{\circ}, m', s'', Hemi]$	33,57,31.16,S
3	Rx Latitude $[d^{\circ}, m', s'', Hemi]$	18,27,36.36,E
4	AREPS Rx Project Folder Name	MenziesRx96.5
5	Antenna Pattern [*.mat file]	See Exceptions (Section C.1)
6	Rx Sector Start $[0^{\circ} - 359^{\circ}]$	0
7	Rx Sector End $[0^{\circ} - 359^{\circ}]$	359
8	Receiver Noise Figure, F_n [dB]	20
Additional Information		
1	PL Data Calculation Choice [y/n]	y
2	Free Space PL Calculation [y/n]	y
3	Altitude [m]	See Exceptions (Section C.1)
4	SNR and SNIR Processing Bandwidth, B [Hz]	1
5	Target RCS $[m^2]$	10
6	Antenna Noise Temperature T_a [K]	290

Appendix D

Receiver Components

D.1 Antenna

Four folded dipole antenna elements were purchased from SpaceTV. One element can be seen in Figure D.1.

Figure D.1: Single folded dipole element.

D.2 Transmission Line and Connectors

The transmission line used was Ellies RG 6 dual shield white coaxial cable (Series 6). Further technical features of this cable can be seen in Table D.1.

Table D.1: Technical features.

Product Code	ACRG6
Inner Conductor	1.02 mm C.C.S.
Dielectric	4.70 mm Physical Foam PE
Foil	ALu/Pet
Braid	32/0.12 mm ALu
Jacket	6.80 mm PVC
Impedance	75 Ω

D.3 Attenuator

Tee attenuators were built for channel 1 and 4 of the target array. The schematic with resistors is shown in Figure D.2. The attenuator was designed to have a nominal impedance of 75 Ω and the resistor values were found to be $R_1 = R_2 = 36.5\,\Omega$ and $R_3 = 59\ \Omega$ using Pozar [26].

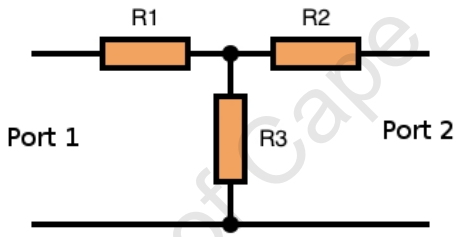

Figure D.2: Tee attenuator schematic and resistors.

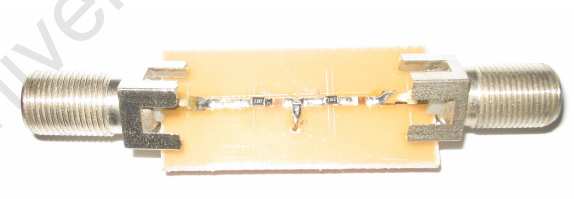

Figure D.3: Tee Attenuator.

D.4 Combiner

The combiner was sourced for Ellies. Technical details were not provided and subsequently the combiner was characterised following the measurement procedure detailed by Pozar [26] and a Mini-Circuits application note [37].

Figure D.4: Ellies splitter/combiner.

Table D.2: Combiner characteristics at 96.5 MHz

Frequency	Insertion Loss [dB]			
[MHz]	S-1	S-2	S-3	S-4
90	7.02	7.08	7.04	7.04
95	7.03	7.09	7.06	7.04
100	7.05	7.11	7.08	7.06
105	7.08	7.13	7.11	7.1

(a) Insertion Loss

Frequency	Isolation [dB]					
[MHz]	1-2	1-3	1-4	2-3	2-4	3-4
90	25.83	27.98	28.3	28.13	28.6	25.63
95	25.86	28.03	28.34	28.2	28.6	25.7
100	25.95	27.96	28.41	28.23	28.7	25.78
105	25.96	27.98	28.39	28.21	28.68	25.88

(b) Isolation

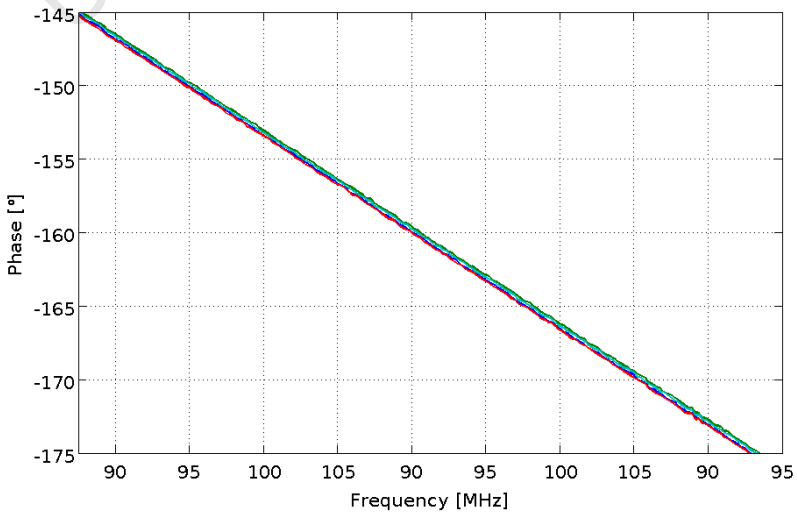

Figure D.5: Combiner Phase Shift

Bibliography

[1] Cherniakov M, Moccia A, D'Errico M, Moreira A, Krieger G, Dubois-Fernandez P, et al. Bistatic Radar: Emerging Technology. Cherniakov M, editor. John Wiley & Sons, Ltd; 2008.

[2] Howland PE, Maksimiuk D, Reitsma G. FM radio based bistatic radar. In: IEE Proceedings on Radar, Sonar and Navigation. vol. 152. Institute of Electrical Engieers (United Kingdom); 2005. p. 107–115.

[3] Barton DK. Modern Radar System Analysis. Artech House; 1988.

[4] Balanis CA. Antenna Theory: Analysis and Design. 3rd ed. John Wiley & Sons; 2005.

[5] Milligan TA. Modern Antenna Design. 2nd ed. Hoboken, New Jersey: John Wiley & Sons, Inc.; 2005.

[6] Mawela C. Final Terrestrial Broadcast Frequency Plan. Independent Communications Authority of South Africa - ICASA; 2004. General Notice, Notice 1513 of 2005. Available from: `http://www.info.gov.za/view/DownloadFileAction?id=61800` [Accessed May 2007].

[7] Willis N. Bistatic Radar. Artech House, Inc.; 1991.

[8] Skolnik MI. Introduction to Radar Systems. 3rd ed. McGraw-Hill Book Company; 2001.

[9] Haimovich AM, Blum RS, Cimini LJJ. MIMO Radar with Widely Separated Antennas. IEEE Signal Processing Magazine. 2008 January;25(1):116 – 129.

[10] Zoeller CL, Budge MCJ, Moody MJ. Passive Coherent Location Radar Demonstration. System Theory, 2002 Proceedings of the Thirty-Fourth Southeastern Symposium on. 2002;p. 358 – 362.

[11] Peebles PZ. Radar Principles. John Wiley & Sons; 1998.

[12] Griffiths HD, Long NRW. Television-based bistatic radar. IEE Proc F, Commun Radar Signal Process. 1986 December;133(7):649–657.

[13] Howland PE. Television Based Bistatic Radar [PhD Thesis]. University of Birmingham; 1997.

[14] Howland PE. Target Tracking Using Television-Based Bistatic Radar. IEE Proceedings on Radar, Sonar and Navigation. 1999 June;146(3):166–174.

[15] Baker CJ, O'Hagan DW, Griffiths HD, Inggs MR, Lord RT, Morrison N. Passive Radar Tracking. In: The Institution of Engineering and Technology Seminar on The Future of Civil Radar. Institution for Engineering and Technology; 2006. p. 57–67.

[16] Baniak J, Baker DG, Cunningham AM, Martin L. Silent Sentry Passive Surveillance: Lockheed Martin Mission Systems; 1999.

[17] Sandenbergh S. A Low-Cost Time Synchronization Method For a Netted Radar System using Multi-Channel Common View GPS Time Transfer; 2008. Available from: `https://rrsg.ee.uct.ac.za/members/stephan/index_files/phdtopic.html` [Accessed December 2008].

[18] Brooker M. The Design and Implementation of a Simulator for Multistatic Radar Systems [PhD Thesis]. University of Cape Town; 2008.

[19] Skolnik M. Radar Handbook. 2nd ed. Skolnik M, editor. McGraw-Hill Book Company, Inc; 1990.

[20] Baker CJ, Griffiths HD, Papoutsis I. Passive coherent location radar systems. Part 2: Waveform properties. In: IEE Proceedings on Radar, Sonar and Navigation. vol. 152. Institute of Electrical Engineers (United Kingdom); 2005. p. 160–168.

[21] ;. Private Communication from D. O'Hagan, November 2009.

[22] Griffiths HD, Baker CJ. Passive coherent location radar systems. Part 1: Performance prediction. In: IEE Proceedings on Radar, Sonar and Navigation. vol. 152. Institute of Electrical Engineers (United Kingdom); 2005. p. 153–159.

[23] Tobias M, Lanterman AD. Multitarget tracking using multiple bistatic range measurements with probability hypothesis densities. vol. 5429. Orlando, FL, USA: SPIE; 2004. p. 296–305. Available at `http://link.aip.org/link/?PSI/5429/296/1`.

[24] Wan H, Li S, Wang Z. Direct Path Interference Cancellation in FM Radio Based Passive Radar. In: ICSP2006 Proceedings; 2006. .

[25] Sahr JD, Lind FD. The Manastash Ridge radar: A passive bistatic radar for upper atmospheric radio science. Radio Science. 1997 December;32(6):2345–2358.

[26] Pozar DM. Microwave and RF Design of Wireless Systems. John Wiley & Sons, Inc.; 2001.

[27] User's Manual for Advanced Refractive Effects Prediction System. San Diego, CA; 2006. Atmospheric Propagation Branch.

[28] Barrios AE, Anderson K, Lindem G. Low Altitude Propagation Effects - A Validation Study of the Advanced Propagation Model (APM) for Mobile Radio Applications. IEEE Transactions on Antennas and Propagation. 2006 October;54(10):2869–2877.

[29] Barrios AE, Sprague DR. Propagation Modeling. 2008;Available from: www.onr.navy.mil/obs/reports/docs/05/mmbarrio.pdf [Accessed 9 June 2008].

[30] Sentech. Transmitter Data; 2007. Transmitter data was obtained through correspondance with Sentech (http://www.sentech.co.za/).

[31] Cape Town - World Aeronautical Chart (3422); 1996. Private Bag X10, Mowbray, South Africa. Published by the Chief Directorate: Surveys and Land Information.

[32] Villeneuve A. Taylor patterns for discrete arrays. Antennas and Propagation, IEEE Transactions on. 1984 Oct;32(10):1089–1093.

[33] Schelkunoff SA. A mathematical theory of linear arrays. Bell System Technical Journal. 1943;22:80–107.

[34] Laxpati S. Planar array synthesis with prescribed pattern nulls. Antennas and Propagation, IEEE Transactions on. 1982 Nov;30(6):1176–1183.

[35] Castella FR, Marable DL. Optimized planar array antenna nulling with phase only control. In: European Microwave Conference, 1993. 23rd; 1993. p. 886–888.

[36] Orchard HJ, Elliott RS, Stern GJ. Optimising the synthesis of shaped beam antenna patterns. IEE Proceedings. 1985 Feburary;132H(1):63–68.

[37] Mini-Circuits. Understanding Power Splitters; 2005. AN-10-006. Available from: http://www.minicircuits.com/pages/pdfs/an10006.pdf [Accessed January 2009].

[38] Schleher DC. MTI and Pulsed Doppler Radar. Artech House, Inc.; 1991.

[39] Straw RND, editor. The ARRL Antenna Book. 17th ed. The American Radio Relay League, Newington, CT 06111; 1994.

[40] Recioui A, Azrar A. Use of genetic algorithms in linear and planar antenna array synthesis based on Schelkunoff method. Microwave and Optical Technology Letters. 2006 April;49:1619–1623.

[41] Vu TB. On null steering in rectangular planar array. Antennas and Propagation, IEEE Transactions on. 1992 August;40:995–997.

[42] Zainud-Deen SH. On null steering in rectangular planar array using external elements. In: Antennas and Propagation Society International Symposium, 1995. AP-S. Digest. vol. 2; 1995. p. 942–945.

[43] Burke GJ. Numerical electromagnetic code - NEC-4 method of moments, part I: Users manual. Lawrence Livermore National Laboratory; 1992. UCRL-MA-109338.

[44] PoyntingAntennas. Direction Finding Antennas; 2009. Available from: `http://www.poynting.co.za/productlist.php?id=1&app=30&type=0` [Accessed May 2009].

[45] ThalesRaytheonSystems. Home Alerter 100; 2009. Available from: `http://www.thalesgroup.com/eurosatory2008/standthales3.htm` [Accessed Feburary 2009].

[46] Baker C, O'Hagan DW, Baker CJ, Griffiths HD, Inggs M, Lord R, et al. Passive Radar Tracking. The Future of Civil Radar, 2006 The Institution of Engineering and Technology Seminar on. 2006 June;p. 57–67.

[47] Hoyuela CM, Terzuoli AJ, Jr, Wasky RP. Determining possible receiver locations for passive radar. Radar, Sonar and Navigation, IEE Proceedings. 2005 June;.

[48] O'Hagan DW, Baker CJ, Griffiths HD. Signal and Interference Analysis: Proposed Analogue Signal Suppression Techniques for PCL Radar. Radar Conference, 2006 EuRAD 2006 3rd European. 2006 Sept;p. 296–298.